# Dépendance de la production de photons durs avec le paramètre d'impact dans les collisions entre ions lourd aux énergies intermédiaires

Gines Martinez Garcia

# GANIL

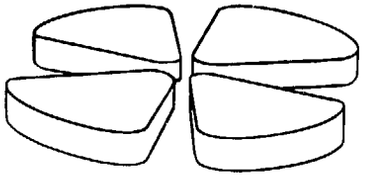



# Multiparticle correlations and intermittency in high energy collisions

Piotr Bożek

GANIL T 92 02

# Multiparticle correlations and intermittency in high energy collisions

Piotr Bożek
Institute of Nuclear Physics
Cracow

Ph.D. Dissertation
H. Niewodniczański Institute of Nuclear Physics
Cracow, Poland

# Multiparticle correlations and intermittency in high energy collisions

Piotr Bożek
H. Niewodniczański Institute of Nuclear Physics
Cracow, Poland
February 1992

Ph.D. Dissertation prepared under the supervision of
Dr. Marek Płoszajczak in the Department of Theoretical
Physics of the H. Niewodniczański Institute of Nuclear Physics,
Cracow, Poland

Date of the degree : 27.05.1992
Referees :
Prof. A. Białas, Jagiellonian University, Cracow
Prof. R. Peschanski, CEN-Saclay
Prof. K. Zalewski, Institute of Nuclear Physics, Cracow

I am greatly indebted to my thesis supervisor, Professor M. Płoszajczak, for proposing me the theme of this work, for many fruitful discussions, for much patience and great help.
I would like to thank Dr. A. Tucholski for collaboration, help and many useful discussions. I have the pleasure to acknowledge the remarkable collaboration with Dr. Z. Burda. For useful discussions I want to thank Dr. R. Peschanski, Dr. J. Alberty and Dr. G. Auger. I thank also Dr. P. Kamiński for help and discussions. I would like to thank Professor J. Kwieciński, Professor S. Harar and Professor W. Nörenberg for their help and encouragment to work on the subject.
This work was possible due to the financial support of the Polska Agencja Atomistyki, Gesellschaft für Schwerionenforschung (GSI) in Darmstadt and Commissariat à l'Énergie Atomique, France. The support of the Polish Government grant KBN 2.0204.91.01 is also acknowledged. I would like to thank GSI in Darmstadt and Grand Accélérateur National d'Ions Lourds (GANIL) in Caen for hospitality and for the permission to use their computer facilities. My stay at GANIL was possible due to the scholarship from Commissariat à l'Énergie Atomique for which I am grateful. I would like to thank all collegues from the Department of Theoretical Physics of the Institute of Nuclear Physics in Kraków, the Theory Group at GSI and from the Physics Department at GANIL for creating a stimulating and friendly atmosphere and for the help extended to me during my stay in these institutions.

# Abstract

In this work the analysis of the intermittency signal observed in high energy experiments is done using multiparticle distributions and correlation functions. The effect of the dimensional projection of the multiparticle distributions on one or two-dimensional subspace is discussed. The structure of the multiparticle cumulants is analyzed for the DELPHI $e^+e^-$ annihilation data. The language of the self-similar distribution functions, which is used in this work, is shown to be largely equivalent to the well known $\alpha$-model. In the case of the ultrarelativistic nuclear collisions, where the Monte-Carlo simulations fail to reproduce the data, we argue that the observed intermittency pattern is a signal of some nonlinear effect beyond the simple superposition of nucleon-nucleon collisions. The model of spatiotemporal intermittency is discussed in details and is shown to reproduce qualitatively the dependence of the intermittency strength on the target and projectile nuclei. Similar effects are also observed in the statistical systems undergoing a higher order phase transition. We study in particular a 1-dimensional (1D) cellular-automaton (CA) and a 1D forest-fire model. On the example of the noncritical 1D Ising model we illustrate the difficulties of the scaled factorial moment (SFM) method in extracting genuine scaling behaviour. The problem of the finite-size effect in connection to the dimensional projection can be easily exemplified in the case of the 2D critical system with conformal symmetry. All these studies could serve as tools to test the sensibility of the SFM method as used in the analysis of the high energy production.

# Streszczenie

W tej pracy analiza sygnału intermitentnego obserwowanego ekserymentalnie jest wykonana za pomocą wielocząstkowych funkcji rozkładu i funkcji korelacji. Dyskutowany jest efekt rzutowania z przestrzeni wielowymiarowej, w której powstają niefaktoryzowalne korelacje. Pokazano dobrą zgodność opisu za pomocą funkcji rozkładu niezależnych od skali i za pomocą modelu $\alpha$ . Ciekawe jest zjawisko intermitencji dla ultrarelatywistycznych zderzeń jądrowych, w których symulacje Monte-Carlo nie odtwarzają danych eksperymentalnych. Pokazujemy, że obserwowany sygnał intermitencji jest zjawiskiem nielinowym, wychodzącym poza proste złożenie zderzeń nukleon-nukleon. W szczególności analizowany jest model intermitencji czasoprzestrzennej. Odtwarza on jakościowo obserwowaną eksperymentalnie zależność od rodzaju pocisku i tarczy. Podobne efekty zastały stwierdzone w systemach statystycznych w pobliżu punktu przejścia fazowego wyższego rzędu. Pokazano tego typu zachowanie dla pewnego jednowymiarowego automatu komórkowego i dla jednowymiarowego modelu pożaru lasu. Na przykładzie niekrytycznego jednowymiarowego modelu Isinga pokazujemy problemy związane z identyfikacją skalującego zachowania rozkładów w metodzie momentów faktorialnych. Na prostym dwuwymiarowym modelu z symetrią konforemną ukazujemy efekt skończonych rozmiarów w połączeniu z rzutowaniem wymiarowym. Wszystkie te badania mogą służyć do sprawdzenia czułości metody skalowanych momentów faktorialnych używanej w analizie produkcji przy wysokich energiach.

# Contents

# 1. Introduction

Since few years intermittency in the phase-space distributions of produced particles is studied experimentally in the high energy collisions. Intermittency, which was discussed first in the connection with turbulence bursts in classical mechanics [1], is a manifestation of the scale-invariance of the physical process.

It was conjectured that the multiplicity fluctuations in small bins can reveal important aspects of the multiparticle production mechanism such as the intermittent pattern of fluctuations [2, 3]. Intermittency is characterized by large nonstatistical fluctuations at all scales , i.e. the SFMs $F_i$ of a studied distribution rise like $F_i(\delta y) \propto (\delta y)^{-\nu_i}$ with decreasing bin size $\delta y$ (for the definitions see sect. 2.1). Even though the underlying physical interpretation in the spirit of some multifractal structures in the multiparticle distributions is experimentally not clear, the method of the SFMs in limited rapidity intervals, proposed by Białas and Peschanski, became a powerful tool in the studies of nonstatistical fluctuations in the multiparticle production.

The two basic results of the work of Białas and Peschanski [2] were the proposition of applying SFMs in order to reduce the statistical noise and the study of the SFMs with changing resolution scale. The SFMs reduce the statistical noise which is present in the events with a finite multiplicity, and they remove it completely in the case of the Poissonian noise. Thus, this method permits to study effects of the nonstatistical, dynamical fluctuations in the probability distributions of produced particles without the bias from the statistical fluctuations.

The dependence of the SFMs on the resolution scale in rapidity, azimuthal angle, transverse momentum or any combination of these variables was proposed as a tool to search for fractal probability distributions in multiparticle production. The method of the SFMs is a beautiful method to investigate the multiparticle correlations on small scales and/or for high order correlations which otherwise would be inaccessible. The SFMs have also the advantage of selecting spikes in the particle distributions. The SFM of rank $i$ has contributions only from bins with at least $i$ particles, so higher moments are sensitive to the clusters of particles well collimated in momentum. An important tool in these studies is the $\alpha$-model of density fluctuations [4] which was introduced in the high energy phenomenology by Białas and Peschanski [2, 3]. This model was used to study the different questions of the intermittency analysis, giving predictions in agreement with the experimental results. It is also the only model which predicts consistently the relations between the SFMs of different rank.

In the present work, we shall study the intermittency phenomena in a different approach, which is based on the relation between the multiparticle distribution functions and the SFMs [5]. This approach was used extensively with non-singular parametrization of the correlations [6, 7, 8, 9]. We shall mostly assume the presence of singularities in the multiparticle distributions and study in this language the different issues of the intermittency phenomenology. These include the dimensional projection, the finite-size scaling (FSS), the regimes of strong and weak intermittency, the scaled factorial correlators (SFCs) and the relation between the two-particle distributions and the higher multiparticle distributions. In all these questions, with the exception of this last issue,

the singular multiparticle distribution is largely equivalent to the $\alpha$-model. As it was already mentioned, the $\alpha$-model is the only one that relates consistently the SFMs of different ranks. In this domain the singular (or nonsingular) multiparticle distribution approach is much less successful. A related problem is the phase-structure of the $\alpha$-model allowing for different regimes of fluctuations [10]. Of course, this very interesting problem cannot be studied in the approach presented in this work.

The nonstatistical fluctuations in ultrarelativistic nuclear collisions deserve in our opinion special attention. We argue that it is a nonlinear effect, which cannot be accounted for by the simple nucleon-nucleon superposition models and may have strong implication on our understanding of the collision dynamics. The presence of spatiotemporal intermittency in the interaction region could explain the essential features of the experimentally observed intermittency patterns (impact parameter and projectile dependence). Assuming that the onset of the spatiotemporal intermittency is due to the higher order phase-transition [11], the detailed calculations with the inclusion of the non-ideal inside-outside dynamics and the resonance decay are presented. Also the behaviour of the fluctuations during the hydrodynamical evolution of the colliding system and the implication of the fractal structures in space-time for Bose - Einstein (B-E) correlations are studied.

Another domain where the study of the SFMs was performed are the fluctuations in the critical Ising systems [12, 13]. We analyze in a similar way the SFMs behaviour for two simple CA models, finding a scaling behaviour in the SFMs for 1D (non-projected) and 2D analysis. In order to study the noncritical intermittent-like behaviour we calculate the SFMs for the distributions of the number of particles or links (nearest neighbour interactions) in the 1D lattice gas model. The intermittent-like behaviour present in this model could serve as an illustration of the difficulties in the procedures searching for some fractal source of the phenomena observed in the experimental data. The intermittency signals in the particles and links are compared and a possible influence of the clustering in hadronization on the fluctuations is also discussed. The effect of the finite size of a critical system on intermittency pattern is studied. It is shown that the correlations in a system of the infinitely long strip with a finite width exhibit different behaviour on the distances of the order of the induced effective correlation range than the correlations in the infinite system. It is difficult however to discuss the possible implications of this effect on the observation of the intermittency signal at the present stage of the experimental results.

The study of fluctuations in the density of particles produced in ultrarelativistic collisions attracted much attention from the experimental groups [14] - [33] .

To close this chapter, we list below most of the published experimental data on the intermittency analysis by the SFM method. The $e^+e^-$ annihilation was first analyzed by the TASSO Collaboration [14]. The analysis was performed in the 1D rapidity ($y$) distribution along the sphericity axis and in the 2D rapidity-azimuthal angle ($y$-$\phi$) distributions. At LEP energies, DELPHI [15], ALEPH [16] and OPAL [17] Collaborations performed the intermittency analysis in 1D or 2D distributions. The LUND model predictions were found to be consistent with the data. The CELLO Collaboration analyzed the 3D intermittency signal in $e^+e^-$ annihilation and also found a good agreement with the LUND model [18]. The 1D analysis was made also for the $\mu$-p scattering, the data could not be reproduced by the LUND and Marchesini-Webber

models [19]. Unlike in the other experiments, the authors found that a significant part of the effect could be due to the B-E correlations.

The multiparticle production in the $\nu$-nucleus interactions was analyzed, finding an intermittency signal in 1D rapidity analysis for $\nu$-Ne interactions and no intermittency for $\nu$-D interactions [20]. The intermittency in this case was interpreted as an effect of rescattering in the $\nu$-nucleus interaction.

The $\pi^+/K^+$-$p$ collisions were extensively analyzed by the NA22 Collaboration [21, 22] which calculated also the SFCs for their data [23]. In this process, neither the magnitude, nor the $p_T$-dependence of the effect are reproduced by the FRITIOF Monte-Carlo. The data of the UA1 collaboration for $p\bar{p}$ collisions at 630 GeV indicated an increase of the intermittency signal for the low multiplicity sample [24]. Again, this tendency is not reproduced by the models. The $pp$ collisions at 360 GeV were analyzed in 1D for different multiplicity samples. The Monte-Carlo generators also do not reproduce the multiplicity dependence of the fitted intermittency slopes [25]. The NA22 Collaboration performed the intermittency analysis of the particles produced in $\pi^+/K^+$-nucleus interactions [26], using the same experimental setup as for the $\pi^+/K^+$-$p$ collisions studied earlier by this group [21, 22, 23]. The results show weaker intermittency signal for larger targets.

The proton-nucleus and nucleus-nucleus collisions were first analyzed by the KLM Collaboration [27, 28] in 1D and 2D distributions. The intermittency signal decreased for larger projectiles, but this decrease was smaller than expected from the increase of the mean multiplicity in the collision. It was impossible to reproduce this nonlinear dependence on the multiplicity by the models independent collisions. The EMU01 Collaboration performed also the intermittency analysis for different nuclear projectiles and targets [29, 30] and found a similar dependence as the KLM Collaboration. Generally, the intermittency signal decreased rapidly for increasing incident energy (14.6, 60 and 200 GeV). The NA35 Collaboration analyzed the multiparticle production in the nuclear collisions also in the 3D momentum space [31]. 1D and 2D analysis of the nuclear collisions was also performed for emulsion experiments at different energies [32]. Few events from cosmic ray experiments were analyzed finding rather strong intermittency effect [33].

In summary, one can say that all processes show an increase of fluctuations with increasing resolution. However, the SFMs dependence on the bin size flattens for small bins in 1D analysis. An intermittency signal was found stronger in 2D and even stronger in 3D analysis, where no sign of flattening is seen. Recent results for the SFMs in 3D for $e^+e^-$ annihilation [34], $\mu$-$p$ [35], $\pi^+/K^+$-$p$ [36] and nucleus-nucleus collisions [31] show that the dependence of the SFM on the resolution is stronger than a power-law. Fiałkowski showed that these results could be explained if only a part of the two-particle distribution is scale-invariant [37], in contrast to the predictions of the $\alpha$-model where the whole two-particle distribution is scale-invariant [2]. The $e^+e^-$ annihilation results are consistent with the predictions of the LUND model. The hadron-hadron collisions show however a reverse dependence of the intermittency signal on the multiplicity cuts as the FRITIOF model. In the nuclear collisions, the Monte-Carlo calculations fail to reproduce the strength of the intermittency signal.

# 2. Scale-invariant multiparticle distributions

This chapter gives the essential definitions for the factorial moments and their relation to the correlation functions. The rise of the SFMs was explained by some authors using the extrapolation of the known non-singular short range correlations to very small rapidity bins [6, 7]. In this chapter we give the description of the dependence of the SFMs on the resolution scale by the *singular* multiparticle distributions in 2D or 3D space. This leads, after the dimensional projection, to similar results as in the non-singular 1D description. The description of the intermittency patterns in the language of the $n$-particle distributions is discussed in the relation to $\alpha$-model and to some experimental results.

## 2.1 Basic definitions

In this section we shall give same basic definitions of the quantities that we shall study and some relations between them. We shall assume in this work the existence of only one particle specie, which is what in most of the experiments is classified as *charged particles*. The total inelastic cross section $\sigma_I$ can be written as a sum of the cross sections $\sigma_n$ for the production of exactly $n$-particles in an event :

$$\sigma_I = \sum_{n=0}^{\infty} \sigma_n \tag{2.1}$$

Further, one can define the probabilities $P_n = \sigma_n/\sigma_I$ of observing $n$-particles in an inelastic event. From those probabilities one can construct the moments of the multiplicity distribution, the $i$-th moment is given as :

$$< n^i >= \sum_{n=1}^{\infty} n^i P_n \ , \tag{2.2}$$

or the scaled moments

$$C_i = \frac{< n^i >}{< n >^i} \ . \tag{2.3}$$

The scaled moments $C_i$ are frequently used to compare multiplicity distribution for different processes in restricted rapidity intervals or for different energies, i.e. for distributions with different $< n >$ . In particular the energy independence of $C_i$ was expected to be a consequence of the KNO scaling of the multiplicity distributions. As we shall see below the SFMs are a better tool to study the multiplicity distributions, because they are not contaminated by the statistical noise. Actually, they deconvolute the observed multiplicity distributions from the Poisson distribution, which is a natural *ansatz* for statistical noise superimposed on top of the "physical" distribution. The factorial moment is defined as :

$$< n(n-1)\ldots(n-i+1) >= \sum_{n=1}^{\infty} n(n-1)\ldots(n-i+1)P_n \ , \tag{2.4}$$

and the SFM as

$$F_i = \frac{< n(n-1)\dots(n-i+1) >}{< n >^i} . \tag{2.5}$$

Let us write the discrete multiplicity distribution $P_n$ in form of a Poisson transform (see ref. [38] for a discussion of the Poisson transform in the context of high energy phenomenology) :

$$P_n = \int_0^\infty f(x) \frac{(x\bar{n})^n e^{-x\bar{n}}}{n!} dx , \tag{2.6}$$

where $\bar{n} =< n >$ and $f(x)$ fulfils the normalization conditions :

$$\begin{aligned} \int_0^\infty f(x)dx &= 1 \\ \int_0^\infty x f(x)dx &= 1 . \end{aligned} \tag{2.7}$$

The Poisson transform means a convolution of the statistical Poissonian noise of mean $\bar{n}$ with the "physical" distribution $f(x)$. The SFMs of the discrete distribution $P_n$ are related to the moments of the function $f(x)$ :

$$F_i = \int_0^\infty x^i f(x)dx . \tag{2.8}$$

This analysis was used to study the multiplicity distributions in the full phase-space or in some restricted rapidity windows. Some bin to bin correlations and, in particular the forward-backward correlations were studied.

The studies of the multiplicity distribution cannot show the structure of the correlations between the momenta of the produced particles. In the independent particle production, the probability of producing a particle does not depend on the fact that and how many other particles are produced. If, on the contrary, some correlations are present, the production of $i$ particles enhance the probability of the production of the $(i+1)$-st particle. As a result, the multiplicity distributions are broader then the Poisson distribution. This gives us information on the global number of the particles produced, *i.e.* on the integrated correlation functions and not on the correlations between particles with definite momenta.

The information about $n$-particle correlations is contained in the $n$-particle distribution function $\rho_n(y_1,\dots,y_n)$ , where $y_i$ denotes generally the momentum vector of the $i$-th particle. This quantity denotes the probability density of observing $n$-particles with momenta $y_1,\dots,y_n$ irrespective of the number and positions of any other particles. These distribution densities are related to the $n$-particle inclusive cross sections :

$$\begin{aligned} \rho_1(y_1) &= \frac{1}{\sigma_I}\frac{d\sigma}{dy_1} , \\ \dots & \quad \dots \\ \rho_n(y_1,\dots,y_n) &= \frac{1}{\sigma_I}\frac{d^n\sigma}{dy_1\dots dy_n} . \end{aligned} \tag{2.9}$$

The integration of the $n$-particle distribution over a domain $\Omega$ of the phase-space, gives us the factorial moments of the multiplicity distribution in that domain [5] :

$$< n >_\Omega = \int_\Omega dy\ \rho_1(y)$$

$$< n(n-1)\dots(n-i+1) >_\Omega = \int_\Omega dy_1 \dots \int_\Omega dy_i \ \rho_i(y_1,\dots,y_i) \ , \qquad (2.10)$$

and correspondingly the SFM :

$$F_i = \frac{\int_\Omega dy_1 \dots \int_\Omega dy_i \ \rho_i(y_1,\dots,y_i)}{\left(\int_\Omega dy \ \rho_1(y)\right)^i} \ . \qquad (2.11)$$

If the one-particle inclusive distribution is approximately constant, *i.e.* in the "plateau" region, we can rewrite the above relation as :

$$F_i = \frac{1}{\Omega^i} \int_\Omega dy_1 \dots \int_\Omega dy_i \ d_i(y_1,\dots,y_i) \ , \qquad (2.12)$$

where the $d_i$ represents the $i$-particle reduced density :

$$d_i(y_1,\dots,y_i) = \frac{\rho_i(y_1,\dots,y_i)}{\rho_1(y_1)\dots\rho_1(y_i)} \ . \qquad (2.13)$$

The use of the reduced density is very common in phenomenological parametrizations of the $i$-particle distribution, in the cases where the one-particle distributions are assumed to factorize. Furthermore, we shall mostly assume in the model comparisons that the one-particle density is almost constant. The $n$-particle distribution can be written using the $n$-particle correlation function :

$$\rho_n(y_1,\dots,y_n) = \rho_1(y_1)\dots\rho_1(y_n) + C_n(y_1,\dots,y_n) \ , \qquad (2.14)$$

and analogously one can define the reduced correlation function :

$$c_n(y_1,\dots,y_n) = \frac{C_n(y_1,\dots,y_n)}{\rho_1(y_1)\dots\rho_1(y_n)} \ . \qquad (2.15)$$

The $n$-particle correlation function consists mainly of statistical combination of lower order correlations. In order to study genuine $n$-particle correlations, one has to define the $n$-particle cumulant $K_n(y_1,\dots,y_n)$ , which enters into the expression for $\rho_n$ together with cumulants of the order lower than $n$. The first few densities are :

$$\rho_2(y_1,y_2) = \rho_1(y_1)\rho_1(y_2) + K_2(y_1,y_2) \ , \qquad (2.16)$$

*i.e.* $K_2 = C_2$ ,

$$\begin{aligned}
\rho_3(y_1,y_2,y_3) &= \rho_1(y_1)\rho_1(y_2)\rho_1(y_3) + \sum \rho_1(y_i)K_2(y_j,y_k) + K_3(y_1,y_2,y_3) \\
\rho_4(y_1,y_2,y_3,y_4) &= \rho_1(y_1)\rho_1(y_2)\rho_1(y_3)\rho_1(y_4) + \sum \rho_1(y_i)\rho_1(y_j)K_2(y_k,y_l) \\
&\quad + \sum \rho_1(y_i)K_3(y_j,y_k,y_l) + \sum K_2(y_i,y_j)K_2(y_k,y_l) + K_4(y_1,y_2,y_3,y_4) \\
\rho_5(y_1,\dots,y_5) &= \rho_1(y_1)\rho_1(y_2)\rho_1(y_3)\rho_1(y_4)\rho_1(y_5) + \sum \rho_1(y_i)\rho_1(y_j)\rho_1(y_k)K_2(y_l,y_m) \\
&\quad + \sum \rho_1(y_i)\rho_1(y_j)K_3(y_k,y_l,y_m) + \sum \rho_1(y_i)K_2(y_j,y_k)K_2(y_l,y_m) \\
&\quad + \sum \rho_1(y_i)K_4(y_j,y_k,y_l,y_m) + \sum K_2(y_i,y_j)K_3(y_k,y_l,y_m) \\
&\quad + K_5(y_1,\dots,y_5) \ , \qquad (2.17)
\end{aligned}$$

where the sums are taken over all permutation of $\{y_1, \ldots, y_n\}$ without the transposition inside the factors of the sums.

The $n$-particle cumulant measures the statistical dependence of the whole $n$ particle set. The $n$-particle cumulant is zero, if anyone of the $n$ particles is independent of the others. Analogously, the $n$-particle reduced cumulant can be defined :

$$k_n(y_1, \ldots, y_n) = \frac{K_n(y_1, \ldots, y_n)}{\rho_1(y_1) \cdot \ldots \cdot \rho_1(y_n)} \ . \tag{2.18}$$

Białas and Peschanski proposed to look on the dependence of the SFMs on the resolution in the rapidity [2]. The idea was to study in the high energy event the structure of the particle density in rapidity. They showed that the SFMs averaged over M bins of width $\delta y$ in the total rapidity window of length $\Delta Y = M\delta y$ , correspond to the moments of the probability density in these bins :

$$\int_0^\infty dx_1 \ldots \int_0^\infty dx_M \ P(x_1, \ldots, x_M) \frac{1}{M} \left( \sum_{k=1}^{M} x_k^i \right) \sim \frac{M^{i-1} \sum_{k=1}^{M} n_k \ldots (n_k - i + 1)}{N(N-1)\ldots(N-i+1)} \ , \tag{2.19}$$

where $n_k$ is the number of particles in the bin $k$ in the event of the total multiplicity $N$ in the whole rapidity interval $\Delta Y$ . An average of the r.h.s. of the above equation over a large number of events with fixed multiplicity $N$, should converge to the l.h.s. The multiplicity distribution in different bins $P_{mul}(n_1, \ldots, n_M)$ is a convolution of the probability distribution $P$ and the multinomial distribution :

$$P_{mul}(n_1, \ldots, n_M) = \frac{N!}{n_1! \ldots n_M! M^N} \int_0^\infty dx_1 \ldots \int_0^\infty dx_M P(x_1, \ldots, x_M) x_1^{n_1} \ldots x_M^{n_M} \tag{2.20}$$

Thus, the factorial moments of the multiplicity distribution in different bins give the moments of the probability distribution $P$. The intermittent behaviour[1] is defined as a power-law dependence of the SFMs on the number of bins :

$$F_i \sim (M)^{\nu_i} = \left( \frac{\Delta Y}{\delta y} \right)^{\nu_i} \sim (\delta y)^{-\nu_i} \ , \tag{2.21}$$

where $\nu_i$ is called the intermittency exponent of rank $i$ . This analysis was applied to the JACEE event [2], confirming the observation of Takagi [39] that the rapidity density fluctuations are of a nonstatistical origin. The SFMs can also be averaged for a sample of many events. This allows to perform similar studies also in low multiplicity events such as discussed in $e^+e^-$ or hadron-hadron collisions [2, 3]. The SFM is calculated for each event in a definite bining, *i.e.* for each event the sum over all the $M$ bins is taken, and then the average over all events is taken. Generally, the events in the sample have different multiplicities so the normalization $N(N-1)\ldots(N-i+1)$ from eq. (2.19), which accounts for the Bernoulli character of the statistical fluctuations around the

[1] We shall use the name intermittency signal or intermittency patterns to describe the increase of the SFMs with the resolution, but not necessarily a power-law. We shall also call an intermittency signal a stronger one if the corresponding local slopes of the dependence of the SFM on the resolution are bigger.

studied probability $P$, is replaced by $< n >^i$, where $< n >$ is the mean multiplicity in the sample of events. This gives the horizontally averaged SFMs [3] :

$$F_i = \frac{M^{i-1}}{< n >^i} \sum_{k=1}^{M} < n_k(n_k - 1)\ldots(n_k - i + 1) > , \tag{2.22}$$

where $< \ldots >$ means an average over events. Generally, even if the particles are uncorrelated (all correlation functions $C_n = 0$) the defined above $F_i$ contains a spurious dependence on the scale due to the shape of the one-particle distribution $\rho_1(y)$ . So the horizontal SFMs should be corrected for this dependence by a factor [40] :

$$R_i = \frac{M^{i-1}}{< n >^i} \sum_{k=1}^{M} < n_k >^i \ . \tag{2.23}$$

The corrected SFMs :

$$\tilde{F}_i = \frac{F_i}{R_i} , \tag{2.24}$$

are less biased by the variations in the single-particle spectrum. Białas, Gaździcki and Ochs proposed to look at the fluctuations in a different variable [41]:

$$X(y) = \frac{\int_{y_{min}}^{y} dy' \ \rho_1(y')}{\int_{y_{min}}^{y_{max}} dy' \ \rho_1(y')} , \tag{2.25}$$

now $0 \leq X(y) \leq 1$ . This change of variables before the intermittency analysis is especially important for rapidly changing $\rho_1$, such as for the transverse momentum distribution, where this procedure was shown to better follow the true intermittent correlation than the corrected horizontal analysis. The experimental data are almost entirely analyzed using the corrected, horizontally averaged SFMs $\tilde{F}_i$ . The SFMs calculated in that way for each chosen bin width are then fitted to the intermittent relation :

$$ln(F_i) \sim a - \nu_i ln(\delta y) . \tag{2.26}$$

One can also define the vertically averaged SFMs [42] :

$$F_i = \frac{1}{M} \sum_{k=1}^{M} \frac{< n_k(n_k - 1)\ldots(n_k - i + 1) >}{< n_k >^i} . \tag{2.27}$$

This corresponds to the average of the SFMs calculated in each of the $M$ bins over all the bins. This form of averaging is equivalent to the previous one for the case of the flat one-particle distribution. However, there are till now not many experimental data on the vertical SFMs. The EMU01 data on the nuclear collisions [29] show little difference between the vertical SFMs and the corrected horizontal SFMs. From the theoretical point of view, it is particularly easy to relate the vertical SFMs to the integrals of the $n$-particle distributions :

$$F_i(\delta y) = \frac{1}{M} \sum_{k=1}^{M} \frac{\int_{y_{min}+(k-1)\delta y}^{y_{min}+k\delta y} dy_1 \ldots \int_{y_{min}+(k-1)\delta y}^{y_{min}+k\delta y} dy_i \ \rho_i(y_1, \ldots, y_i)}{(\int_{y_{min}+(k-1)\delta y}^{y_{min}+k\delta y} dy \ \rho_1(y))^i} . \tag{2.28}$$

For slowly varying $\rho_1(y)$, SFMs can be written using the reduced densities as follows :

$$F_i(\delta y) = \frac{1}{M}\sum_{k=1}^{M}\frac{1}{(\delta y)^i}\int_{y_{min}+(k-1)\delta y}^{y_{min}+k\delta y} dy_1 \ldots \int_{y_{min}+(k-1)\delta y}^{y_{min}+k\delta y} dy_i \; d_i(y_1,\ldots,y_i) \; . \qquad (2.29)$$

Generally, one assumes translational invariance of the reduced densities and consequently, of the SFMs in different bins. The reduced densities depend then only on the relative variables $y_i - y_k$, so that one has :

$$F_i(\delta y) = \frac{1}{(\delta y)^i}\int_0^{\delta y} dy_1 \ldots \int_0^{\delta y} dy_i d_i(y_1,\ldots,y_i) \; . \qquad (2.30)$$

The comparison of the horizontal SFMs to the phenomenological parametrization of the reduced density is difficult because the contribution of different bins is weighted by the single-particle distribution $\rho_1(y)$ for that bin. The vertical moments have the contribution of each bin scaled so that all of them enter on equal footing to the sum over the bins. For sufficiently small bins they are closer to the integrals of the reduced density (eq. 2.30) than the horizontal moments even if the one-particle distribution is not flat. One expects to have simple and approximately translationally invariant parametrization for the reduced densities, which can be used in the expression (2.30). In the next sections we shall extensively use this relation between the SFMs and the reduced densities.

Till now, there are no experimental data on the dependence of the SFMs in small bins on the position of the bin. Due to large experimental errors all results for the SFMs in small bins are averaged over the whole rapidity window $\Delta Y$ . There is some experimental evidence for the dependence of the bin averaged SFMs on the position of the rapidity window used in the analysis. Thus, one observes some change in the results for the corrected horizontal SFM, depending on whether the target and projectile fragmentations region are included into the analysis [19]. However, it is difficult to draw definite conclusions from the horizontal SFMs, which are dominated by the contributions from bins in the central region, where the single-particle density is maximal. It would be interesting to make the analysis using vertical SFMs in different windows, which would give information on the correlations in the different regions of the phase-space. Another indirect evidence for the lack of the translational invariance is provided by the SFCs (eq. 2.32) which are not symmetric :

$$F_{i,j} \neq F_{j,i} \; , \qquad (2.31)$$

for $i \neq j$ in the asymmetric $\pi^+/K^+$-$p$ collisions [23]. This shows that in this case the fluctuations are different in the target fragmentation region and in the projectile fragmentation region.

The SFM in a rapidity window $\delta y$ is equivalent to the $n$-particle distribution function integrated from the scale 0 to $\delta y$ (eq. 2.30). Thus, $F_i(\delta y)$ has contributions from the $i$-particle distribution on all this range of scales in rapidity. This makes difficult to disentangle the true scaling behaviour of the multiparticle distributions in a certain range of rapidity separations from other effects, which could be present at the limiting scales. This concerns especially the behaviour of the $n$-particle distribution for particle separation going to 0. The presence of some limit on the scaling behaviour

in this region, can change dramatically the dependence of the integrated $n$-particle distribution on the upper integration limit $\delta y$ (see [43, 44] and sects. 2.3, 4.2). On the other hand, the limit $\delta y \to 0$ tests only a limited part of the $i$-particle phase-space ($\mid y_i - y_k \mid < \delta y \to 0$). To cure this disadvantage of the SFMs Białas and Peschanski proposed to study the SFCs, which are the observables relating the fluctuations in separated bins [3]. The SFC $F_{i,j}$ for two bins of width $\delta y$ separated by the distance $D$ is defined as :

$$F_{i,j}(\delta y, D) = \frac{< n_1(n_1-1)\dots(n_1-i+1)n_2(n_2-1)\dots(n_2-j+1) >}{< n_1(n_1-1)\dots(n_1-i+1) >< n_2(n_2-1)\dots(n_2-j+1) >} , \quad (2.32)$$

where $n_{1(2)}$ is the number of particles in the first (second) bin. The so defined SFC is then averaged over all the pairs of bins distant by $D$ in the rapidity window $\Delta Y$, what corresponds to the vertical averaging. In was shown in the $\alpha$-model that the SFCs are independent of the bin size $\delta y$ and exhibit a power-law dependence on the bin distance D :

$$F_{i,j} \sim (D)^{-\nu_{i,j}} . \quad (2.33)$$

$\nu_{i,j}$ in the above expression is called the intermittency exponent of the SFC $F_{i,j}$ . The SFCs can also be directly related to the integrals of the $(i+j)$-particle distribution function :

$$\begin{aligned} F_{i,j}(\delta y, D) = \frac{1}{M}\sum_{k=1}^{M} & \int_{y_{min}+(k-1)\delta y}^{y_{min}+k\delta y} dy_1 \dots \int_{y_{min}+(k-1)\delta y}^{y_{min}+k\delta y} dy_i \\ & \int_{y_{min}+D+(k-1)\delta y}^{y_{min}+D+k\delta y} dy_{i+1} \dots \int_{y_{min}+D+(k-1)\delta y}^{y_{min}+D+k\delta y} dy_{i+j}\ \rho_{i+j}(y_1,\dots,y_{i+j}) \ / \\ & \left( \int_{y_{min}+(k-1)\delta y}^{y_{min}+k\delta y} dy_1 \dots \int_{y_{min}+(k-1)\delta y}^{y_{min}+k\delta y} dy_i\ \rho_i(y_1,\dots,y_i) \right. \\ & \left. \int_{y_{min}+D+(k-1)\delta y}^{y_{min}+D+k\delta y} dy_1 \dots \int_{y_{min}+D+(k-1)\delta y}^{y_{min}+D+k\delta y} dy_j\ \rho_j(y_1,\dots,y_j) \right) , \end{aligned} \quad (2.34)$$

where $M = (\Delta Y - D)/\delta y$ is the number of the bin pairs in the rapidity window $[y_{min}, y_{min} + \Delta Y]$ . For slowly varing single-particle density, the SFCs can be approximated by simple integrals of the $(i+j)$-particle reduced distributions. This form will be used in the further investigations. Moments similar to the SFCs have also been proposed by Seibert and Voloshin [45]. They proposed the split-bin correlators, *i.e.* the bin of width $\delta y$ is divided in two parts and the correlations in the left and right part of the bin are calculated :

$$F_2^{(SB)} = \frac{1}{M}\sum_{k=1}^{M} \frac{< n_L n_R >}{< N_L N_R >} . \quad (2.35)$$

This definition corresponds to the SFC $F_{1,1}$ for the case $\delta y = D$. Due to the approximative independence of the SFCs on the bin width $\delta y$ both in the $\alpha$-model [3] and in the experiment [23], SFCs and the split-bin correlators are largely equivalent. The split-bin moments have also the advantage that they allow the analysis of the fluctuations in continuum observables such as the transverse energy in certain subdomains

of the rapidity and/or azimuthal angle. Dealing with the small scale correlations in the case of a thermodynamic model, Haglin and Seibert [46] made an interesting observation of the difference in the results for the SFMs and the split-bin moments. The split-bin correlation are sensitive to the scale on which they are calculated and are not contaminated at all the scales by the zero scale behaviour. This could be important if the experimental data are contaminated by some double track counting, which introduces spurious correlations at the scale of the resolution of the detectors. The analysis by the split-bin moments or the SFCs could disentangle these spurious correlations from other nontrivial correlation at other scales.

The SFCs and SFMs are all related to the $n$-particle distribution function and so there exist relations between them [47]. These relations are true for any type of translationally invariant distributions. In the case of self-similar distributions, one obtains relations also between the intermittency exponents of the SFMs and SFCs :

$$\nu_{i,j} = \nu_{i+j} - \nu_i - \nu_j \ . \tag{2.36}$$

The $n$-particle distribution is the sum of the trivial product of the single-particle distributions and of the $n$-particle correlation functions. Generally, one studies the behaviour of the SFMs which tests the whole $n$-particle distribution function. Self-similar behaviour in this variable is expected in the $\alpha$-model, but in the experimental data it is not yet clear whether the self-similar behaviour is present in the SFMs or in the scaled factorial cumulants. The scaled factorial cumulants have the advantage of testing the genuine $n$-particle correlations, and so it is always interesting to test their contribution to the higher order correlation for each process. The indirect analysis of the factorial cumulants for the KLM data [9] leads to the conclusion that the three or more particles cumulants are zero. The self-similar parametrization in the $n$-particle distribution or in the $n$-particle correlations can both reproduce the data after the dimensional projection [48, 49] (see sects. 2.3 and 2.4). Probably more data on 3D SFMs and scaled factorial cumulants would help to select the better of these two parametrizations. In sect. 2.4, it will be assumed that a singular aggregation function is present in 3D, leading to a structure involving nonsingular terms and singularities of different exponents in the $n$-particle distribution. In the remaining parts of the work we shall assume that the self-similarity is present in the $n$-particle densities. In the chapter 3, the discussion will be confined to the second SFM, leaving apart the problem of the presence of any higher order cumulants [8, 9].

## 2.2 The dimensional projection

It was observed by Ochs and Wosiek that the 2D intermittency analysis in rapidity and azimuthal angle gives a stronger intermittency signal than the 1D analysis in the rapidity alone [50]. This was interpreted as an effect of the pencil-jet structure in the branching model studied in [50]. Later Ochs showed that the effect is quite general and it is expected that the 1D projected distributions have no longer scale-invariant fluctuations, even though the system possess such a structure in its full-dimensional version [51]. He studied in particular the dimensional projection in the $\alpha$-model. Similar studies have been performed by Bialas and Seixas for a phenomenological model of

singular multiparticle distributions in 3D momentum space [48]. They have observed that the effect of the dimensional projection depends on the range of the transverse momentum, over which one averages the fluctuations. The discussion of the importance of the factorization properties of the 2D multiparticle distributions was made in ref. [52]. The effect of the dimensional projection in space-time was studied in the model of phase-transition for the nuclear collisions. There the strength of the effect was linked with the transverse size of the interaction region [52]. The dependence of the attenuation of the intermittency signal on the transverse size of the system or on the transverse momentum cuts can be studied quantitatively [53].

Our discussion will concentrate on the second SFM, for which it is particularly easy to relate its behaviour with the singular structures of the two-particle density $\rho_2(\vec{r_1},\vec{r_2})$. For slowly varying $\rho_1(\vec{r})$, i.e. in the "plateau" region, one gets for the second SFM (eq. 2.12) :

$$F_2^{(n)}(\delta\Omega) = \frac{1}{\Omega\ \delta\Omega}\sum_{i=1}^{M^n}\int_{\Omega_i} d\vec{r_1}\int_{\Omega_i} d\vec{r_2}\ d_2(\vec{r_1},\vec{r_2})\ , \tag{2.37}$$

where the $n$ - dimensional volume $\Omega$ is divided in $M^n$ cubes $\Omega_i$ of volume $\delta\Omega$ . The intermittent fluctuations in the density distribution should be observed as a power law behaviour of the factorial moment :

$$F_2^{(n)}(\delta\Omega) \sim (\delta\Omega)^{-\nu_2}\ . \tag{2.38}$$

This type of behaviour for small cubes $\delta\Omega$ is equivalent to the existence of singularity in the reduced density $d_2$ . In the following we shall assume , that this singularity is dominating and hence, in the calculation of $F_2^{(n)}$ we shall omit all non-singular terms in $d_2$ . This corresponds to the power-law behaviour of the SFM and not of the scaled factorial cumulant. Below, we consider translationally invariant densities with two different parametrizations of the singularity. The factorized parametrization :

$$d_2^{(fac)}(x_1,\vec{X}_1,x_2,\vec{X}_2) = \frac{C_2}{\mid x_1 - x_2 \mid^{\nu_2}\ \mid \vec{X}_1 - \vec{X}_2 \mid^{(n-1)\nu_2}}\ , \tag{2.39}$$

where $\vec{r_i} \equiv [x_i,\vec{X}_i]$ , and the isotropic parametrization :

$$d_2^{(iso)}(\vec{r_1},\vec{r_2}) = \frac{C_2}{\mid \vec{r_1} - \vec{r_2} \mid^{n\nu_2}}\ . \tag{2.40}$$

Results do not change if one rescales one of the components of $\vec{r}$ in (2.40), allowing in this way for non-isotropic shapes of $d_2$ . In this case, by a suitable coordinate transformation which changes only the integration domain $\Omega$, one can bring the singularity back to the isotropic form (2.40). This latter modification is negligible for small bins, and hence the behaviour of the factorial moments is similar in these two cases. Thus, it does not change the qualitative behaviour of the SFM for the projected distributions, i.e. the flattening of the SFMs for small bins in rapidity. The variation of the integration region $\Omega$ changes, however the resulting "effective slope" in the 1D intermittency analysis (sects. 3.2 and 4.3) and can be analyzed by the FSS method [53].

Both factorized $d_2^{(fac)}$ and isotropic $d_2^{(iso)}$ types of singularities give a power law behaviour for $F_2^{(n)}$ with the exponent $\nu_2$ . However, they have a different behaviour in

the $(n-1)$-dimensional subspace $\vec{X}$ . The $(n-1)$-dimensional SFM can be obtained from the density $d_2$ by integrating over $x_i$ :

$$F_2^{(n-1)}(\delta\omega) = \frac{1}{\Omega\ \delta\omega} \sum_{i=1}^{M^{n-1}} \int_{\Delta x} dx_1 \int_{\Delta x} dx_2 \int_{\omega_i} d\vec{X}_1 \int_{\omega_i} d\vec{X}_2\ d_2(x_1, \vec{X}_1; x_2, \vec{X}_2) \ . \quad (2.41)$$

The factorized singularity $d_2^{(fac)}$ (eq. 2.39) gives a power law dependence also in $(n-1)$-dimensions :

$$F_2^{(n-1)}(\delta\omega) \sim A'(\delta\omega)^{\nu_2} \ . \quad (2.42)$$

On the contrary, the reduced isotropic density has no more a singularity in $\vec{X}$ variables and, consequently, it does not show a power law behaviour of the SFM. In particular, in the case $n = 2$ such as for the $(y\text{-}\phi)$-distribution, the 1D SFM in the limit $\delta X \to 0$ can be written as :

$$F_2^{(1)}(\delta X) = (\delta X)^{-1} \int_0^{\delta X} dX d_2(X) \ , \quad (2.43)$$

where $d_2(X) \equiv \int_{\Delta x} dx_1 \int_{\Delta x} dx_2\ d_2(x_1, x_2, X)$ and $X \equiv X_1 - X_2$ . The intermittency exponent at the scale $\delta X$ is given by :

$$\nu_2(\delta X) = -\frac{d\ ln F_2^{(1)}(\delta X)}{d\ ln \delta X} \ . \quad (2.44)$$

After a substitution of (2.43) into eq. (2.44) one obtains :

$$\nu_2(\delta X) = \frac{\delta X\ d_2(\delta X)}{\int_0^{\delta X} dX\ d_2(X)} - 1 \ . \quad (2.45)$$

For $\delta X \to 0$ , the intermittency exponent $\nu_2(\delta X)$ tends to zero if the density $d_2(X)$ has no singularity at $X = 0$ . Using the similar arguments as above, one can argue that for finite bins $\delta X$ one should observe a flattening of the SFM. As an example of such a behaviour we show in Fig. 2.1 the dependence of the 1D SFM $F_2^{(1)}$ on the rapidity resolution $\delta y$ for the singular density $d_2^{(iso)}(\vec{r}_1, \vec{r}_2)$ ( $\vec{r}_i \equiv [y_i, \phi_i]$ , $i = 1,2$ ) and also in the case when the scale-invariant correlations have a finite value of the correlation range :

$$d_2(\vec{r}_1, \vec{r}_2) = \begin{cases} C_2\ (\Delta R)^{-\nu_2} \ , & \text{for } \Delta R < R_{corr} \\ C_2\ (R_{corr})^{-\nu_2} \ , & \text{for } \Delta R \geq R_{corr} \end{cases} \quad (2.46)$$

where $\Delta R \equiv \ | \vec{r}_1 - \vec{r}_2 \ |$ . The 1D factorial moments shown in Fig. 2.1, have been calculated for the singular 2D reduced density (2.46) with $\nu_2 = 0.153$ . This value of the singularity exponent corresponds to the observed slope of $F_2^{(2)}$ in $(y-\phi)$ bins in the $e^+\ e^-$ annihilation process [14] . The 1D moments show no power law behaviour. Moreover, the behaviour of $F_2^{(1)}(\delta y)$ depends not only on the singularity but also on the cut-off parameter even for small rapidity bins. A similar type of behaviour in small rapidity bins can be obtained from the non-singular reduced density [54] :

$$d_2(y_1 - y_2) = 1 + \gamma\ exp(-\ | y_1 - y_2 \ | /\xi) \ . \quad (2.47)$$

An even stronger effect of the dimensional projection is observed when projecting a 3D singular density. In this case the flattening of the 1D SFM is stronger and the

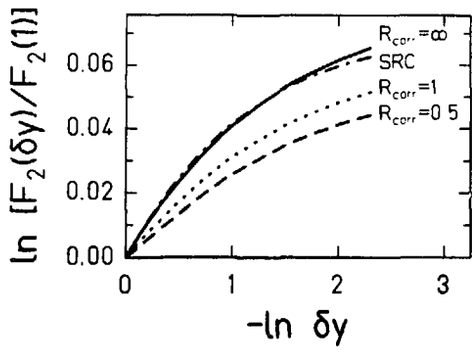


Figure 2.1: The dependence of the second SFM $F_2$ on the size of the rapidity bin $\delta y$ , as obtained from eq. (2.41) with $n = 2$ for three different values of the correlation range $R_{corr}$ . The dashed-dotted line represents the results obtained using the non-singular, short range correlation ansatz for the reduced density (2.47) with the parameters $\gamma = 0.25$ and $\xi = 1.1$ . All the curves are normalized at $\delta y = 1$.

"effective" slopes are smaller than the ones resulting from a 2D to 1D projection. An example of this double projection is given in sect. 2.4, where such a singular 3D correlation function projected on rapidity is used to describe the $e^+e^-$ annihilation data of the DELPHI Collaboration [15]. Recent experimental results confirm that the strongest intermittency exists in the 3D analysis, and that the intermittent signal decreases with the number of the effective projections of the multiparticle distribution [18, 31, 28]. This could be taken as an evidence for the non-factorized type of singularity in the reduced density. A similar behaviour of the correlation function has been found in the proton - emulsion data [55] : the hadron pairs with small pseudorapidity separation $| \Delta\eta | < 0.2$ are correlated in the azimuthal angle, and hence $(\eta - \phi)$ - correlations do not factorize.

The discussion of different behaviour of the $\alpha$—model in different regimes was performed by Brax and Peschanski [56]. They found that the three phases of the $\alpha$—model behave differently in the dimensional projection. One of such phases could explain the appearance of anomalous events such as seen by the NA22 Collaboration [57] and another one the jet structure observed in the $e^+e^-$ annihilation. In the language of distribution functions, all these regimes should have different parametrization in 2D.

The dimensional projection from different transverse sizes, discussed in relation to the nuclear collision geometry (sect. 3.2) and to the finite size effect in a critical system (sect. 4.3), could be the dominant effect in the observed dependence of the intermittency signal on the $p_T$-cut [22], as proposed by Białas and Seixas [48]. This would mean that the intermittency effect is not due to hard processes, since it is present and even stronger in low $p_T$ samples. Below we investigate the observable evidences of this effect, which moreover allow to extract the intermittency exponents from the analysis of the projected 1D data [53].

Let us write the SFMs as integrals of the multiparticle reduced distribution func-

tions :

$$F_i(\delta y) = \frac{1}{(\delta y)^i (\Delta L)^{n\,i}} \int_{-\Delta L/2}^{\Delta L/2} \dots \int_{-\Delta L/2}^{\Delta L/2} d^n \vec{P}_1 \dots \int_{-\Delta L/2}^{\Delta L/2} \dots \int_{-\Delta L/2}^{\Delta L/2} d^n \vec{P}_i$$
$$\int_0^{\delta y} dy_1 \dots \int_0^{\delta y} dy_i \; d_i(\vec{P}_1, y_1, \dots, \vec{P}_i, y_i) \; , \tag{2.48}$$

where $\Delta L$ is the size of the transverse dimension over which the integration takes place. $\Delta L$ should be regarded as an effective transverse size in momentum after the change of variables, so that the integration limits over the transverse momentum $\int_0^\infty p_t dp_t$ are finite [41]. We keep explicitely the number of transverse dimensions $n$, because as we will see the results do not depend on it. The $i$-particle scale-invariant distribution function :

$$d_i(\lambda \vec{P}_1, \lambda y_1, \dots, \lambda \vec{P}_i, \lambda y_i) = \lambda^{-\nu_i} d_i(\vec{P}_1, y_1, \dots, \vec{P}_i, y_i) \tag{2.49}$$

gives rise to the power-law behaviour of the SFMs in the "full" $(n+1)$-dimensional analysis (eq. 2.38).

The SFMs from the 1D analysis (eq. 2.48) have no longer a power-law behaviour as a function of the bin size $\delta y$ . Nevertheless, they exhibit interesting scaling which can be observed experimentally. Let us consider $F_i(\delta y; \lambda \Delta L)$ calculated from the $i$-particle distribution after the projection over the $n$ transverse dimensions, but with a different size $\lambda \Delta L$ of the allowed values of the transverse variables. Such a change in the range of transverse variables can be achieved by imposing cuts in the transverse momentum or biases on the centrality of the event. Indeed, as predicted by Białas and Seixas [48], the intermittency signal was found to be sensitive to the cuts in the transverse momentum [21]. Generally, the intermittency signal is weaker and the effective slopes are smaller for larger allowed range of transverse momenta. By a change of variables, the SFM in a system of the transverse size $\lambda \Delta L$ can be related to the SFM of the system of size $\Delta L$ :

$$\begin{aligned}
F_i(\delta y; \lambda\, \Delta L) &= \frac{1}{(\delta y)^i (\lambda \Delta L)^{n\,i}} \int_0^{\lambda \Delta L} \dots \int_0^{\lambda \Delta L} d^n \vec{P}_1 \dots \int_0^{\lambda \Delta L} \dots \int_0^{\lambda \Delta L} d^n \vec{P}_i \\
&\quad \int_0^{\delta y} dy_1 \dots \int_0^{\delta y} dy_i \; d_i(\vec{P}_1, y_1, \dots, \vec{P}_i, y_i) \\
&= \frac{1}{(\delta y)^i (\lambda \Delta L)^{n\,i}} \int_0^{\Delta L} \dots \int_0^{\Delta L} d^n \lambda \vec{P}_1 \dots \int_0^{\Delta L} \dots \int_0^{\Delta L} d^n \lambda \vec{P}_i \\
&\quad \int_0^{\delta y/\lambda} dy_1 \dots \int_0^{\delta y/\lambda} dy_i \; d_i(\lambda \vec{P}_1, \lambda y_1, \dots, \lambda \vec{P}_i, \lambda y_i) \\
&= \frac{\lambda^{-\nu_i}}{(\delta y)^i (\Delta L)^{n\,i}} \int_0^{\Delta L} \dots \int_0^{\Delta L} d^n \vec{P}_1 \dots \int_0^{\Delta L} \dots \int_0^{\Delta L} d^n \vec{P}_i \\
&\quad \int_0^{\delta y/\lambda} dy_1 \dots \int_0^{\delta y/\lambda} dy_i \; d_i(\vec{P}_1, y_1, \dots, \vec{P}_i, y_i) \\
&= \lambda^{-\nu_i} F_i(\delta y/\lambda; \Delta L) \; .
\end{aligned} \tag{2.50}$$

In the above expression we have used the scale-invariance of the distribution function (2.49) to relate the densities in the scaled variables. The above relation is similar to the FSS relations in the critical systems [58] :

$$G(x, L) = L^{-\nu} G(x/L^{\mu}) \; . \tag{2.51}$$

This analogy allows to treat the experimental data obtained for different effective sizes of the transverse variables by the methods of the statistical physics.

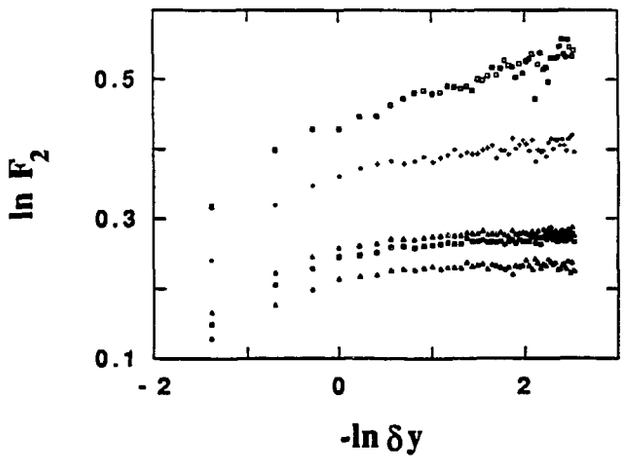


Figure 2.2: The experimental data for the SFMs $F_2$ of the NA22 Collaboration, before FSS analysis. Different data sets correspond to different cuts in transverse momentum : $p_T \leq 0.15$ GeV (the empty boxes), $p_T \leq 0.30$ GeV (the crosses), all $p_T$ (the empty triangles), $p_T \geq 0.15$ GeV (the full boxes) and $p_T \geq 0.30$ GeV (the full triangles). The experimental errors are not shown on the figures for clarity.

We illustrate the method using the NA22 data for $\pi^+/K^+$-$p$ collisions at 250 GeV [21]. The SFMs are calculated for five different cuts in transverse momentum of the produced particles. The NA22 results for $F_2$ are shown in Fig. 2.2 and one can see that the SFMs have different magnitudes and local slopes. The scaling hypothesis means that by a shift of the origin of the curves, one can superimpose them on top of each other with the shifts in the horizontal and vertical directions equal to $-\ln\lambda$ and $-\nu_i \ln\lambda$ respectively. As a result, the two shifts should be proportional with the same proportionality factor $\nu_i$ for different data sets. The result of applying this procedure to the NA22 data is shown in Figs. 2.3a-c for $F_2$, $F_3$ and $F_4$ respectively .

As it is shown in Fig. 2.3a , the procedure works well for all NA22 data except for the set with $p_T \leq 0.15$ GeV (the open boxes). The values of the shifts for different data sets are shown in the Table 2.1. The shifts in the vertical and horizontal directions follow closely the linear relation confirming the existence of scaling with the exponent $\nu_2 \simeq 0.3$ .

The data set with $p_T \leq 0.15$ GeV does not lie on the same universal curve as the other data. In Fig. 2.3a we plot this data set using the linear relation between the horizontal and vertical shifts with the exponent $\nu_2 = 0.3$ . Shifting of this curve to the region of the universal curve with a comparable local slope can be achieved by taking $\ln\lambda \sim -1.5$ and $\nu_2 \sim 0.1$ . This strong difference of parameters could mean that the two-particle distribution function has a different behaviour for small $p_T$ with, perhaps, a different scaling index.

For $F_3$ and $F_4$ in Figs. 2.3b-c we have taken the same value of $\ln\lambda$ as for the moment $F_2$. This is consistent with the idea, that different moments of the same data

| Data set | Horizontal shift $(-\ln\lambda)$ | Vertical shift $(-\nu_2 \ln\lambda)$ |
|---|---|---|
| $p_T \leq 0.15$ GeV | -0.4 | -0.12 |
| $p_T \leq 0.30$ GeV | 0 | 0 |
| all $p_T$ | 0.4 | 0.12 |
| $p_T \geq 0.15$ GeV | 0.5 | 0.14 |
| $p_T \geq 0.30$ GeV | 0.6 | 0.17 |

Table 2.1: The horizontal and vertical shifts of the FSS analysis for the different data sets of the NA22 Collaboration

set should be described with the same effective transverse size. We have found that if $\nu_2$ is taken from the shift of $F_2$ for the same data set (see the Table 2.1) then the NA22 data is consistent with the quadratic relation $\nu_i = \frac{i(i-1)}{2}\nu_2$ between scaling indices and the third and fourth factorial moments $F_3$, $F_4$ show the finite size scaling. One may conclude from these fits that the multiparticle production in hadronic collisions shows intermittent behaviour in higher dimensional phase-space and, after the dimensional projection, the resulting SFMs show FSS. The FSS analysis allows to find the true intermittency indices for the respective moments. These indices are approximately equal 0.3 , 0.9 and 1.2 for the second, third and fourth SFMs, *i.e.* they correspond to the quadratic dependence on the rank of the moment as expected for random gaussian multiplicative processes.

The procedure gives also the relations between the transverse scales corresponding to different data sets. This transverse size is not directly related to the $p_T$-cuts for two reasons. Firstly, due to the strong dependence of the one-particle distribution on the transverse momentum, we are using the effective transverse variables [41]. Secondly, the different shapes of the integration region for various conditions imposed on the data ( e.g. $p_T \geq p_{cut}$ or $p_T \leq p_{cut}$ ) impose a different definition of the transverse "effective size" for the data set. It is obvious from the definition of the projected distributions that a good estimate of the transverse size could be the mean two-point distance in the data set :

$$\Delta L = \frac{\int_{\delta\Upsilon} d^n\vec{P}_1 \int_{\delta\Upsilon} d^n\vec{P}_2 \; |\vec{P}_1 - \vec{P}_2|}{(\delta\Upsilon)^2 \int_0^1 \ldots \int_0^1 d^n\vec{P}_1 \int_0^1 \ldots \int_0^1 d^n\vec{P}_2 \; |\vec{P}_1 - \vec{P}_2|} , \qquad (2.52)$$

where $\delta\Upsilon$ is the transverse integration region imposed by the given cut (we are working in the variables where the one-particle distribution is flat). Then, one can rewrite the averaging over the transverse domain $\delta\Upsilon$ as an integration over the $n$-dimensional cube of size $L$ (eq. 2.48), for which the size rescaling can be performed. This definition of the transverse size of the data set is different from the estimate $\delta\Upsilon$ and in fact gives different behaviour. The SFMs for the data set "all $p_T$" (the empty triangles in Fig. 2.2) lie above and have larger slopes than for the data sets "$p_T \leq p_{cut}$" , in spite of the

fact that its naive size measured by the corresponding cross section is larger. Moreover, it also contradicts the widely discussed $\frac{1}{dN/dy}$ scaling [59, 7, 60, 61].

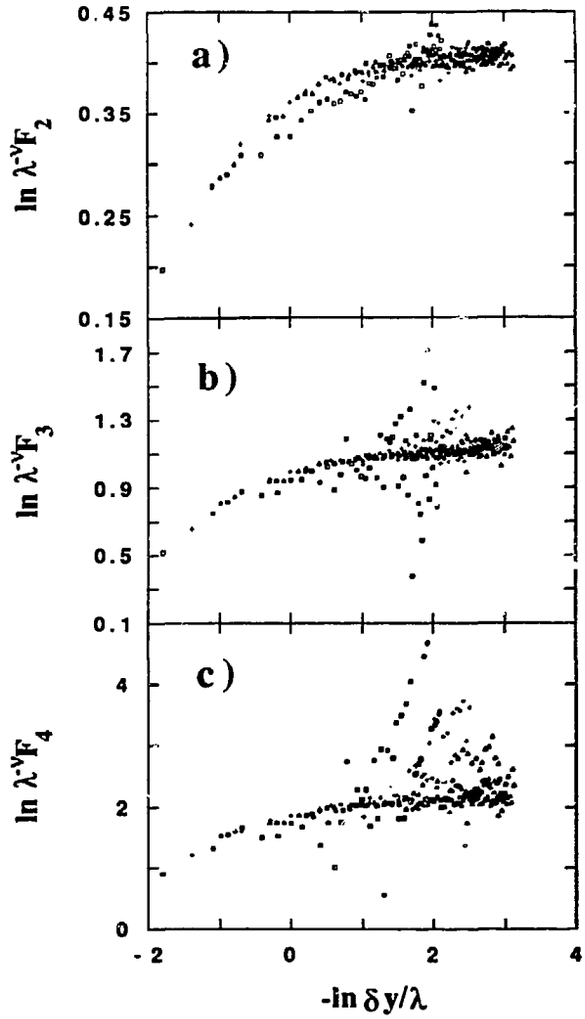


Figure 2.3: The SFMs of the N..22 Collaboration, after the FSS analysis, *i.e.* after rescaling of $\delta y$ and $F_i$. In parts a) , b) and c) are shown the SFMs $F_2$, $F_3$ and $F_4$ respectively. The results are depicted using the same symbols as in Fig. 2.2 .

The whole discussion is important because in fact one does not know what are the transverse dimensions and what is the shape of the regions of averaging corresponding to different $p_T$-cuts. All the above reasoning is exactly the same if as the transverse variables we take not the transverse momentum but some other variable. As inspired from the Reggeon field theory, the scaling may not be present in the 3D momentum space but in the rapidity-impact parameter space [62]. In that case the correspondence between cutting parameters for different data sets and the shape and size of the transverse integration region is not known. Consequently, the finite size scaling is the

only way to analyze the underlying multiparticle scaling distributions, since one has no access experimentally to the impact parameter corresponding to the produced particle. Finally, we observe that the similar analysis can be done for the 2D data, the only assumption needed is the scaling of the multiparticle distributions (eq. 2.49). This feature is not conserved in a nonlinear change of variables, so one must be careful in extracting the relevant variables. It is generally assumed that such a scaling can be expected in the rapidity and transverse momentum or impact parameter variables as discussed here.

The SFCs are related to the SFMs by appropriate sum rules [47, 63]. Therefore, introducing in these sum rules the universal scaling functions (eq. 2.50) found for the SFMs, gives directly the corresponding scaling functions of the SFCs. The SFCs would then obey a similar FSS with those scaling functions.

To conclude this discussion, we would like to stress once more that the FSS analysis of the $\pi^+/K^+$-$p$ data of the NA22 Collaboration confirms the existence of scaling in the multiparticle distributions. This analysis gives the access to intermittency indices. The recent preliminary NA22 data on SFMs in 3D momentum space indicate, that the full phase-space multiparticle distribution is not scale-invariant [36]. This means that the observed FSS in 1D distributions is not due to the projection from the 3D momentum space. The FSS in the rapidity distributions could be a signal of some scaling behaviour taking place in a space inaccessible for direct experimental studies as in the Reggeon field theory scenario [62] or in the model of spatiotemporal intermittency for nuclear collisions [52, 64]. If this is true, then the method of FSS is the only way of the deconvolution of the dimensional projection effect. It would be interesting to perform the same analysis for other reactions. This should consist of creating different data sets by using cuts in multiplicity or, better, in transverse momentum and doing the above described FSS analysis. Although we have not performed the FSS analysis for other reactions, some qualitative features of other data allow to conclude that the FSS is not fulfilled in the $e^+e^-$ anihilation and in the nuclear reactions. The FSS implies that a relation exists between the magnitude and the slope of the 1D SFM for a given data set. Generally, for lower local slopes one obtains lower values of the SFMs. This qualitative feature is not present in the $e^+e^-$ anihilation data of the DELPHI Collaboration [34] and in the nuclear collisions [30]. For the case of the $e^+e^-$ collision this could mean that the multiparticle distributions do not have a simple, translationaly invariant parametrization (2.49) and the SFMs behave very differently for different $p_T$-cuts. On the other hand, the multiparticle correlations in the nuclear collisions have many different sources and the strongly restrictive form of the multiparticle distributions (2.49) could be wrong. In particular, one expects the nonsingular components destroying the FSS to be present. It would be interesting to compare the results of the FSS scaling here presented to other hadron-hadron collisions. If this feature of the SFM is confirmed in other hadron-hadron reaction, it could mean that the fluctuations in hadron-hadron collisions have a very special structure, perhaps also with specific relevant variables (rapidity-impact parameter).

## 2.3 The singular multiparticle distribution function and the $\alpha$-model

The $\alpha$-model of a multiplicative cascade was proposed as a general scheme explaining intermittent fluctuations in the multiparticle production in both elementary particle and nuclear collisions [2, 3]. This model gives intermittency exponents for the SFMs and the SFCs [2, 3, 65]. Also the experimental data on the intermittency slopes can be described by this simple model. However, the dimensionality of the intermittency analysis was found to be important for the strength of the intermittency signal if the non-factorizable, self-similar correlations are present in the 2D or 3D phase-space [51, 48, 52]. Another phenomenological description of the data was proposed using singular multiparticle reduced distributions in 1D [48, 52] (sect. 2.2). The phenomenological, singular parametrization of the correlation functions gives, similarly as in the $\alpha$-model, a power-law behaviour of the SFMs [48, 52] (sect. 2.2).

In this section we study a relation between descriptions using either the singular distribution function or the $\alpha$-model and, in particular, we study the implications of the dimensional projection and a regularization of the singularity [44]. We shall also compare the results of these two approaches for the SFCs in 1D and 2D.

In a framework of the $\alpha$-model the distinction is made between the case of the strong and weak intermittency [65, 43]. Let us consider the $\alpha$-model with the branching number $\lambda$ and a certain probability distribution function $P(w)$ of the random multiplicative factors [2]. The case of the weak intermittency corresponds to probability distributions satisfying :

$$< w^i > < i - 1 . \tag{2.53}$$

In this case, the self-similar cascade can be infinite and the total multiplicity has a limit distribution [65]. If the condition (2.53) is not satisfied, then the cascade must be finite. For the rapidity intervals of length $\delta y \gg l$ , where $l$ is the limiting minimal scale of the cascade, one obtains the following behaviour of the SFMs :

$$F_i \sim (\delta y)^{1-i} , \tag{2.54}$$

i.e., the intermittency exponents are now $\nu_i = i - 1$ .

In the parametrization using the singular distribution function, the SFMs are related to the integrals of the reduced distribution functions (eq. 2.30). We have seen that the singular scale-invariant distribution function :

$$d_i(\lambda y_1, \ldots, \lambda y_i) = \lambda^{-\nu_i} d_i(y_1, \ldots, y_i) \tag{2.55}$$

gives rise to the intermittent behaviour of the SFM :

$$F_i \sim (\delta y)^{-\nu_i} . \tag{2.56}$$

However, this is correct only if the integral in eq. (2.30) exists. This gives bounds on the values of the intermittency exponents $\nu_i$ . Let us consider the case when all the $n$-particle distributions have the form :

$$d_i(y_1, \ldots, y_i) \sim \{ \prod_{(m)} \mid y_k - y_l \mid^{-\nu} \}_{sym} , \tag{2.57}$$

where the number $m$ of the pairs $\mid y_k - y_l \mid$ is at least $i-1$ and at most $i(i-1)/2$, and the whole expression is symmetrized over the permutations of $\{y_1, \ldots, y_i\}$. If the integral in eq. (2.30) exists, then the SFM has an intermittent behaviour with the intermittency exponent $\nu_i = m\nu$. For the above written distribution functions, the integral (2.30) exists if the intermittency exponents satisfy :

$$\nu_i < i - 1 \,. \tag{2.58}$$

In this case one obtains intermittent behaviour of the SFMs for all scales and there is no need to introduce any regularization of the singularity in the distribution function. This situation corresponds to the weak intermittency in the $\alpha$-model [65]. However, if the distribution function (eq. 2.55) shows a self-similar behaviour with the exponent $\nu_i > i - 1$, then to ensure the existence of the integral in eq. (2.30), one should introduce some regularization for $\mid y_k - y_l \mid \to 0$. Let us suppose that if the distance between any pair of points $y_k$, $y_l$ is smaller than a certain cut-off value $l$, then $\mid y_k - y_l \mid$ will be replaced by $l$. For $\delta y \gg l$, the SFMs have then the following behaviour :

$$F_i(\delta y) = a\, l^{i-1-\nu_i} (\delta y)^{1-i} + b\, (\delta y)^{-\nu_i} + O(\delta y^2) \,. \tag{2.59}$$

Clearly, the above expression is divergent for $l \to 0$ if $i - 1 < \nu_i$. For $\delta y \gg l$, the first term is dominant giving the behaviour :

$$F_i(\delta y) \sim (\delta y)^{1-i} \,, \tag{2.60}$$

similarly as in the $\alpha$-model for the case of the strong intermittency. Here, analogously as in the $\alpha$-model where the number of steps in the cascade must be finite, a non-singular behaviour has to be assumed in the distribution function, i.e. a finite scale below which the scale-invariance breaks down. Similarly, we recover the scale-invariant behaviour of the SFMs (eq. 2.60) at scales $\delta y \gg l$, but with the exponents of the strong intermittency $\nu_i = i - 1$.

Let us now consider the SFC calculated from the $(i+j)$-particle reduced density :

$$F_{i,j}(D, \delta y) = \frac{\int_0^{\delta y} dy_1 \ldots \int_0^{\delta y_i} dy_i \int_D^{D+\delta y} dy_{i+1} \ldots \int_D^{D+\delta y} dy_{i+j}\, d_{i+j}(y_1, \ldots, y_{i+j})}{(\delta y)^{i+j} F_i(\delta y) F_j(\delta y)} \,. \tag{2.61}$$

For further simplicity we take $F_{1,1}$, which is given by the uniquely determined two-particle reduced distribution function :

$$d_2(y_1, y_2) = \frac{A}{\mid y_1 - y_2 \mid^{-\nu}} \,. \tag{2.62}$$

This gives :

$$F_{1,1}(D, \delta y) = A \frac{(D+\delta y)^{2-\nu} + (D-\delta y)^{2-\nu} - 2D^{2-\nu}}{(2-\nu)(1-\nu)\,(\delta y)^2} \,. \tag{2.63}$$

The above expression follows closely the power-law behaviour in D :

$$F_{1,1}(D, \delta y) \sim D^{-\nu} \,. \tag{2.64}$$

Similarly as in the $\alpha$-model, the intermittency exponent $\nu$ equals $\nu_2$, i.e. it is the same as for the SFM $F_2$. Fig. 2.4 shows the dependence of the SFC $F_{1,1}(D, \delta y)$ on $\delta y$ for

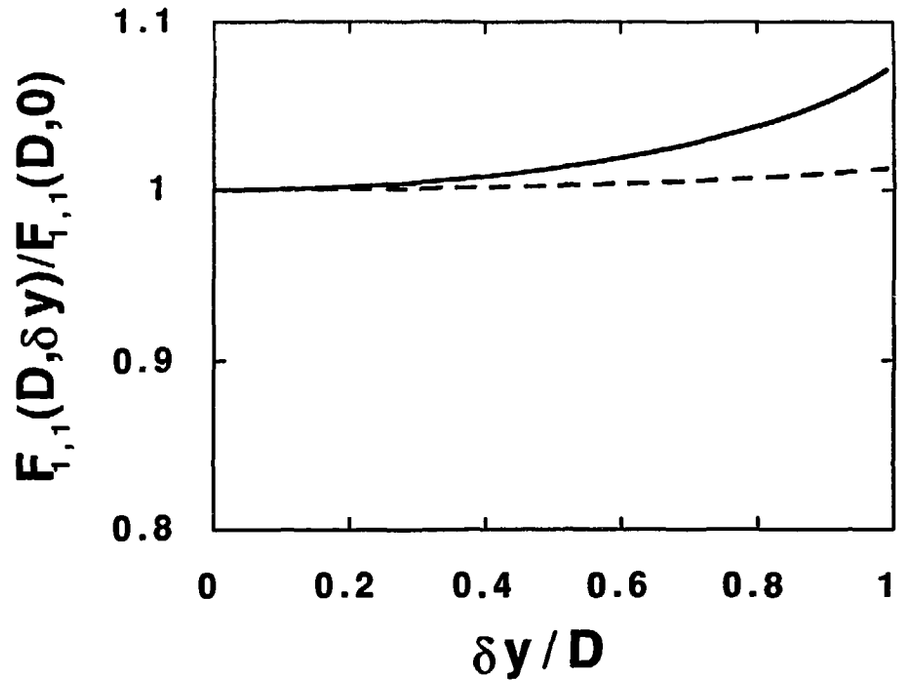


Figure 2.4: The dependence of the SFC $F_{1,1}(D, \delta y)$ on the bin size $\delta y$ as calculated from eq. (2.63) for the intermittency exponents $\nu = 0.1$ (the dashed line) and $\nu = 0.4$ (the solid line) .

$\nu = 0.1$ , $0.4$ . One can see that $F_{1,1}$ is approximately independent of $\delta y$ . Moreover, as long as $D - \delta y$ is larger than the minimal scale of the self-similarity, the SFCs do not depend on whether the distribution function is regularized or not. These features of the $\alpha$-model in 1D can be reproduced by the singular or regularized scale-invariant distribution function (eq. 2.55) .

As was noticed in refs. [51, 48, 52], the intermittency signal depends dramatically on the dimensionality of the analysis if the correlations are multidimensional and non-factorizable. The projected distributions of the 2D $\alpha$-model [51] or of the 2D and 3D singular distributions [48, 52] are not intermittent. Their respective effective slopes are smaller than in the unprojected case and the dependence of the SFM on the binning flattens out for small bins.

Let us now consider the $\alpha$-model in 2D having the transverse size $L$, and let us calculate the SFC $F_{1,1}$ in this model for the projected distribution which is obtained by averaging over the transverse size. The SFC $F_{1,1}(D, \delta y) = < n_1 n_2 > /(< n_1 > < n_2 >)$ , where $n_1$ and $n_2$ are the number of particles in the region 1 and 2 respectively (see Fig. 2.5), become :

$$F_{1,1} = \sum_{i=1}^{L/\delta y} \sum_{j=1}^{L/\delta y} < n_{1i}\, n_{2j} > /(< n_1 > < n_2 >)$$

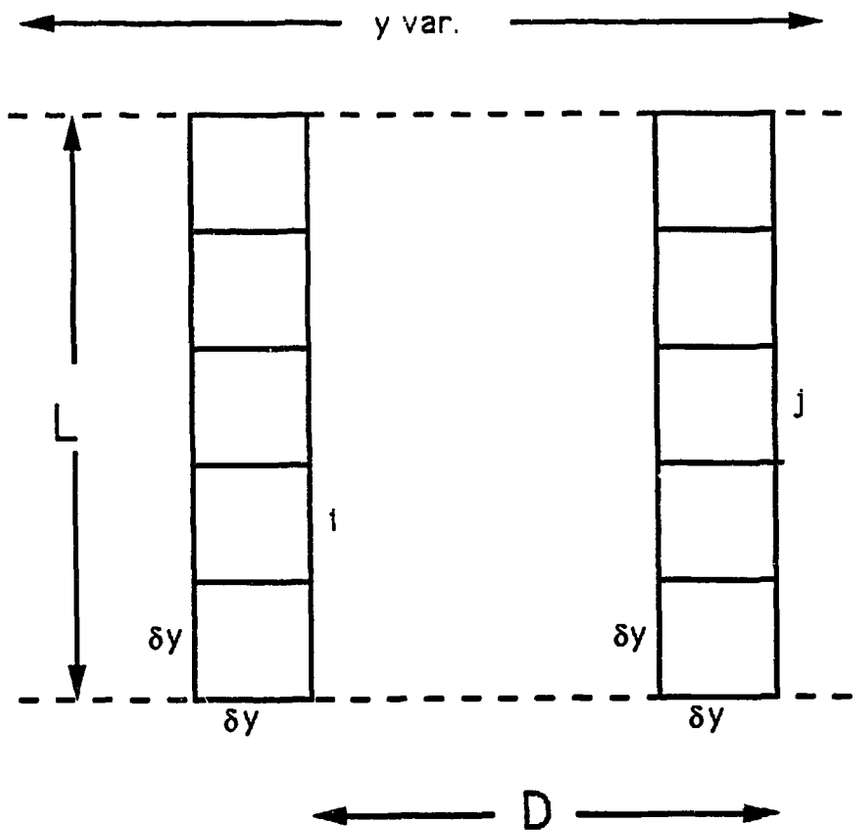


Figure 2.5: The summation region for the scaled factorial correlator $F_{1,1}$ of the 2D $\alpha$-model. The two regions are subdivided into $L/\delta y$ squares $\delta y \times \delta y$.

$$= A \sum_{i=1}^{L/\delta y} \sum_{j=1}^{L/\delta y} \left( \sqrt{D^2 + (i-j)^2 \, (\delta y)^2} \right)^{-\nu} (\delta y)^2 / L^2$$

$$\sim \frac{A}{L^2} \int_0^L dy_1 \int_0^L dy_2 \left( \sqrt{D^2 + (y_1 - y_2)^2} \right)^{-\nu} \quad \text{for } \delta y \ll L \qquad (2.65)$$

Hence, as in the unprojected $\alpha$-model and in the experiment [23], the SFC are approximately independent of $\delta y$. In the case of the 2D singular distribution, similar arguments can be put forward as for the $\alpha$-model. This shows that also in this case one expects the bin size independence of the projected SFCs. We have also calculated numerically the SFCs in 1D from the formula :

$$F_{1,1}(D, \delta y) = \frac{1}{L^2 (\delta y)^2} \int_0^L dx_1 \int_0^L dx_2 \int_0^{\delta y} dy_1 \int_0^{D+\delta y} dy_2 \; d_2(x_1, y_1; x_2, y_2) \; . \qquad (2.66)$$

The dependence of the SFC on the bin size $\delta y$ is shown in Fig. 2.6 . As already noticed by Peschanski and Seixas [47], the SFCs fulfil approximately the requirement of the

independence on the bin size. This is even better satisfied than in the 1D case (compare

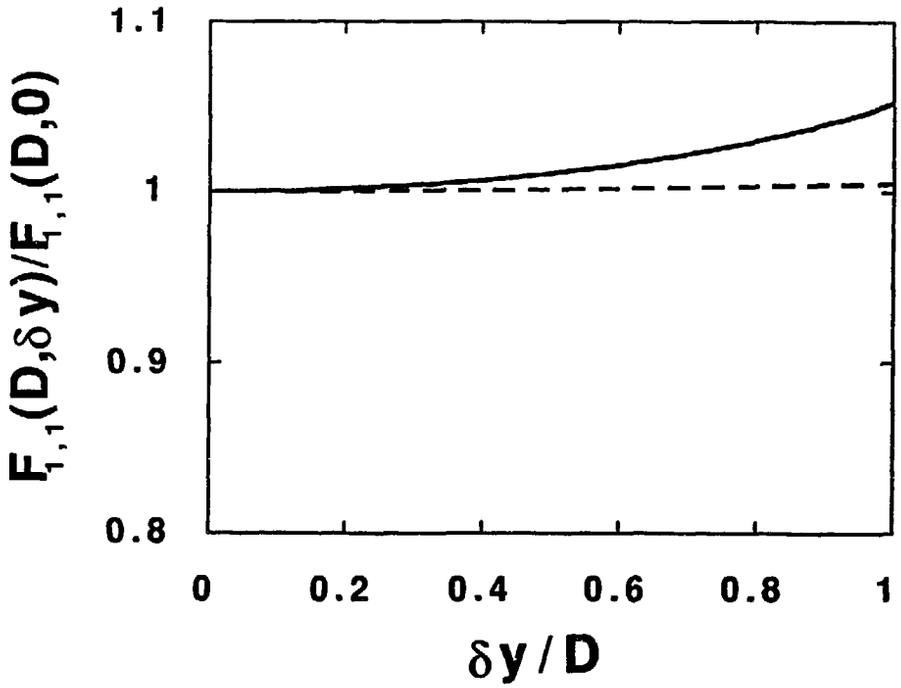


Figure 2.6: The dependence of the SFC $F_{1,1}(D, \delta y)$ on the bin size $\delta y$ as calculated from eq. (2.66) for the intermittency exponents $\nu = 0.1$ (the dashed line) and $\nu = 0.4$ (the solid line). For the transverse size we take $L = 4D$ .

Figs. 2.4 and 2.6).

The experimental data show different relations between the slopes of the SFCs and the slopes of the SFMs than predicted by the $\alpha$-model :

$$\nu_{i,j} = \nu_{i+j} - \nu_i - \nu_j \ . \tag{2.67}$$

This difference can be understood as being due to the effect of the projection in a higher-dimensional model. In ref. [47], a general relation was derived which relates the SFC $F_{1,1}$ to the SFM $F_2$ :

$$F_{1,1}(D, \delta y) = F_{1,1}(D, D) = 2F_2(2D) - F_2(D) \ . \tag{2.68}$$

From the above equation one can calculate the local slope of the SFC :

$$\frac{d\ lnF_{1,1}(D, \delta y)}{d\ ln(D)} = \left( 2F_2(2D) \frac{d\ lnF_2(2D)}{d\ ln(2D)} - F_2(D) \frac{d\ lnF_2(D)}{d\ ln(D)} \right) (2F_2(2D) - F_2(D))^{-1} \ . \tag{2.69}$$

Due to the projection, the local slopes of the SFMs flatten out for small bins and, in general, the slope is decreasing for the decreasing bin size. This gives :

$$\frac{d\ lnF_2(2D)}{d\ ln(2D)} > \frac{d\ lnF_2(D)}{d\ ln(D)} \ . \tag{2.70}$$

Substituting this relation into eq. (2.69) one obtains :

$$\frac{d\ lnF_{1,1}(D,\delta y)}{d\ ln(D)} > \frac{d\ lnF_2(D)}{d\ ln(D)} \tag{2.71}$$

This feature is found in the experimental data [23] for which :

$$\nu_{i,j} > \nu_{i+j} - \nu_i - \nu_j\ . \tag{2.72}$$

The above relation follows from the saturation of the SFMs and from the general identity (2.68), which is true for any kind of translationally invariant distribution functions. This observation can explain the breaking of the relation (2.67) between slopes of the SFCs and the SFMs which holds in the original $\alpha$-model and in the description using the scale-invariant distribution function but is no longer fulfilled in the projected 1D distributions.

We have shown that the $\alpha$-model and the singular distribution functions give similar behaviour of the SFMs and the SFCs. This covers the cases of both strong and weak intermittency, which can be correctly described by the singular and regularized scale-invariant distribution functions respectively or, in the $\alpha$-model, by the infinite and finite self-similar cascade respectively. The SFCs, as obtained from the integration of the scale-invariant distribution functions, are similar to those obtained from the $\alpha$-model. The dimensional projection does not change this similarity. Both descriptions show the same behaviour in the projected SFMs and SFCs. These two descriptions give an approximate independence of the SFCs on the bin size, and moreover, the relations between the slopes of the SFCs and SFMs are changed by the dimensional projection. This last observation which was confirmed by the experimental data [23], allows to explain the recent data on SFCs using the higher dimensional $\alpha$-model of the multiparticle correlations. Together with results of previous works, which used the scale-invariant distribution function to describe the power-law behaviour of the SFMs [48, 52] (sect. 2.2), this result completes an analysis of similarities between the two approaches. These two approaches are in agreement with the experimental data on both SFMs and SFCs if the dimensional projection is taken into account.

## 2.4 Structure of the multiparticle correlations

In the previous sections we have concentrated mainly on the structure of the two-particle correlations, which are related to the second SFM $F_2$ and to the SFC $F_{1,1}$ . The study of the higher SFMs and SFCs can give some insight into the structure of the multiparticle correlations. In sect. 2.1 the relation between the $n$-particle density and the $n$-th SFM was given. The experimental analysis of the SFMs allowed for the first time to have an estimate of the behaviour of the multiparticle correlations on small distances in rapidity. Those features could not be seen in the study of the correlation functions, due to the large experimental errors in these direct, non-integrated observables which conceal the intermittent behaviour. One can then ask what is the relation between the structure of the multiparticle correlations and the structure of the simplest one, the two-particle correlation. In this section we try to identify this relation in the $e^+e^-$ annihilation data of the DELPHI Collaboration [15].

Much experimental data on multiplicity distributions have been fitted using the negative binomial (NB) distribution [66]. NB fits have been applied both to the whole rapidity range as well as to the symmetric or shifted subintervals of the rapidity, down to the rapidity width $\delta y = 0.4 - 0.5$. The intermittency analysis revived the interest in the studies of the multiplicity distributions in small rapidity bins and especially its dependence on the bin width. In numerous studies, the values of the intermittency exponent $\nu_i$ and its scaling with the rank $i$ have been discussed. The experimental data for $\pi^+/K^+$-$p$, $\mu$-$p$ collisions and $e^+e^-$ annihilation [21, 19, 15] , show an approximately quadratic scaling of the intermittency exponents :

$$\nu_i \sim \frac{i(i-1)}{2}\nu_2 \,. \tag{2.73}$$

From the above relation, conclusions can been extracted concerning the underlying particle production mechanism [3]. On the other hand, the rise of SFMs should be related to the shape of the multiplicity distribution in small rapidity intervals or in some restricted regions of the phase-space and several authors have tried to extrapolate the NB distribution down to the very small intervals in rapidity [67, 68]. This problem concerns not only the relation between intermittency exponents of different rank, but also the relation between the magnitude of the factorial moments. The magnitude of the SFMs in small rapidity bins shows deviations from the prediction of the NB law [68, 51] :

$$(\frac{F_i}{F_{i-1}} - 1) = (i-1)(F_2 - 1) \,, \tag{2.74}$$

and, in general, SFMs grow slowlier than predicted by (2.74). This feature is not confirmed by the DELPHI data for $e^+e^-$ annihilation [15] for which the SFMs grow faster than (2.74) and, therefore, one may ask the question whether the same scheme of multiparticle correlations is present both in the $e^+e^-$ annihilation and in the hadron - hadron collisions.

Several authors have tried to describe the measured SFMs in small rapidity bins by postulating various expressions for the higher correlation functions [68, 6, 69]. Probably the most consistent procedure, which in the limiting case reproduces the NB distribution, has been proposed by Van Hove [69, 70]. In this procedure one assumes that all multiparticle correlations can be expressed in terms of the single-particle distribution $\rho_1(y)$ and a two-particle aggregation function $a(y, y')$. The experimental data for $F_2$ have been successfully reproduced using the two-particle reduced density of the form $1 + \gamma exp(- \mid y_1 - y_2 \mid /\xi)$ [68, 6, 7]. The second term in this expression can be identified with the aggregation function :

$$a(y_1, y_2) = \gamma \; exp(- \mid y_1 - y_2 \mid /\xi) \,. \tag{2.75}$$

Following Van Hove [69], the $n$-particle inclusive distribution is determined by the one-particle distribution $\rho_1(y)$ and the aggregation function $a(y, y')$ (which is nothing else than the reduced two-particle correlation function defined in sect. 2.1) by means of the recursive formula :

$$\rho_{n+1}(y_1, \cdots, y_n, y_{n+1}) = \{\rho_n(y_1, \cdots, y_n)\rho_1(y_{n+1})(1 + na(y_1, y_{n+1}))\}_S \tag{2.76}$$

where $\{\}_S$ means symmetrization over all $y_i$ . A similar procedure, which gives the same results in small rapidity bin, has been used extensively by De Wolf to reproduce the higher SFMs in various processess [68]. One should stress that all these approaches deal with the structure of the correlation function and hence, they are directly connected to the behaviour of the scaled factorial cumulants. In other words, a singularity in the aggregation function and in the resulting higher order cumulants, would give a power-law or an approximately power-law behaviour of the scaled factorial cumulants and not of the SFMs.

From the fits one can observe that the NB formula overestimates the experimentally observed SFMs in small rapidity bins for hadronic collisions [68]. The reverse behaviour is seen in the $e^+e^-$ (see Fig. 2.7) and $\mu$-$p$ data. The curves corresponding to the

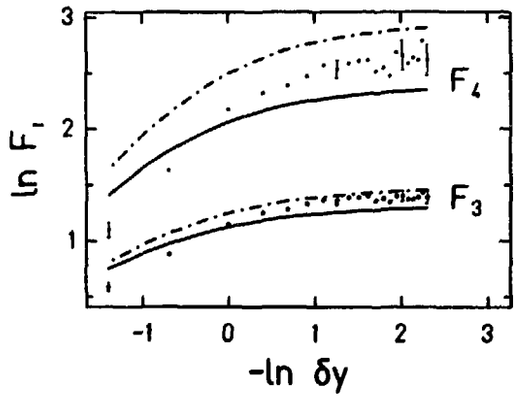


Figure 2.7: The dependence of SFMs on the bin size as obtained for the NB-like correlation scheme given by eq. (2.76) (the solid lines) and for the power-like correlation scheme (2.77) (the dashed-dotted line), with the aggregation function given by eq. (2.75) with parameters $\gamma = 0.64$ and $\xi = 1.48$ . The experimental data are denoted by the points and correspond to the $e^+e^-$ annihilation data of the DELPHI Collaboration.

NB like structure of the higher correlation functions (2.76) in this case lie below the experimental points, possibly indicating a different structure of the $n$-particle inclusive distributions in the $e^+e^-$ than in the hadron-hadron collisions. Below, we propose a new, power-like scheme of the multiparticle correlations [49] :

$$\rho_{n+1}(y_1,\cdots,y_n,y_{n+1}) = \{\rho_n(y_1,\cdots,y_n)\rho_1(y_{n+1})\prod_{i=1}^{n}(1+a(y_i,y_{n+1}))\}_S\ , \qquad (2.77)$$

which is related to the multiplicative process of particle production. Independently of the details of the underlying branching scheme, all these models give the log-normal distribution for high numbers of branching steps [71]. For the case of constant $a(y,y')$ in this correlation scheme, we obtain the following expression :

$$< n(n-1)\cdots(n-i+1) >_\Omega = \bar{n}_\Omega^i (1+a)^{i(i-1)/2} \qquad (2.78)$$

for the factorial moment in an interval $\Omega$ of rapidity, where $\bar{n}_\Omega = \int_\Omega \rho_1(y)dy$ is the mean multiplicity in the interval $\Omega$. In this perhaps oversimplified case, the SFMs follow the quadratic law :

$$F_i = F_2^{i(i-1)/2}\ , \qquad (2.79)$$

which is a general feature of the random multiplicative processes in the gaussian approximation [72]. For the symmetric aggregation function $a(i,j) \equiv a(y_i,y_j) = a(y_j,y_i)$ , the reduced $n$-particle correlation functions can be expressed as follows :

$$\begin{aligned}
c_2(y_1,y_2) &= a(1,2) \\
c_3(y_1,y_2,y_3) &= \{3a(1,2)a(2,3) + a(1,2)a(1,3)a(2,3)\}_S \\
c_4(y_1,\cdots,y_4) &= \{12a(1,2)a(2,3)a(3,4) + 4a(1,2)a(1,3)a(1,4) \\
&\quad +12a(1,2)a(1,3)a(2,3)a(2,4) + 3a(1,2)a(1,3)a(2,4)a(3,4) \\
&\quad +6a(1,2)a(1,3)a(1,4)a(2,3)a(2,4) \\
&\quad +a(1,2)a(1,3)a(1,4)a(2,3)a(2,4)a(3,4)\}_S
\end{aligned} \tag{2.80}$$

The structure of the above correlation functions differs strongly from those derived for the Van Hove *ansatz* given by eq. (2.76) ( see also eqs. (22), (23) of ref. [69]). In general, the $n$-particle correlation function in the power-like scheme (2.77), contains products of $n-1$ up to $n(n-1)/2$ functions $a(y,y')$. For real cascading the powers of $a(y,y')$ would not occur with the weights predicted by the log-normal distribution because, due to the finite energy and the non-negligible particle masses, the number of branching steps is finite. At higher energies, however, one might expect that the multiparticle distributions would be better described by a very long branching process which would imply an even closer agreement with the formula (2.77). Even at presently available energies the log-normal distribution has been successfully applied to fit the full phase-space multiplicities of charged particles produced in $e^+e^-$ annihilation [71].

We have used the same parametrization of the aggregation function (2.75) in the two correlation schemes (2.76), (2.77). The resulting predictions for $F_3$ and $F_4$ are shown in Fig. 2.7 . The experimental SFMs are clearly overestimated by the SFMs calculated for the power-like correlation scheme (2.77). However, for small rapidity binning both schemes fail to reproduce the experimental data which lie between the curves calculated for these two correlation schemes.

Here one should comment that the log-normal distribution can be obtained in a multiplicative random process using the gaussian approximation. This is not correct in the tails of the distributions, which are especially important in the calculation of the highest moments. In fact it was shown by Alberty and Białas [73] that for high moments the intermittency indices should be linear in the rank of the moment :

$$\nu_i \sim i \,. \tag{2.81}$$

Another possibility is allowed if one considers the Levy-stable random variables [74]. Brax and Peschanski have shown that then the intermittency exponents depend in the following way on the rank of the moment :

$$\nu_i \sim \frac{i^\mu - i}{2^\mu - 2}\nu_2 \,, \tag{2.82}$$

with $0 \leq \mu \leq 2$ . The things become even more complicated if one considers the finite cascades or the regime of the strong intermittency. Moreover, the scaling in the values of the SFMs and not in the intermittency exponents requires additional assumptions, which will be discussed below.

Another very important problem is related to the effective number of dimensions in which the correlations are built [51, 48]. This question was raised in discussing the observable consequences of intermittency in projected distributions such as the rapidity or rapidity-azimuthal angle multiplicity distributions. It has been shown [51, 48, 52], that the occurrence of intermittency in two or in three dimensions does not lead to the power law behaviour of the SFM in the projected 1D distributions (sect. 2.2). This leads naturally to the question about the number of dimensions in which the correlation functions could be described by some simple *ansatz*. In studying this problem, we have assumed that the $n$-particle inclusive distributions in 3D phase-space obey the relations (2.76) or (2.77), where now $y_i$ is the 3D momentum $\vec{p_i}$ of the on-shell particle $i$. In order to reproduce the behaviour of the 1D SFMs we have assumed a singularity in the 3D momentum space. However, unlike in refs. [48, 52, 44] and in the previous sections, we do not assume that the whole reduced density is given by the singularity, but that only the aggregation function is singular :

$$a(\vec{p_1},\vec{p_2}) = \frac{\gamma}{(\sqrt{-p_\mu p^\mu})^\nu} \ . \tag{2.83}$$

This leads to a power law behaviour of the second factorial cumulant. However, the higher order cumulant do not share that because the $i$-particle cumulant contains singularities of the exponents from $n\nu$ to $n(n-1)\nu/2$ (eq. 2.80). One should observe that the singular structure of the aggregation function is incompatible with the scheme given by eq. (2.77). Indeed, the $n$-particle correlations contain the singularity with the exponent $n(n-1)\nu/2$ , so for the sufficiently high order of the correlations the singularity becomes non-integrable. This would require some regularization of (2.83), but since we confine our studies to $F_2$ and $F_3$ , no such procedure is needed. A detailed discussion of a regularization of the integrals of the singular correlation function and of its implication is presented in section 2.3.

For the single-particle distribution we have taken $\rho_1(\vec{p}) = exp(-\sqrt{m_\pi^2 + p_T^2}/m_T^0)$ . Using (2.83) with all momenta expressed in GeV, we have obtained a reasonable fit to the experimental values of $F_2$ for the parameter values $\gamma = 0.11$ and $\nu = 1.2$ . Both the non-singular 1D (eq. 2.75) and the singular 3D (eq. 2.83) aggregation functions can correctly describe the rapidity width dependence of $F_2$ in the range $(\delta y = 0.1 - 1)$ (Fig. 2.8). This confirms again that the 1D non-singular dependence of the second SFM can be due to the existence of the intermittent behaviour in the 3D momentum space [51, 48, 52].

The singular parametrization (2.83) was used to calculate $F_3$ in the two schemes of correlations given by eqs. (2.76) and (2.77). Similar features can be observed as for the 1D non-singular aggregation function, for which the experimental points are situated between the two curves calculated in the two different correlation schemes (Figs. 2.8 and 2.9). However, these two curves for $F_3$ are shifted up in comparison with the 1D parametrization.

In order to compare the scaling of the SFMs of different rank, we have studied the dependence of $ln\ F_i$ $(i = 3, 4)$ on $ln\ F_2$ . This way of analyzing the results is less sensitive to the details of the parametrization of the two-particle correlations, which are not equally good in reproducing the data for $F_2$ (see Fig. 2.8). It was observed by Ochs [51] that for $e^+e^-$ annihilation at $\sqrt{s} = 35\ GeV$ and $p\bar{p}$ collisions at various

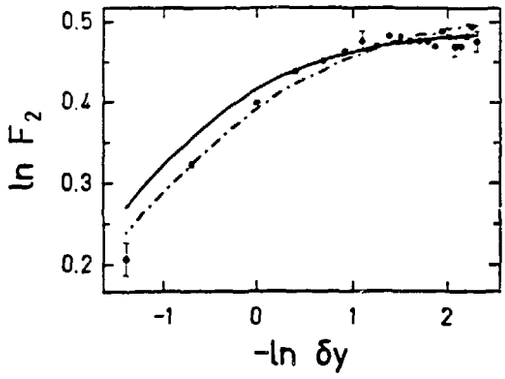


Figure 2.8: Dependence of the second SFM $F_2$ on the bin size for different assumptions about the correlations. The solid line represents the non-singular parametrization in 1D (eq. 2.75). The dashed-dotted line represents the SFM of the projected 3D distribution containing the singularity (eq. 2.83) with $\gamma = 0.11$ and $\nu = 1.2$.

energies, and also for a scale-invariant branching model, the 2D $\alpha$-model and the QCD parton model HERWIG, $ln\ F_i$ $(i > 2)$ depends linearly on $\ln F_2$ :

$$\ln F_i = k_i + \beta_i \ln F_2 \ . \tag{2.84}$$

This relation is only approximately satisfied by the NB law (2.74). Nevertheless, in the range of rapidity bins studied in this work, the scheme given by eq. (2.76), which is based on the NB, can be well approximated by a linear dependence. In the Table 2.2, we show the fitted parameters $k_i$ and $\beta_i$ for various schemes of correlations and for the experimental data. One can see that, independent of the details of the parametrization, the experimental slope ratios $\beta_i$ lie between the values obtained from the two models both in the 1D and in the 3D case. For the scheme given by eq. (2.77) and the non-singular aggregation function, the parameters of the linear dependence (2.84) approach the values $k_i = 0$ and $\beta_i = i(i-1)/2$ for small bins, in accordance with the relation (2.79). For the projected 3D densities with the singular aggregation function (2.83), the scheme (2.76) leads to deviations from the NB law, whereas the scheme (2.77) departs from the power law (2.79). In both cases, the numerically calculated values of $F_3$ are larger, and thus the first scheme is closer to the data points and the second one deviates even more from the data points than in the non-singular case.

In summary, the analysis of the data on the SFMs of the multiplicity distribution for $e^+e^-$ annihilation leads to several interesting observations. First we observe that the scaling of the magnitudes of the SFMs exceeds the prediction of the NB, unlike for the $\pi^+/K^+$-$p$ and $p\bar{p}$ collisions [68, 51]. This is a striking feature and could indicate a different behaviour of the multiparticle production mechanism in the $e^+e^-$ annihilation at this energy. Motivated by the properties of the random multiplicative processes, we have proposed a scheme relating the $n$-particle inclusive distribution function to the

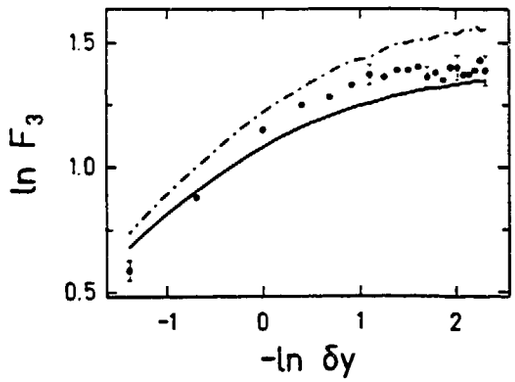


Figure 2.9: Dependence of the third SFM $F_3$ on the bin size for different assumptions about the correlations. The curves have been obtained by integrating the 3D singular three-particle distribution obtained either from the NB like correlation scheme (eq. 2.76) (the solid line) or from the power like correlation scheme (eq. 2.77) (the dashed-dotted line).

single-particle distribution and to the two-particle aggregation function. This scheme gives faster growing SFMs than the scheme proposed by Van Hove [69] which is based on the NB law. The experimental data for $F_3$ and $F_4$ fall in between these two predictions. This conclusion is confirmed by the analysis of the dependence of $\ln F_i \ \ (i > 2)$ on $\ln F_2$ in the different correlation schemes and for the data.

In this section we have also addressed the problem of the effective dimensionality of the correlations. Assuming the presence of a singularity in the aggregation function in the 3D momentum space, we have reproduced the experimentally measured factorial moments $F_2$ using the projected 1D two-particle distribution. We have generalized the two schemes of correlations for the 3D momentum space, but we have not found any substantial change in comparison to the data. This would mean, assuming the presence of intermittency in the 3D momentum space, that each of the two schemes represents an effective description of the projected 1D rapidity distributions. In order to clarify this, it would be interesting to compare the predictions of the two correlation schemes for the projected singularity both in the rapidity-azimuthal angle and in the azimuthal angle distributions.

In the 1D case, the multiplicative scheme (eq. 2.77) reproduces the experimental slope ratios $\beta_i$ better than does the NB scheme (eq. 2.76) (Table 2.2). The slope ratios are unchanged by the projection from higher dimensions [51] and thus provide a more clear characteristic of the particle production mechanism than the 1D intermittency slopes. On the other hand, the coefficients $k_i$ have no such general meaning. This favours an interpretation of the log-normal scheme (eq. 2.77) as an effective description of the 1D correlations, which takes into account the basic properties of the particle

Table 2.2: Parameters of the linear fit (2.84) of the SFMs for various correlation schemes and different effective dimensionalities of the correlations, as well as for the $e^+e^-$ annihilation data of DELPHI Collaboration .

| | Data Ref. [15] | Eq. (2.76) 1D | Eq. (2.77) 1D | Eq. (2.76) 3D | Eq. (2.77) 3D |
|---|---|---|---|---|---|
| $k_3$ | -0.05 | 0.08 | 0.01 | 0.07 | -0.03 |
| $\beta_3$ | 2.99 | 2.51 | 2.99 | 2.57 | 3.2 |
| $k_4$ | -0.14 | 0.25 | 0.03 | - | - |
| $\beta_4$ | 5.72 | 4.33 | 5.93 | - | - |

production mechanism but not its dimensionality. Consequently, it fails to reproduce the coefficients $k_i$. However, both these schemes, when generalized to 3D, fail to reproduce the data. This is caused by the singular 3D aggregation function. So there is, until now, no general scheme of multiparticle correlations giving the scaling properties of SFMs, *i.e.* the slope ratios $\beta_i$ and the expected in 3D intermittent dependence on the binning.

The $\alpha$-model predicts [65] that the moments of the multiplicity distribution in a rapidity interval $\delta y$ should be related to the moments in the full rapidity interval $\Delta y$ as follows :

$$F_i(\delta y) = F_i(\Delta y)\left(\frac{\delta y}{\Delta Y}\right)^{-\nu_i} . \tag{2.85}$$

This leads in the Gaussian approximation to the log-normal scaling relation between the intermittency slopes $\nu_i \sim i(i-1)/2\nu_2$ . This relation can then be only approximately fulfilled for the first few intermittency exponents, because in order for the eq. (2.85) to be true the weak intermittency bound on the intermittency slopes must be ensured [65] :

$$\nu_i < i - 1 . \tag{2.86}$$

The random cascade model could explain the different behaviour of the multiplicity distributions on different scales. For the full phase-space or for the large rapidity windows, the NB distribution is a correct fit to the data [15] However, for small rapidity bins, the SFMs of the multiplicity distribution increase and differ from the NB. In the case of the projected 1D densities one cannot expect intermittent power-law behaviour (eq. 2.85). However, if the relative increase of the SFMs with increasing resolution is log-normal, one would expect the following relation to be fulfilled [51] :

$$F_i(\delta y) = F_i(\Delta y)G(\delta y/\Delta Y)^{\beta_i} , \tag{2.87}$$

with a universal function $G$ and $\beta_i = i(i-1)/2$ for the log-normal case. As we can see in Table 2.2, the experimental values of the coefficients $\beta_i$ are slightly below the log-normal prediction. It is an open question whether it is a result of the limitation of the log-normal approximation to the random multiplicative processes or it is an effect

of the finite c.m. energy available in the process. Concerning the second possibility, it would be interesting to study the dependence of the coefficients $\beta_i$ on the energy. Resuming the results of this section, we see that neither of the two correlation schemes is correct for all scales in the rapidity. Neither of them reproduces the tendency of the data to be NB-like in large rapidity windows and log-normal for small rapidity bins. This feature of the data could be explained by the self-similar, random multiplicative cascade production (the $\alpha$-model). However, even in the framework of the $\alpha$-model the multiplicity distributions are determined only up to the choice of the initial values [65]. No phenomenological scheme of multiparticle correlations exists for this model. As we discussed above, such a scheme should describe multiparticle correlation at all scales. Motivated by a simple structure of the SFM in the $\alpha$-model, it seems natural to parametrize directly of the $n$-particle distribution and not the $n$-particle cumulant. From the discussion in this section we must conclude, that the approach based on the "iteration" of the $n$-particle cumulants is not satisfactory and unlike the $\alpha$-model, it does not give correct predictions on both the multiplicity distribution in the full phase-space and on the intermittency indices.

# 3. Spatiotemporal intermittency in ultrarelativistic nuclear collisions

The experiments on the relativistic heavy-ion collisions raised the question about a possible existence of exotic phenomena, such as the creation of the quark-gluon plasma. It is expected that in central collisions of the heavy-ions accelerated to the energy of 200 GeV/nucl the critical energy density is reached, offering the possibility of a phase-transition to the state of free quarks and gluons. The intermittency analysis was first applied to high multiplicity events such as the JACEE event with a multiplicity $\sim 1000$ [2] and the events produced in ultrarelativistic proton-emulsion and nucleus-emulsion interactions [27] with a multiplicity of the order of 100. The high multiplicity of the produced particles was expected to help in this analysis, allowing to disentangle the interesting particle density fluctuations from the statistical ones. The study of the fluctuations in the rapidity distribution of the produced particles could be a signal of some exotic phenomena occuring during the collision [39], and the method of the SFMs gave a possibility to quantitatively estimate the effect. Indeed, the fluctuations in the nuclear collisions seem to have another source than in the $e^+e^-$ and hadron-hadron collisions. It could be a signal of some collective phenomena occurring in nuclear collisions, or even could be caused by the quark-gluon plasma phase-transition. In this chapter we will try to discuss why the intermittency patterns observed in nuclear collisions could be an indication of some collective phenomena. We shall also calculate the intermittency signal resulting from a phase-transition [52, 64].

## 3.1 Geometrical models of nuclear collisions

In the first approximation, the nucleus-nucleus collision may be considered as a superposition of independent nucleon-nucleon collisions, the number of which is determined by the geometry of the reaction. This picture of the ultrarelativistic dynamics leads to accurate predictions for a number of observables. Many geometrical models are successful in describing the relation between hadron-hadron and hadron-nucleus collision, and other models can relate within the same framework both the hadron-nucleus and the nucleus-nucleus collisions. The main contribution to the change of the observed multiplicity distributions for different collisions is due to the change in the geometry of the collision when passing from smaller to larger projectile or target. Models, such as the wounded nucleon model [75] or the additive quark model [76], were elaborated to calculate the number of primary collisions, which is not a directly observable quantity. The mean multiplicity in different collisions is directly reproduced using such simple models. Also the geometrical arguments permit to describe the experimental multiplicity distribution of the produced particles [77, 78, 79], as well as the experimental transverse energy distribution [80, 81].

The fundamental assumption of all those models is that the primary excited objects such as nucleons, quarks, tubes, strings or ropes, produce particles independently and, hence, the final particle distribution can be considered as the superposition of

distributions from elementary collisions (sources). Also the more elaborate models of heavy-ion collisions such as the dual parton model [82] or the FRITIOF model [83], describe the multiparticle production as an independent fragmentation of strings and the geometry determines only the number of strings in those models [84]. Obviously, neither of the above mentioned models of the independently emitting sources, contain genuine nonlinear effects and, consequently, the comparison of their predictions to the experimental data provides only a starting point in the quest for exotic phenomena in ultrarelativistic nuclear collisions.

The hydrodynamical approach offers an alternative picture of both the dynamics of the collision and the treatment of possible nonlinear effects. In this approach, the excited matter equilibrates rapidly and its further evolution is governed by the equations of the relativistic hydrodynamics involving only locally averaged quantities such as the energy density, the pressure, the velocity, the temperature and not any kind of microscopic degrees of freedom. This presupposes both a very short mean free path and a short memory of the primary collisions.

In the models based on the concept of the creation and subsequent decay of strings, the picture of independent fragmentation of strings seems to be not justified. The density of generated strings which is $2-3$ strings/fm$^2$ [85], denies the reliability of such a scenario and leads to the necessity of taking the string interaction into account. The first attempt to study these effects in the interacting string model has been done by Andersson and Hennig [85], but still the existence of various nonlinear phenomena and nontrivial correlations remains an open question. In the treatment of nonlinear effects, such a flux-tube model [85] with a possible phase-transition would stand *halfway* between the simple nucleon-nucleon superposition models and the hydrodynamics with a phase-transition. Van Hove proposed to use the parton-shower model including a perturbative stage of parton production and the hadronization through the string fragmentation during the final stage [84]. This picture needs a very soft parton cascade in order to reproduce the experimental effects, and it is not clear whether a perturbative approach could be justified.

In the present work we concentrate on the multiparticle correlations. Those correlations can be built up at any stage of the collision. They can arise either from random cascading structure of the parton cascade or from the string fragmentation process. However, as we will show below, they are not a product of independent fragmentation of strings (sources). The inclusion of a non-negligible interaction between the strings is crucial in order to reproduce the experimental data.

## 3.2 Fractal structures in the collision dynamics

It was claimed that the presence of nonstatistical fluctuations in the spectra of hadrons produced in ultrarelativistic nuclear collisions could be a signal of the quark-gluon plasma formation [39, 2]. The effect of nonstatistical fluctuations can be extracted and the comparison between different processes is possible using the method of the SFM [2, 3]. The experimental data in $e^+e^-$ and hadron-hadron collisions confirm the existence of such fluctuations and the dependence of SFM on the resolution in rapidity can be fitted using a power law relation. In the case of a large number $N$ of

independent fluctuating sources, the superimposed distributions would follow a similar law with the slopes $\nu_i$ which are $N$ times smaller than for one source [7, 59, 60, 61]. This motivates the so called Białas plot, *i.e.* the intermittency slopes versus the particle rapidity density $\frac{dn}{dy}$. Comparing on such a plot different nuclear collisions at similar energies leads to the conclusion that the intermittency slopes are anomalously high for heavy targets [30]. The discussion of the independent collision model was performed by Capella et al. [7] who concluded that this model give values of the intermittency slopes $4 - 20$ times too low and, consequently, the observed intermittency slopes in nuclear collisions cannot be interpreted as an effect of superimposed nucleon-nucleon collisions. One should notice that even if the mechanism responsible for the fluctuations in nucleus-nucleus collisions is different than in hadron-hadron collisions, still there is a lack of consistency in the observed parameters for different projectiles (p, O, S) [52]. In

| Moment | Reaction | Data [28] | Data (rescaled multiplicity) | Model |
|---|---|---|---|---|
| $F_2$ | p-Em | 0.019 | 0.019 | 0.016 |
| $F_2$ | O-Em | 0.016 | 0.003 | 0.006 |
| $F_3$ | O-Em | 0.042 | 0.010 | ... |
| $F_2$ | S-Em | 0.012 | 0.0015 | 0.003 |
| $F_3$ | S-Em | 0.028 | 0.006 | ... |

Table 3.1: Slopes of the SFMs $F_2$ and $F_3$ for different reactions are compared to the rescaled multiplicity data for $p - Em$ reaction (eq. 3.1). The estimate of the slope from the theoretical model presented in this chapter is given for $F_2$ .

table 3.1 we show the experimental data for $F_2$ and $F_3$ for three projectiles [28] and the predictions for the projectile nucleus $A$ from the p−Em data rescaled in accordance with the change of the mean multiplicity :

$$F_i^A = \frac{F_i^p < N_p >}{< N_A >} . \tag{3.1}$$

As was already discussed in the ref. [52], the observed decrease of the intermittency slopes is not as large as the corresponding increase of the multiplicity.

Białas and Hwa proposed that the intermittency patterns of fluctuations in the nuclear collisions could be a consequence of a higher order phase-transition from quark-gluon plasma into hadrons [11]. More generally, it could also be understood as an effect of some strong space-time correlations in the nuclear dynamics. In the picture of partons and strings it means that the main contribution to the observed intermittency patterns does not come from the stage of parton cascade or independent string fragmentation but instead from the stage of dynamical evolution of the interacting string network with a possible phase-transition similar to the percolation [86].

In ref. [52], the two-particle density in space-time was taken to be a scale-invariant function, like in the critical point for a second order phase-transition. The correlation

function at the proper time $\tau_2$ of the freeze out, can be written in the covariant form :

$$d_2(\vec{r_1},\vec{r_2}) = \begin{cases} C_2\ (\tau_{12})^{-\nu_2}\ |_{t_i=\sqrt{\tau_2^2+\vec{r_i}^2}} & \text{for } \tau_{12} < \tau_{corr}\ , \\ C_2\ (\tau_{corr})^{-\nu_2} & \text{for } \tau_{12} \geq \tau_{corr}\ , \end{cases} \tag{3.2}$$

where $\tau_{12} \equiv \sqrt{(\vec{r}_2 - \vec{r}_1)^2 - (t_2 - t_1)^2}$ and $\tau_{corr}$ is the range of the correlations. The finite range of the correlations in this model is exclusively due to the causality constraints. Assuming that the phase-transition takes place at a certain proper time $\tau_1$ and that the correlations cease to build at some other value of the proper time $\tau_2$ , one obtains $\tau_{corr} = (\tau_2^2 - \tau_1^2)/\tau_1$ for the range of the fluctuations (Fig. 3.1). The intermittency

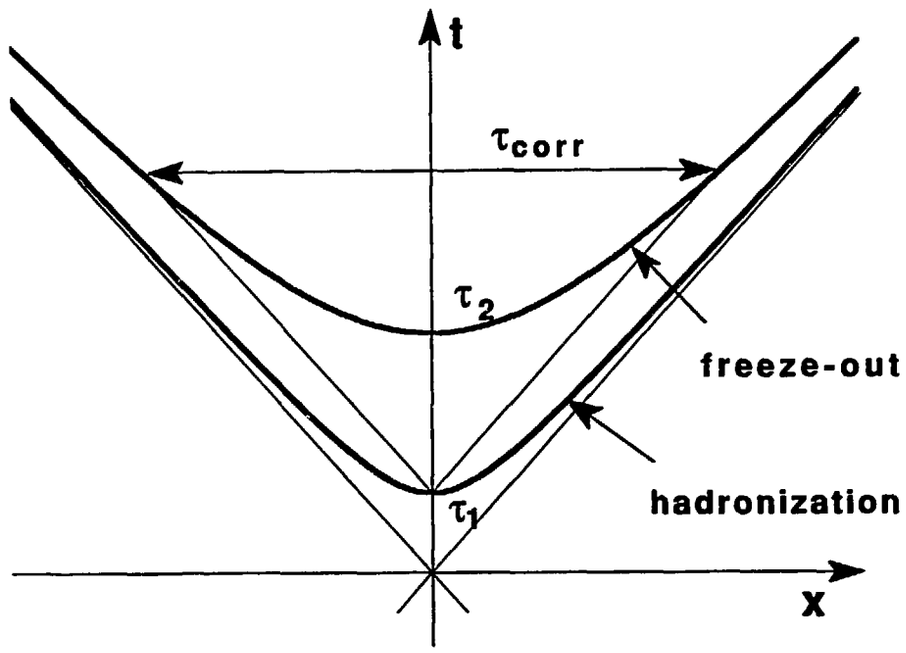


Figure 3.1: The space-time evolution of the system in the nuclear collision. The maximal range $\tau_{corr}$ of the correlations, which are build between the two proper times $\tau_1$ and $\tau_2$ is shown. The variable $|\ x\ |$ corresponds to $|\ \vec{r}\ |$ in $(3+1)$-dimensions.

exponent $\nu_2$ describes the strength of the singular correlations and is given by the nature of the mechanism by which the spatiotemporal intermittency is build up. In our calculation we took $\nu_2 = 1.0$ .

For the dynamics of the reaction we assume the Bjorken's scaling in the longitudinal direction. The ideal inside-outside correspondence will be smeared out, to simulate realistically the dynamics of the interactions at 200 GeV/nucl . The other non-ideal effect taken into account is the presence of the long lived resonances. Here we assume

that a given part $(1-q)$ of the observed pions come from the decay of such resonances[1]. The decay is assumed to be isotropic in the rest frame of the resonance, in which case the rapidity distribution is $1/cosh^2 y$ . Such a distribution is well approximated by a gaussian distribution with the half-width equal 0.75 . The one-particle density is assumed to be constant inside a tube of radius $R_{tu}$ and zero outside. The radius of the tube is given by the geometry of the reaction, i.e. by the impact parameter and the projectile radius. The interaction region for central collisions is determined by the

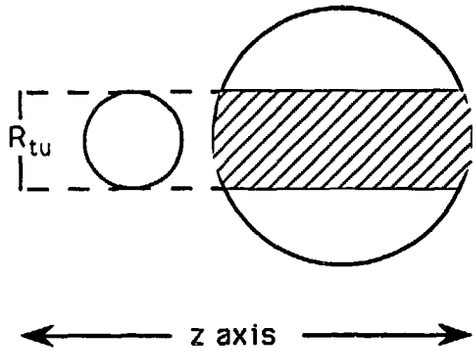


Figure 3.2: Schematic view of the geometry involved in a central collision of two nuclei

radius of the smaller (projectile) nucleus, $R_{tu} = r_0 A^{1/3}$ (see Fig 3.2). Integrating the two-particle reduced density over transverse radii and azimuthal angles, one obtains the one-dimensional reduced density :

$$d_2^{(1-dim)}(y_1,y_2) = \left(\pi^{-2}R_{tu}^{-4}\right)\int_0^{R_{tu}} R_1 dR_1 \int_0^{R_{tu}} R_2 dR_2 \int_{-\pi}^{\pi} d\phi_1 \int_{-\pi}^{\pi} d\phi_2 \; d_2(R_1,\phi_1,y_1;R_2,\phi_2,y_2)\,. \tag{3.3}$$

This represents the two-particle reduced density of the space-time rapidity distribution of the sources. Following our assumptions, this density (3.3) corresponds only approximately to the kinematical rapidity distribution. In order to obtain the distribution in the kinematical rapidity one should fold the space-time rapidity distribution with the phase-space distribution, which we take in the following form [87] :

$$f(y,y^{(st)}) = \frac{exp\left(-(y-y^{(st)})^2/2\sigma^2\right)}{\sigma\sqrt{2\pi}}\,, \tag{3.4}$$

In the case of the ideal inside-outside cascade, the phase-space distribution is given by the $\delta$ function :

$$f(y,y^{(st)}) = \delta(y-y^{(st)})\,. \tag{3.5}$$

The parameter $\sigma$ in the above equation represents the width of the smearing of the rapidity distribution. The rapidity distribution is then :

$$d_2^{(kin)}(y_1,y_2) = \int_{-\Delta Y_{st}/2}^{\Delta Y_{st}/2} dy_1^{(st)} \int_{-\Delta Y_{st}/2}^{\Delta Y_{st}/2} dy_2^{(st)}\; d_2^{(1-dim)}(y_1^{(st)},y_2^{(st)}) f(y_1,y_1^{(st)}) f(y_2,y_2^{(st)})\,. \tag{3.6}$$

[1]Some detailed results from the $e^+e^-$ anihilation indicate that the effect of the resonance decay effectively does not change (or even *increase*) the fluctuations [18], so it is not excluded that the value $q = 1$ could be better suited for this calculation (Fig. 3.6).

This is the kinematical rapidity distribution of the sources of the final pions. As we already mentioned, only about $q = 0.25 - 0.5$ of the total number of pions are produced directly and the rest comes from the resonances decays. Taking this into account, the two-particle rapidity distribution for pions can be written as follows :

$$d_2^{(\pi)}(y_1, y_2) = \int_{-\Delta Y/2}^{\Delta Y/2} dy_1' \int_{-\Delta Y/2}^{\Delta Y/2} dy_2' \; d_2^{(kin)}(y_1', y_2') \\ \Big(q\;\delta(y_1 - y_1') + (1-q)\rho^{(iso)}(y_1 - y_1')\Big)\Big(q\;\delta(y_2 - y_2') + (1-q)\rho^{(iso)}(y_2 - y_2')\Big)\;. \tag{3.7}$$

The decay distribution of a resonance $\rho^{(iso)}$ in the above equation is approximated by :

$$\rho^{(iso)}(y) = \frac{exp(-y^2/1.125)}{0.75\sqrt{2\pi}}\;. \tag{3.8}$$

From the two-particle reduced density one obtains directly the second SFM :

$$F_2 = \frac{1}{(\delta y)^2}\int_0^{\delta y} dy_1 \int_0^{\delta y} dy_2\; d_2^{(\pi)}(y_1, y_2)\;. \tag{3.9}$$

The results for $F_2(\delta y)$ in the range $\delta y = 0.1 - 1$ are plotted in Fig. 3.3 . As one can

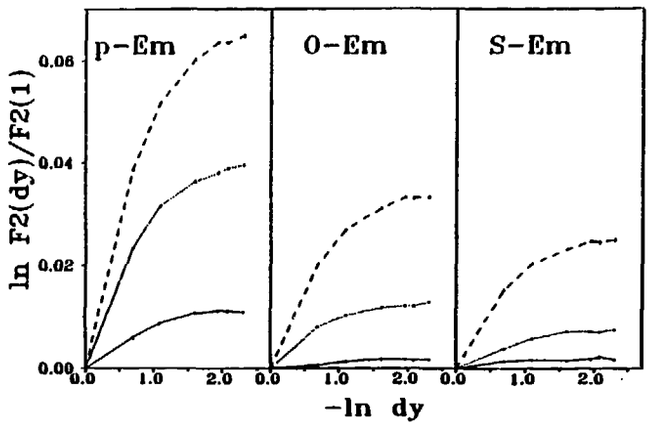


Figure 3.3: The dependence of the second SFM $F_2$ on the size of the rapidity bin $\delta y$, as obtained from eq. (3.9) for three different freeze out times $\tau_2 = 4fm$ (the solid line), $6fm$ (the dotted line) and $10fm$ (the dashed line). The parameters are set to $\tau_1 = 3$fm/c, $q = 0.25$ and $\sigma = 0.3$. All the curves are normalized at $\delta y = 1$ .

see the results depend strongly on the assumed freeze-out time $\tau_2$. The resulting slopes $\nu_2$ of the SFM are of the same order of magnitude as observed experimentally. However, the detailed comparison is not meaningful because the calculated slopes $\nu_2$ depend sensitively not only on the projectile and the impact parameter but also on the unobservable parameters such as the correlation range $\tau_{corr}$ , percentage of the direct pions $q$ and the width $\sigma$ of the rapidity spread around the Bjorken's solution. So the dependence of the SFMs on the projectile and the impact parameter as calculated in this model, can be treated only as a qualitative relation. In Table 3.1 one can see the comparison of the experimental data with results of calculations obtained for the freeze-out

time $\tau_2 = 6\ fm$ . Even though the numerical values of the intermittency slopes $\nu_2$ are systematically underestimated, they depend on the projectile less strongly than the inverse of the mean multiplicity (eq. 3.1).

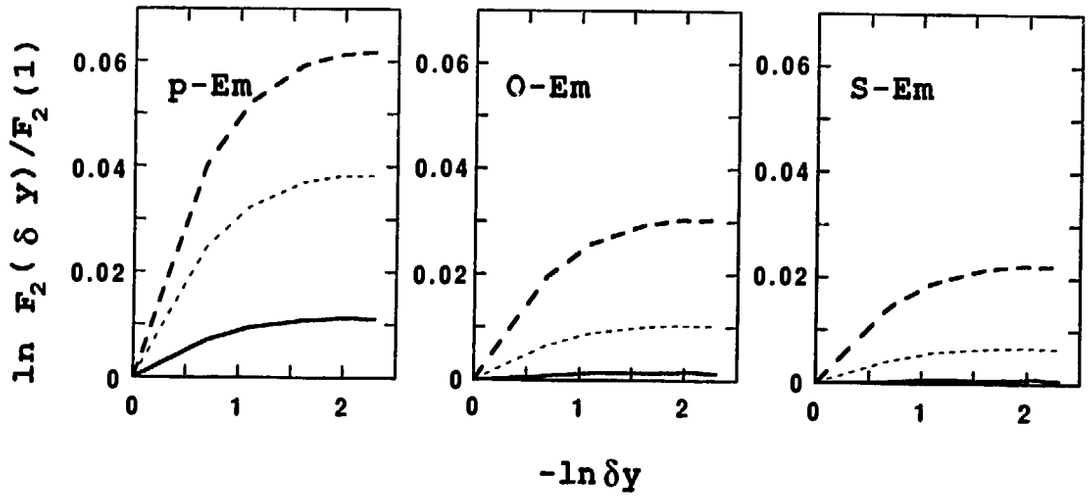


Figure 3.4: The dependence of the second SFM $F_2$ on the size of the rapidity bin $\delta y$, as obtained from eq. (3.9) for three different freeze out times $\tau_2 = 4fm$ (the solid line), $6fm$ (the dotted line), $10fm$ (the dashed line) and $20fm$ (the dash-dotted line). The parameters are set to $\tau_1 = 3$fm/c, $q = 0.5$ and $\sigma = 0.5$. All the curves are normalized at $\delta y = 1$ .

For comparison, we are plotting in Fig. 3.4 the similar results for a different set of parameters. The proportion of the direct pions is now set to $q = 0.5$ and the half-width of the smearing of the rapidity distribution is $\sigma = 0.5$ . The resulting SFMs have a similar dependence on the rapidity bin width $\delta y$ as those plotted in Fig. 3.3. This shows the difficulty in making a quantitative comparison with the data, without having a precise estimate of the unknown parameters.

In Table 3.1 we make a comparison between central nucleus-nucleus collisions in the model (the constant radius of the interaction region) and a sample of central and medium parameter collisions in the experiment. This could be another effect explaining the stronger attenuation of the calculated slopes. On the other side, all ultrarelativistic proton-nucleus collisions are in our model central. So, the model gives relations for central collisions of different projectiles and the experiment gives relations between central proton-nucleus and a mixture of central and medium impact parameter nucleus-nucleus collisions.

Following those arguments, one can take the relations between the "slopes" of the SFMs in our model (see the table 3.1) as the lower bound. Nevertheless, these relations are in much better agreement to the relations followed by the experimental data on $F_2$ than the independent superposition models, and serve as a schematic explanation of the observed relations between intermittency exponents for different projectiles and targets. It would be interesting to compare the results of the model with the experimental results for a sample of only central collisions for different projectiles.

This tendency of the results of the model of spatiotemporal intermittency could

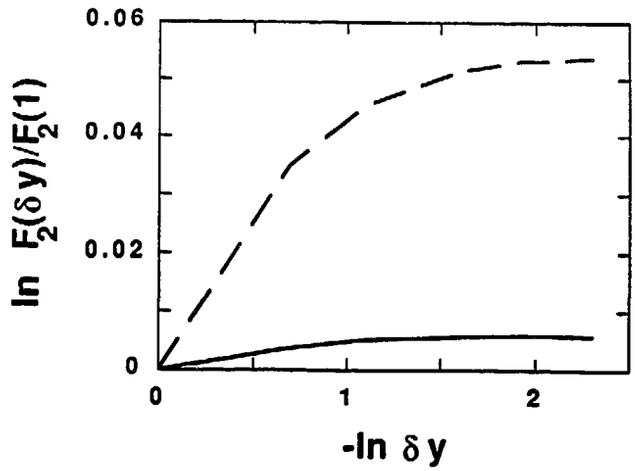


Figure 3.5: The dependence of the second SFM $F_2$ on the size of the rapidity bin $\delta y$, as obtained from eq. (3.9) for O-Au collisions using $\tau_2 = 24 fm/c$, $R_{tu} = 7.2 fm/c$ (the dashed line) and for S-S collisions using $\tau_2 = 5.5 fm/c$, $R_{tu} = 5.5 fm$ (the solid line). The parameters are set to $\tau_1 = 2$fm/c, $q = 0.5$ and $\sigma = 0.5$. All the curves are normalized at $\delta y = 1$ .

certainly be made closer to the experimental data, if we would allow for a projectile dependence on both the spatial and the temporal extensions of the interaction region. This means that taking larger freeze-out time $\tau_2$ for heavier projectiles, one can obtain even weaker attenuation of the slopes with the mass of the interacting nucleus. The recent results of the NA35 Collaboration [88] on the time of the pion emission in ultrarelativistic collisions gives a very high value of the freeze-out time of the order of $20 fm/c$. The lifetime of the pion source in the mid-rapidity was found to be much longer in the asymmetric collisions ($20 fm/c$ for O-Au) than in the symmetric collisions ($6 fm/c$ for S-S) [88]. This strong increase of the emission time with the asymmetry of the collision can explain in the framework of the present model the increase of the slopes of the SFMs with the increase of the mass of the target, as seen by the EMU01 Collaboration [30]. As said before, the interaction time in the asymmetric collisions can take a value of $20 fm/c$ and, as one can see in Figs. 3.5 and 3.6, it gives a substantial increase of the intermittency signal.

The model presented in this section to make allows a comparison between different reactions and explains the dependence of the intermittency parameters on the target and projectile mass. The quantitative analysis of different collisions needs however hints on the values of the parameters $R_{tu}$, $\tau_1$ and $\tau_2$ . We have calculated the intermittency signal for the two different assumptions about the size of the interaction region. First the size of the interaction region was taken to be equal to the size of the projectile nucleus (Figs. 3.3 and 3.4). However, this assumption about the size of the interaction region ($R_{tu} \sim A^{1/3}$) can be justified only at the Dubna and Bevalac energies [89]. For higher energies the scaling of the interaction radius with the rapidity density was

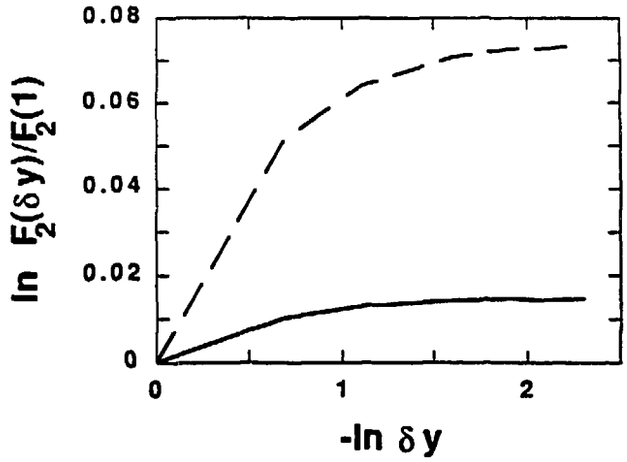


Figure 3.6: The same as in Fig. 3.5 but for $q = 1$ and $\sigma = 0.8$.

observed from B-E correlations [90] :

$$R_{tu}\ [fm]\ \simeq 0.84\ \sqrt{\frac{dn}{dy}}\ . \tag{3.10}$$

This would lead to the increasing interaction radius with the energy. The intermittency signal can be calculated, using the NA35 data on the interaction radius from the B-E correlations (Figs. 3.5 and 3.6). The estimated value of this radius, which depends strongly on the model, is $6 - 8fm$ . The freeze-out time, which depends even stronger on the model of the nonstatic source, equals $24fm/c$ in the central region for the O-Au collisions [88]. Different parameters were estimated for the symmetric S-S collisions [88] leading to a much weaker intermittency, signal independently of the details of the non-ideal effects (see Figs. 3.5 and 3.6). If these results about the length of the interaction time were confirmed then, according to the above model the intermittency signal should be much stronger for the asymmetric O-Au collisions in spite of the larger interaction volume.

The above discussed effects can be due also to some other phenomena, different from the phase-transition from the quark-gluon plasma into hadrons. In that case, even though we have no longer scale-invariant correlations with the range exclusively due to causality constraints, still the correlation range should be of the order of the radius of the interaction region. Consequently, the difference between various projectiles or impact parameters means only the different radius of a single correlated source or, due to differences in the time scales involved, a difference in the correlation length $\tau_{corr}$. On the other hand, if the correlation range is small then the collision would be better described as a superposition of independent sources with the radius equal to the correlation range and would give smaller values of the intermittency exponents for heavy projectiles than observed.

## 3.3 Interferometry measure of the spatiotemporal intermittency

The hypothesis of the spatiotemporal intermittency rises the question if such a strong correlation between the emitting sources in space-time could be observed in B-E correlations between the produced particles. This question was addressed by Białas [91]

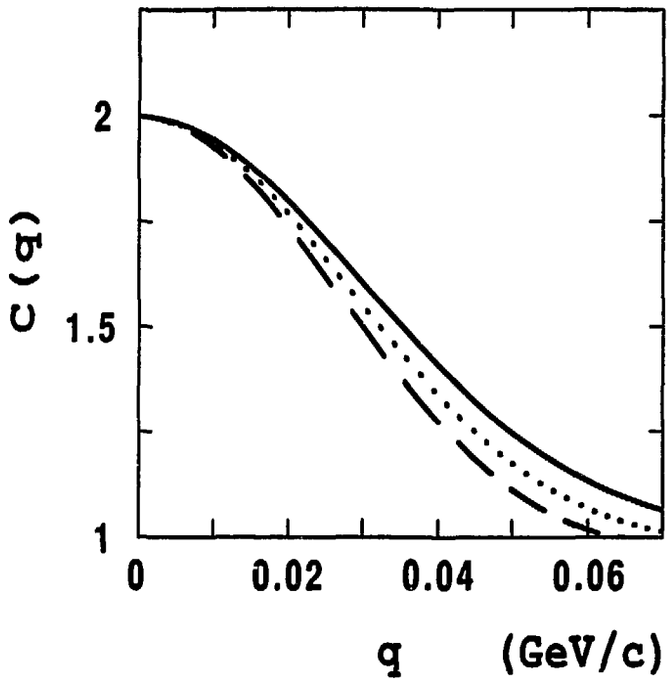


Figure 3.7: The two-particle distribution function $D_2(k)$ , as obtained from eq. (3.16), for different strength of the intermittency correlations $\nu_2 = 1.0$ (the solid line), $\nu_2 = 0.5$ (the dotted line) and for the uncorrelated sources (the dashed line).

in relation to the possible existence of fractal structures in the high energy collisions. The interferometry was first proposed by Hanbury Brown and Twiss [92] as a way to measure the spatial extension of extragalactic sources. Kopylov and Podgoretsky [93] proposed to use the interference of undistinguishable particles to measure the spatiotemporal extension of the interaction region in elementary particles or nuclear collisions. The two-particle distribution :

$$D_2(k_1, k_2) = \frac{\rho_2(k_1, k_2)}{\rho_1(k_1)\rho_1(k_2)} \tag{3.11}$$

is related to the density of the emitting sources by

$$D_2(k_1, k_2) = 1 + \mid d_1(k_1 - k_2) \mid^2 , \tag{3.12}$$

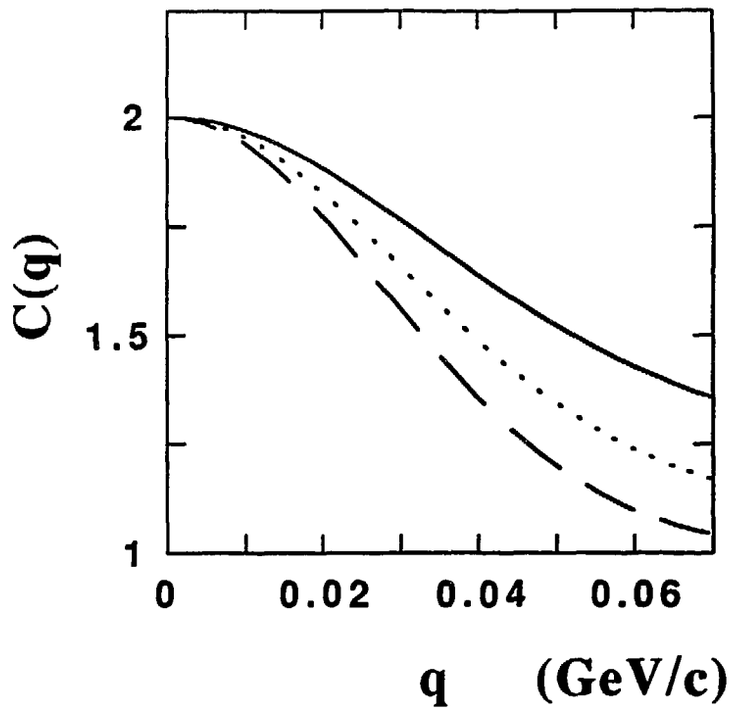


Figure 3.8: The two-particle distribution function $D_2(k)$ for the emission from a surface is shown for different strength of the intermittency correlations $\nu_2 = 1.0$ (the solid line), $\nu_2 = 0.5$ (the dotted line) and for the uncorrelated sources (the dashed line).

where $d_1(k)$ is the four-dimensional Fourier transform of the density of the sources. The experimentally measured like-signed pion correlation function, can be used to study the radius of the interaction region in the collision. The distribution function is related to the radius of the radiating region $R$ and to the mean decay width $\Gamma$ of the emitting sources :

$$D_2(k) = 1 + \frac{I(|\vec{k}\,|\,R)}{1+\omega/\Gamma}\,. \tag{3.13}$$

The derivation of the above equation assumes that the sources emit incoherently and are randomly distributed over the sphere of radius $R$. One can however discard the assumption of uncorrelated sources in space-time and use the two-pion interferometry as a tool to study the correlation of the emitting sources.

The pion interferometry can measure the possible underlying correlations of the emitting sources and its correlation length. For sources correlated in space-time eq. (3.13) takes the form :

$$D_2(k) = \frac{\int d^4x_1 \int d^4x_2\; d_2(x_1,x_2)\Big(1+cos((k_1-k_2)^\mu(x_1-x_2)_\mu)\Big)}{(\int d^4x\; d_1(x))^2}\,. \tag{3.14}$$

If the number of sources is large, then :

$$\int d^4x_1 \int d^4x_2\; d_2(x_1,x_2) \sim (\int d^4x\; d_1(x))^2\,.$$

We calculate the two-pion correlation function assuming a spherical static source in three-dimensions. The source distribution function is in this case :

$$N\frac{d_1(\vec{R}_1)d_1(\vec{R}_2)}{\mid \vec{R}_1 - \vec{R}_2 \mid^{\nu_2}} , \tag{3.15}$$

with the source density $d_1(\vec{R}) = exp(-\lambda\vec{R}^2)$ . The parameter $\lambda = 2/(\pi < R >^2)$ is given by the mean radius $< R >$ and can be related to the radius of a sphere $R_{sph}$ with the same mean radius :

$$\lambda \sim \frac{1.13}{< R_{sph} >^2} .$$

We take $R_{sph} = 3.5fm$ as in the central S-Em collisions. Then the equation for $D_2(\vec{k})$ simplifies to :

$$D_2(\vec{k}) = \frac{\int d^3\vec{R}\ exp(-\lambda\vec{R}^2/2)cos(\vec{R}\vec{k})/\mid \vec{R} \mid^{\nu_2}}{2\pi\Gamma\left(\frac{3-\nu_2}{2}\right)(2/\lambda)^{(3-\nu_2)/2}} + 1 . \tag{3.16}$$

The results for $\nu_2 = 1.0$ , $0.5$ and $\nu_2 = 0$ (uncorrelated sources) are plotted in Fig. 3.7. The different distribution are indistinguishable from the case of the randomly distributed sources according to the density $d_1(\vec{R})$ . The emission from correlated but not necessarily fractal sources, gives distribution function corresponding to an effectively smaller emitting region. In other words, if the sources are correlated then the radius of the interaction region is actually larger than the measured one, but still the effect is very small. The effect of correlated sources can be compensated by a change of about 15% of the radius of the interaction region (Fig. 3.7), and hence it cannot serve as a signal of the spatiotemporal intermittency. The difference between correlated and uncorrelated sources becomes substantial (Fig. 3.7) only in the region of large momentum difference of the pair of pions. This behaviour for large momenta reflects the presence of a singularity for small separation of sources (eq. 3.15). The signal of the singularity in this region of momenta would be probably difficult to disentangle from the background which is present in experimental studies of the correlation function. Its magnitude should be larger if the pion emission would take place on a surface. In this case, the effect of a correlated (fractal) distribution of sources could be better seen even in the Fourier transformed quantity such as the distribution function $D_2$ (Fig. 3.8).

## 3.4 Hydrodynamical evolution of the fluctuations

Another interesting problem is the behaviour of the fluctuations within the relativistic hydrodynamical models. This question was addressed in different context in ref. [94], where the diffusion of plasma droplets through the expansion was discussed. We studied the fluctuations in the $(1+1)$-D hydrodynamical model of nucleus-nucleus collisions with hadronization sources described in ref. [95]. The model was modified by the introdution of the randomness of a gaussian or fractal type in the sources. The hydrodynamical evolution of the system was studied by numerical integration of the equations of the relativistic hydrodynamics in two dimensions :

$$\partial_\mu T^{\mu\nu} = \Sigma^\nu ,$$

where $T^{\mu\nu}$ is the energy-momentum tensor:

$$T^{\mu\nu} = -pg^{\mu\nu} + (\epsilon + p)u^{\mu}u^{\nu} \ , \tag{3.17}$$

with $u^{\mu}$, $\epsilon$ and $p$ being the fluid local velocity, energy density and pressure. In the studied example we assume a simple equation of state which yields the relation :

$$\partial p = {c_s}^2 \partial \epsilon \ ,$$

with a constant sound velocity $c_s$ . Rewriting these equations in the variables:

$$\hat{t} = \frac{1}{2}\log(x^+x^-/\tau_0^2) \tag{3.18}$$

and

$$y = \frac{1}{2}\log(x^+/x^-) \ , \tag{3.19}$$

one obtains [95] :

$$(\partial_{\hat{t}} + \bar{v}\partial_y)\epsilon + (\epsilon + p)(\bar{v}\partial_{\hat{t}} + \partial_y)\Theta = \frac{\exp(\hat{t})}{\cosh(\Theta - y)}(\Sigma^0 \cosh\Theta - \Sigma^1 \sinh\Theta) \ , \tag{3.20}$$

$$(\bar{v}\partial_{\hat{t}} + \partial_y)p + (\epsilon + p)(\partial_{\hat{t}} + \bar{v}\partial_y)\Theta = \frac{\exp(\hat{t})}{\cosh(\Theta - y)}(-\Sigma^0 \sinh\Theta + \Sigma^1 \cosh\Theta) \ , \tag{3.21}$$

where

$$\Theta = \frac{1}{2}\log\left(\frac{1+v}{1-v}\right) \tag{3.22}$$

and

$$\bar{v} = \tanh(\Theta - y) \ . \tag{3.23}$$

The sources $\Sigma^{\nu}$ represent the hadrons forming after the first nucleon-nucleon collisions, so they are a kind of the retarded map of the particle production in direct collisions. For the details see ref. [95], where a functional form of the sources is proposed. All the parameters and initial conditions are taken from ref. [95] and correspond to central U-U collision with 400 GeV/A energy. Those sources are then modified by applying a random factor $\zeta(y)$ :

$$\Sigma_{\nu}^{(r)}(\hat{t}, y) = \Sigma_{\nu}(\hat{t}, y)\zeta(y). \tag{3.24}$$

and we take :

$$\zeta(y) = \exp\left(\xi(y)s - 1/2s^2\right) \tag{3.25}$$

with a normally distributed random variable $\xi(y)$, or a self-similar distribution in rapidity $\zeta(y)$. The simulation shows that the fluctuations induced by the random sources giving the initial conditions for the hydrodynamical evolution are strongly damped in the evolution. It reflects the stability of the Bjorken's solution of the two-dimensional hydrodynamical equations. The energy density is shown in Figs. 3.9 and 3.10 for three evolution times.

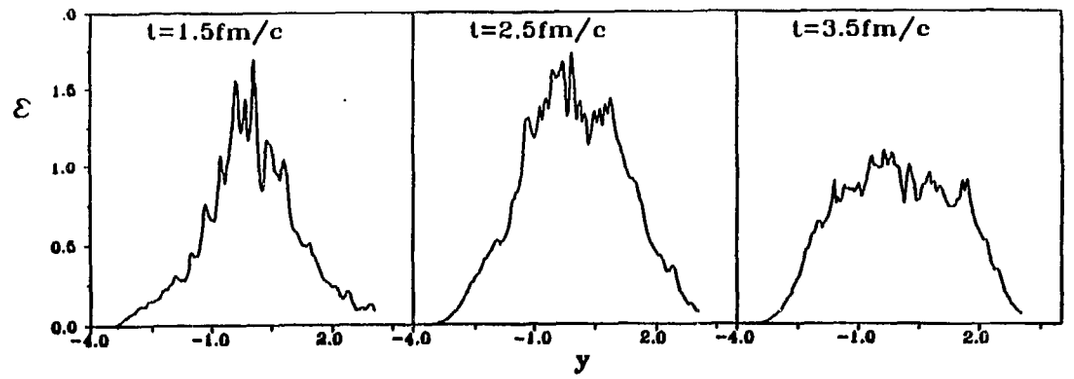


Figure 3.9: Energy density at three different evolution times for the gaussian random hadronization sources with the width $s = 0.2$ .

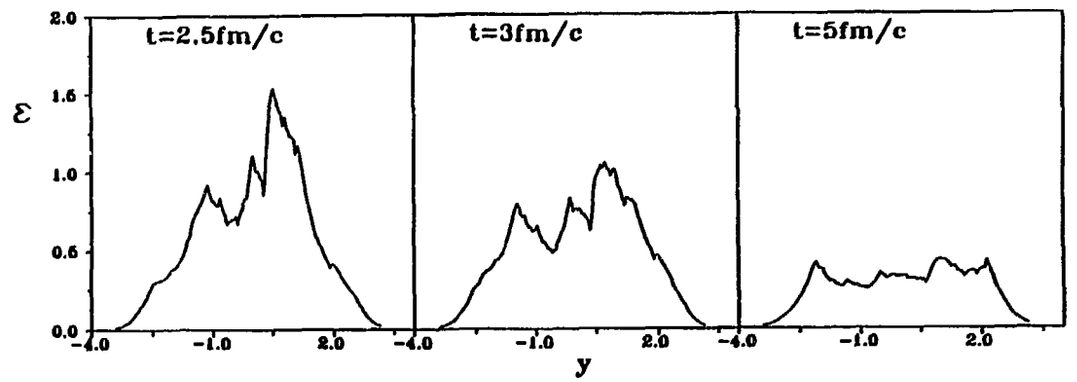


Figure 3.10: Energy density at three different evolution times for the fractal random hadronization sources.

The analysis of the moments of the energy distribution shows a systematic flattening of the distributions (Figs. 3.11 and 3.12). The fitted slopes of SFMs decrease rapidely during the hydrodynamical evolution, *i.e.* the energy distribution smoothes out and its dimension approaches 1.

This mechanism can cause another weakening of the intermittency patterns. The possible appearance of fractal or fluctuating distributions due to a random hadronization would be strongly damped during the hydrodynamical expansion. The assumed independence of the sources on time is of course the most optimistic hypothesis. If we superpose independent random sources at different times in the same rapidity interval, the effect will then be only weaker due to averaging.

evaluated. In Fig. 3.13 we show $2\nu_i/i(i-1)$ for $i = 2$ and 4 as a function of the proper time $\tau$ for three initial distributions (given by different values of the parameter p). One can observe that the intermittency slopes are strongly reduced already after the first fm/c of the evolution. At $t = 1$ fm/c the values of $F_2$ and $F_4$ correspond to 21% and 24% of their initial values respectively. The calculated time dependence of the slopes can be fitted by a power law :

$$\nu_i(t) = \nu_i(1)/t^{\gamma} , \tag{3.26}$$

with the parameter $\gamma = 1.24$ and 1.20 for the moments $F_2$ and $F_4$ respectively.

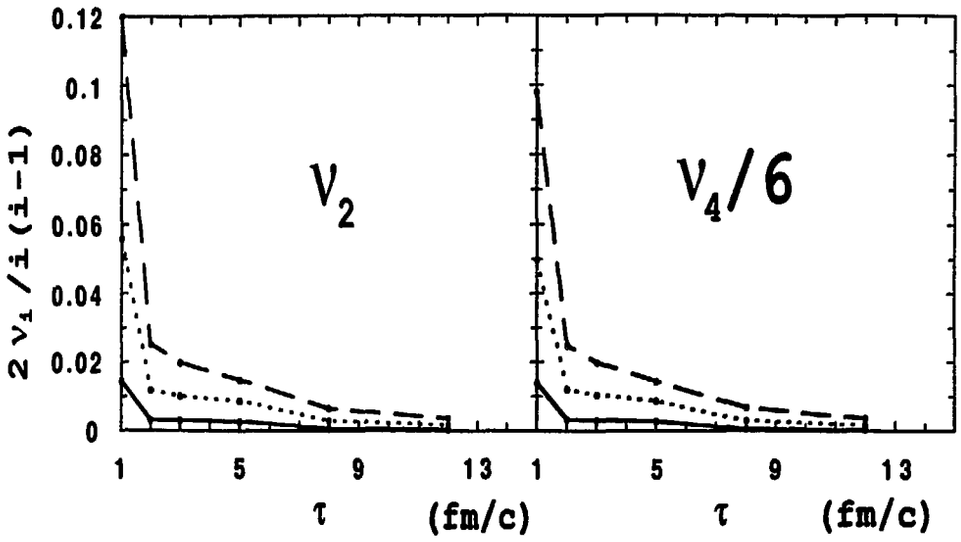


Figure 3.13: The function $\nu_i/i(i-1)$ , where $\nu_i$ is the intermittency exponent for the moment of rank $i$ , is plotted as a function of the proper time of the hydrodynamical evolution of the initially fractal energy density distributions. The results are shown for three different initial fractal distributions, $p = 0.50$ (the solid line), $p = 0.60$ (the dotted line) and $p = 0.65$ (the dashed line).

As was already mentioned, this damping of the fluctuations is a result of the stability of the $(1+1)$-D scaling solution of the perfect fluid hydrodynamics [97]. The general problem of the stability of the scaling solution in $(1+n)$-D for the relativistic viscous fluid was addressed in ref. [98] and the limits on the viscosity coefficients were found for which the scaling solution is stable. There exist however some regions of the parameters were the scaling motion becomes unstable. The authors of ref. [98], using the results of Hosoya and Kajantie [99] for the viscosity coefficients of the quark-gluon plasma, found that the stability condition given by the Reynold's number $R > 1$ is well satisfied. For example, for the initial temperature of the plasma $T = 300$ MeV , one finds $R = 7.22$ for $\alpha_s = 0.3$ and $R = 1.34$ for $\alpha_s = 0.1$ . However, the recent calculation of Baym et al. [100] predicts a larger value of the plasma viscosity and the corresponding Reynold's number is $R = 1.79$ for $\alpha_s = 0.3$ and $R = 0.33$ for $\alpha_s = 0.1$ . This value can

be even lower for a lower value of the initial temperature. According to this predicition [100], the unstable region $R < 1$ could be approached in the nucleus-nucleus collisions and could produce many unexpected results such as the increase of the fluctuations in the rapidity distributions. We have not checked numerically the damping of the fluctuations in the viscous fluid. However, taking a lower value of the sound velocity than for the ideal equation of state ($c_s = 1/\sqrt{3}\ c$), we have found a slower damping of the fluctuations durring the hydrodynamical evolution.

The turbulent origin of the fluctuations was proposed to explain the fluctuations in the distributions of galaxies in the universe [101]. However, in the case of the heavy-ion collision, the short time of the hydrodynamical evolution provides some constraint on the space extention of those fluctuations. Taking for the time of the evolution $t = 4$ fm/c and for the sound velocity $c_s = 1/\sqrt{3}\ c$ , one finds the upper limit on the extension of an eddy $r_{eddy} = 0.7$ fm (one full revolution of the eddy with the sound velocity). Larger eddies simply have no time to build up. So even if the hydrodynamical evolution of a collision would give strong fluctuations, these cannot be thought of as the fully developed turbulence in a broad range of scales.

In conclusion, the ideal hydrodynamics is damping the fluctuations very rapidly. We can deduce that if the observed multiplicity fluctuations come from the stage before or during the hydrodynamical evolution, then this evolution must be very short or the viscosity coefficients must be in the range of values where the scaling solution of relativistic hydrodynamics is unstable [98]. This means that the fluctuations are produced during the final stage of the collision, just before the freeze out, or that the hydrodynamics describing the reaction is near or in the unstable region, in the latter case it could be even the dominant source of fluctuations.

## 3.5 Intermittency and the nuclear collision dynamics

The moments of the multiplicity distributions in rapidity were analyzed in the proton-nucleus and nucleus-nucleus collisions. Assuming a local parton-hadron duality or, in the hydrodynamical model, a local correspondence between the energy density and the multiplicity of the final hadrons, the model of the spatiotemporal intermittency was studied. Here the origin of the intermittency in rapidity distributions comes from the correlations of the hadron sources in the space-time. These correlations were first studied in the context of a higher order phase-transition [52], but can be generalized to any kind of dynamically induced correlations with the correlation range of the order of the size of the system. The scale-invariant form of the correlations is most probably washed out due to :

- the projection from the 3D hyperspace of constant proper time to the 1D rapidity distributions [51, 48, 52],
- the smearing of the distribution due to non-ideal Bjorken's scaling,
- the contribution from the isotropic decay of the metastable resonances,
- the damping of the fluctuations during the hydrodynamical evolution.

So, even if the interacting system possess scale-invariant correlations, there is no reason to expect such a behaviour in rapidity distributions of the final hadrons.

The effect of the dimensional projection is crucial to explain the observed dependence of the SFMs on the projectile and on the impact parameter. The range of the correlation, which is of the order of the size of the interacting region, is a basic assumption to relate the size of the system to the magnitude of the "slopes" of the SFMs. The model presented in sect. 3.2 gives qualitatively similar relations between SFMs as observed experimentally. However, detailed comparison is difficult due to many model-dependent, non-ideal effects. We have found that physically reasonable variations of these parameters can change the resulting dependence of the SFM on the rapidity bin by a factor of $2-3$. Even more important could be the effect of non-singular components in the multiparticle distribution. Motivated by the scaling behaviour of the spin distributions of the Ising model in the thermodynamic limit [103], we have based the calculation of the SFMs on the assumption of the intermittent structure of the two-particle distribution. This could however change if the relevant variable would be the energy density $\epsilon(\vec{r})$ corresponding by some "local energy-hadron duality" to the produced hadrons. The intermittent behaviour of the energy correlator $< \epsilon(\vec{r})\epsilon(\vec{r}') > - < \epsilon(\vec{r}) >< \epsilon(\vec{r}') >$ implies then the scaling for the factorial cumulants of the produced particles. Other phenomena leading to non-singular components of the two-particle distribution could be also the contribution from the particles produced outside the space-time region undergoing the phase transition, or the contribution from events where the phase-transition does not occur.

In accordance with the considerations of this chapter, the study of the fluctuations in the multiparticle distributions provides important informations about the structure of the correlations in the collision dynamics. The detailed nature of the fluctuations in the dynamics remains however unknown and, because of many effects reducing the correlations, it cannot serve as a signal of a higher order phase-transition. Alternative mechanisms involving string interaction and rescattering, could build up correlations giving similar intermittent behaviour [85, 102]. Furthermore, a direct observation of the fractal structure in space-time through B-E correlations does not seem to be possible. However, the possible existence of the spatiotemporal intermittency should be taken into account in the analysis of the B-E correlation data especially if the emission takes place effectively from a surface. Large source composed of few strongly correlated "hot-spots" would look as a smaller source with the radius intermediate between the radius of the source and of the hot-spot. The scaling correlations are an example of the creation of such "hot-spots" on all length scales.

The considerations which were presented in this section, show the importance of the correlated evolution of the hadron sources. Hence, any mechanism aiming at a correct description of the fluctuations in the multiparticle distributions, such as the higher order phase-transition or the string interaction, must include correctly the interactions between hadron sources. The simplest way to describe phenomenologically the nontrivial interactions between the hadron sources is to introduce the space-time correlations between sources and the concept of the correlation range. The observed relations between intermittency exponents for different projectiles give us, in a model independent way, hints that the correlation range is of the order of the size of the interacting system.

# 4. Intermittency in statistical systems

The concept of scaling at the critical point of a statistical system raised very early the question about the existence of nontrivial scaling fluctuations in such systems [12]. Indeed, the scale-invariant fluctuations in the vicinity of the critical point were observed in the 2D Ising model [12]. The SFMs were calculated for a $Z_2$ symmetric definition of the number of spins in a cell [13]. On the other side, the scaling of the number of spins in a cell of a given size was shown to be related to the critical index $\eta$ of the Ising model [103]. It was also noticed that the statistical noise in the cell of $N$ spins is expected to be not of the Poissonian type but of the binomial type [104], so that a slightly different definition of the SFMs was proposed :

$$F_i = \frac{< n(n-1)\dots(n-i+1) > \ N^i}{< n >^i \ N(N-1)\dots(N-i+1)} \ . \tag{4.1}$$

The correct relation between the rise of the SFMs of the number of spins up in a cell and the scaling indices of the Ising model was recently calculated [105]. This problem was resolved for the Ising model with scaling spin correlation function and, generally, one has to find in a similar way the correct estimate of the scaling in the critical system for each particular case (SFMs, scaled factorial cumulants, central moments).

## 4.1 Intermittency in simple cellular automata

In this section the SFMs analysis of a CA system will be performed. We propose to study the fluctuations in a 1D model exhibiting an absorbing transitions between two states [106]. The 1D model has the critical properties similar to the $(1+1)$-D directed percolation and the Reggeon field theory [107]. In the simulation we follow the method of Jensen [107]. We begin the evolution from the three central sites and all the remaining sites empty ($\Phi_i^{(t=0)} = 0$). The evolution of the occupations at the next time step follows a probabilistic rule. The state of the spin $i$ depends on the state of its neighbours in the previous time step. If one defines the sum of the occupation of the spins in its neighbourhood [107] :

$$S_i^t = \sum_{j=i-4}^{i+4} \Phi_j^t \ , \tag{4.2}$$

then the evolution of the spin $i$ follows the rule :

$$\Phi_i^{t+1} = \begin{cases} 1 & \text{with probability p if } \ 3 \leq S_i^t \leq 6 \\ 0 & \text{otherwise} \end{cases} \ . \tag{4.3}$$

The critical value of the probability to survive was estimated to be $p_c = 0.7216 \pm .0002$ [107]. It was observed that this model is in the same universality class as the $(1+1)$-D directed percolation and the Reggeon field theory. It has a power-law dependence of the surviving probability $P(t)$ of an evolution on time. The dependence of the average

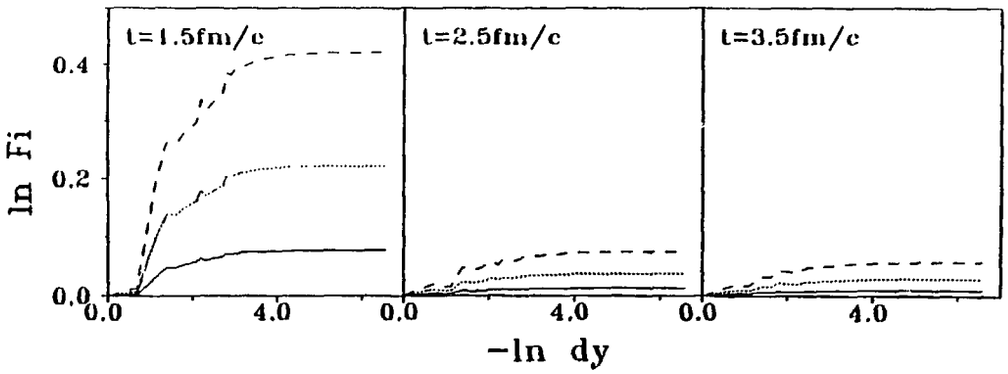


Figure 3.11: The dependence on the size of the rapidity bin $\delta y$ for the moments $F_2$ (the solid line), $F_3$ (the dotted line) and $F_4$ (the dashed line) of the distributions shown in Fig. 3.9 .

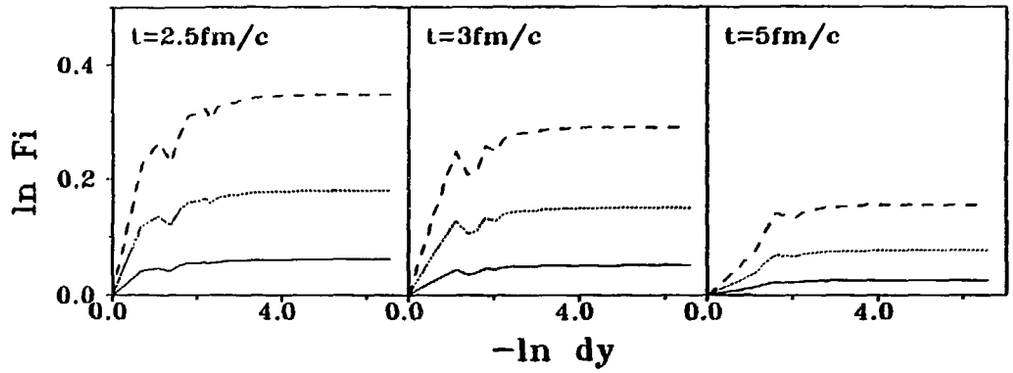


Figure 3.12: The dependence on the size of the rapidity bin $\delta y$ for the moments $F_2$ (the solid line), $F_3$ (the dotted line) and $F_4$ (the dashed line) of the distributions shown in Fig. 3.10 .

The detailed study of the damping of the fluctuations can be performed, for a simpler situation of the hydrodynamical evolution of the initially fractal distribution. For the initial distribution we take a self-similar energy density distribution in a range of rapidity scales, following the $p$-model distribution [96]. The $p$-model is equivalent to a semirandom $\alpha$-model with the number of branching $\lambda = 2$ . The probability distribution for the first random variable is $P(w_1) = 0.5\ \delta(w-1-p)+0.5\ \delta(w-1+p)$ . The second random variable is taken as $w_2 = 2 - w_1$ . For the rapidity distribution $\Theta(y)$ we take the scaling initial condition $\Theta(y, t = 0) = y$. The resulting distributions are analyzed for different times of evolution and the slopes $\nu_i$ of the moments are

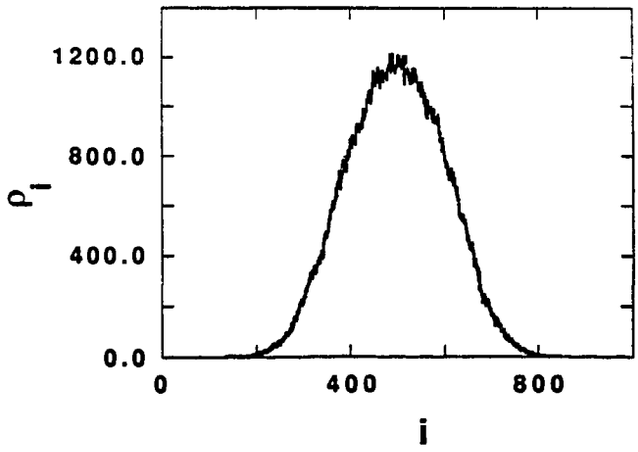


Figure 4.1: The distribution of the occupied cells after 500 time steps for the CA model (arbitrary units).

number of occupied sites $n(t)$ and of the mean-square spreading $R^2(t)$ was also found to be of that form, with the exponents consistent with those of the directed percolation :

$$P(t) \sim t^{-\delta} ,$$
$$n(t) \sim t^{\eta} ,$$
$$R^2(t) \sim t^{z} . \qquad (4.4)$$

The exponents were found to be 0.161, 0.312 and 1.272 [107]. We have tested the behaviour of the fluctuations in the distribution of occupied sites in the model for the critical surviving probability. The 1D intermittency analysis was performed for the fluctuations in the number of occupied sites after 500 time steps ( in a window of width 180 around the central site), also 1D intermittency analysis was applied to the fluctuations in the number of occupied sites in the time history of a given site (the central site $i_1 = 500$ and a shifted one $i_2 = 530$ , for the times between 320 and 500). The 2D SFM analysis in the time-space was performed for the square $410 < i \leq 590$ , $320 < t \leq 500$ . The horizontal SFMs were corrected for the shape of the single particle distribution which is not flat (Fig. 4.1). One expects an almost Gaussian profile of the percolating cone in (1+1)D [108]. The binomial type of statistical noise was assumed and the SFMs were rescaled according to eq. (4.1). The results for the SFMs $F_2$ and $F_3$ are shown in Figs. 4.2 and 4.3 . The results shown in Figs. 4.2 and 4.3 demonstrate the scale-invariance of the fluctuations induced by the local updating rule (4.3) with the critical probability $p_c$. This is related to the structure of the correlations in the percolating system. In the case of the directed percolation, the probability of cluster connectivity between two sites scales with their distance.

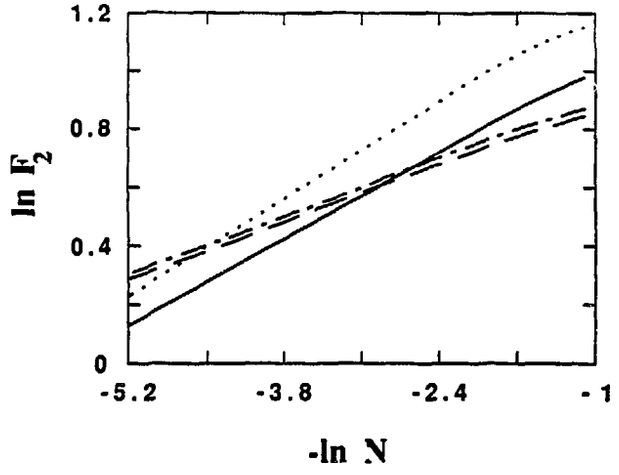


Figure 4.2: The dependence of the SFM $F_2$ on the bin size for the CA model. The dotted line represents the 1D analysis in the space dimension. The dashed line represents the 1D analysis in the time direction for the central site and the dashed-dotted line for the shifted site. The results of the 2D analysis are shown with the solid line.

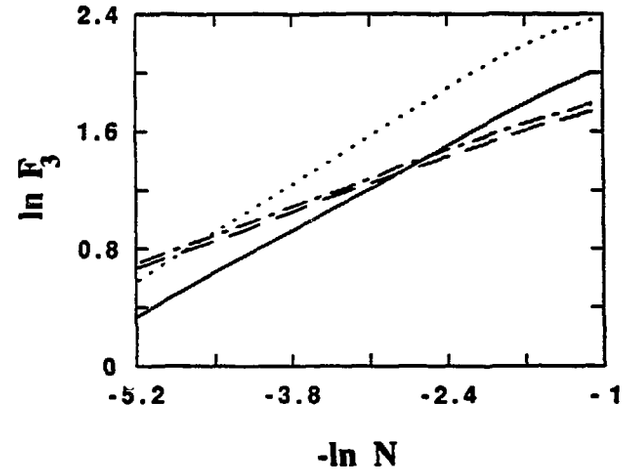


Figure 4.3: The same as in Fig. 4.2 but for $F_3$ .

The intermittency slopes for the moment $F_2$ are 0.23 for the space direction, 0.14 for the time direction and 0.21 for the 2D analysis. As one could expect, the result for the 2D analysis lies in between the two 1D values. The detailed form of the 2D correlation function is however unknown [109]. The value 0.21 for the anomalous dimension of the $(1+1)$-D cellular automaton should be compared with the value 0.19 obtained for the $(1+1)$-D directed percolation [108]. The difference can be attributed to the finite size

effect and/or to the bias due to the correction of the horizontal SFMs on the shape of the 1D distribution. Another effect is also the absence of translational invariance, which can be seen in the difference in the SFMs calculated for two different sites in the time direction (Figs. 4.2 and 4.3).

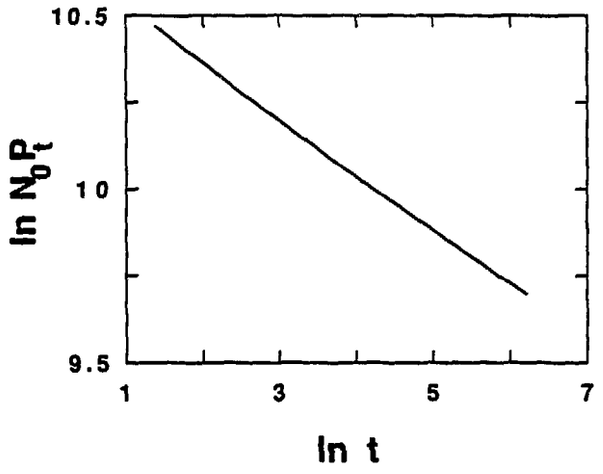


Figure 4.4: The dependence of the number of surviving evolutions of the forest fire on the number of the time steps.

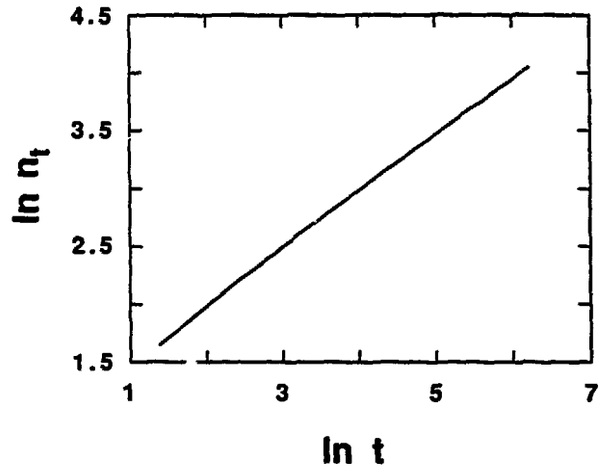


Figure 4.5: The dependence of the number of occupied sites on the number of the time steps for the forest fire model.

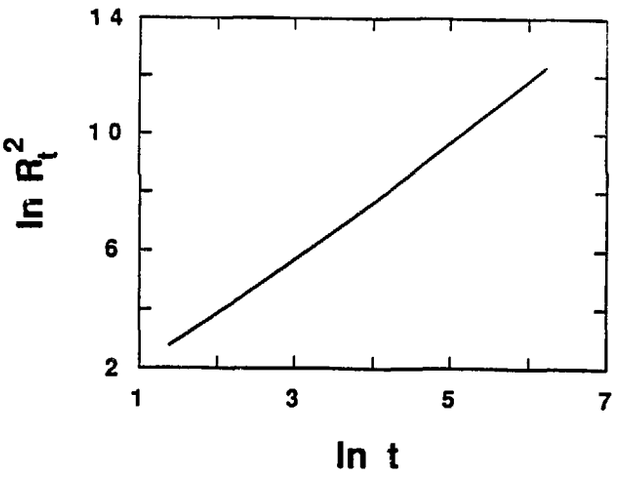


Figure 4.6: The dependence of the mean-square spread of the forest fire on the number of the time steps.

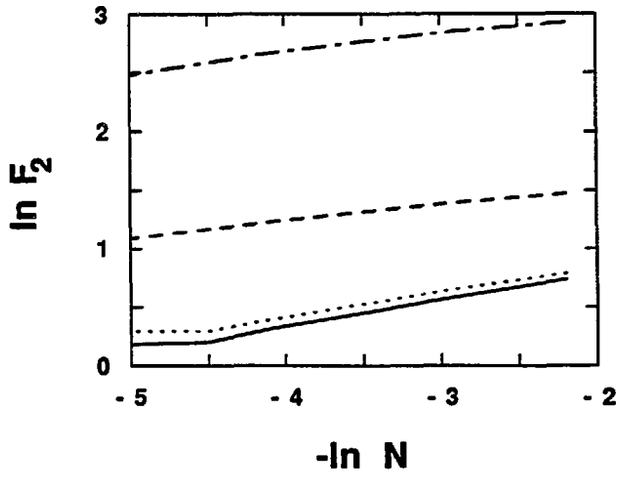


Figure 4.7: The same as in Fig. 4.2 but for the forest fire model.

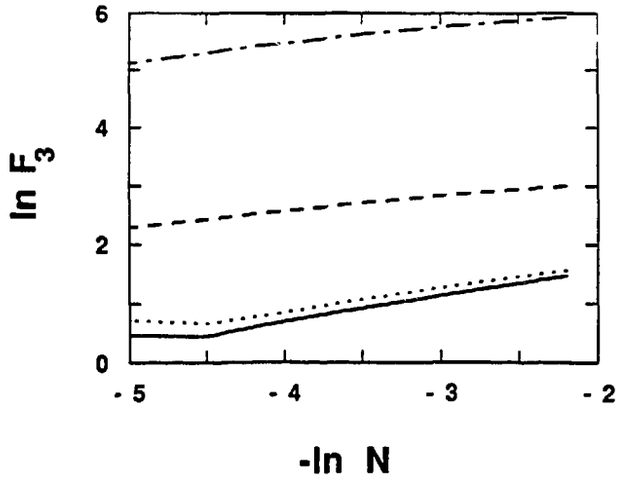


Figure 4.8: The same as in Fig. 4.3 but for the forest fire model.

We have tested the scaling properties for a directed forest fire model. In this model, the occupied site can fire in the next generation the sites $i-1, i, i+1$ , each which the probability p. The initial conditions are now $\Phi_i^{(t=0)} = 0$ except for the central site which is occupied. We have found a reasonable scaling behaviour for $p = 0.5885$. The Figs. 4.4, 4.5 and 4.6 show the dependence of the surviving probability, the number of the occupied sites and the mean-square spreading as a function of the time step.

The results follow the power-law (4.4) with the exponents equal 0.16, 0.5 and 2.0 respectively. Thus, we observe that the forest fire model is probably in a different universality class than the model discussed previously. The same SFM analysis as for the CA was performed for the forest fire model and the results are shown in Figs. 4.7 and 4.8 . The intermittency exponents equal to 0.2, 0.11 and 0.2 for the space, time direction and for the 2D analysis respectively.

## 4.2 Intermittency and clustering in the 1D lattice gas model

Dias de Deus and Seixas have calculated numerically the intermittency signal in the 1D Ising system and shown that for certain values of the parameters some of the features of the experimentally observed intermittency patterns could be reproduced [110]. Even though the 1D Ising system does not possess a critical point, it shows in some range of scales an intermittent-like behaviour which is not related to the scale invariance of the system. The intermittency in this case is not due to scale-invariant correlations with infinite correlation range and, in fact, is present on much larger scales than the scales determined by the finite (and usually small) correlation range in the 1D system.

In this section we perform the analytical study of the model of 1D lattice gas with nearest neighbour interactions, which is equivalent to the Ising model [111]. The system

consists of a lattice of N sites and at each lattice site $i$ the particle number $Y_i$ takes the values 0 or 1. The partition function for this model is given by :

$$Z = \sum_{\{Y_i\}} \exp(E \sum_{i=1}^{N} Y_i Y_{i+1} - M \sum_{i=1}^{N} Y_i) \,, \tag{4.5}$$

where the first sum denotes the sum over all possible particle distributions $\{Y_1, \ldots, Y_N\}$ with periodic boundary conditions $Y_{N+1} = Y_1$. The SFMs $F_i = < n(n-1)\ldots(n-i+1) > / < n >^i$ of the number of $n$ particles in a given bin are calculated as a function of the bin size $l$. Here $< \ldots >$ means an average over the particle configurations with the weight function given by eq. (4.5). The factorial moments of any rank can be calculated from the generating functions defined as follows :

$$G_l(x) = \frac{1}{Z} \sum_{\{Y_i\}} exp(E \sum_{i=1}^{N} Y_i Y_{i+1} - M \sum_{i=1}^{N} Y_i)\, (1+x)^{m(\{Y_i\})} \,, \tag{4.6}$$

where $m(\{Y_i\})$ is the number of particles in the bin of size $l$ for the given configuration $\{Y_i\}$ (similar analytical calculations were performed by Seixas using the two-spin correlation function [112]). The factorial moment of rank $i$ is given by the i-th derivative of $G_l$ :

$$< n(n-1)\ldots(n-i+1) >= \frac{d^i G_l(x)}{dx^i} \mid_{x=0} \,. \tag{4.7}$$

The generating functional $G_l(x)$ can be calculated using the method of the transfer matrix :

$$G_l(x) = Tr\ \sigma_0^{N-l-1} \sigma_{0x} \sigma(x)^{l-1} \sigma_{0x}^T \ / Tr\ \sigma_0^N \,, \tag{4.8}$$

with

$$\sigma(x) = \begin{pmatrix} (1+x)\, e^{E-M} & \sqrt{1+x}\, e^{-M/2} \\ \sqrt{1+x}\, e^{-M/2} & 1 \end{pmatrix} \,, \tag{4.9}$$

$\sigma_0 = \sigma(0)$ and

$$\sigma_{0x} = \begin{pmatrix} \sqrt{1+x}\, e^{E-M} & \sqrt{1+x}\, e^{-M/2} \\ e^{-M/2} & 1 \end{pmatrix} \,. \tag{4.10}$$

Denoting by $\lambda_\pm(x) = 1/2\Big((1+x)e^{E-M} + 1 \pm \sqrt{\big((1+x)e^{E-M}-1\big)^2 + 4(1+x)e^{-M}}\Big)$ the eigenvalues of $\sigma(x)$ and by $|w\pm(x)>$ the corresponding eigenvectors, one can rewrite eq. (4.8) in the thermodynamic limit $N \to \infty$ as follows :

$$G_l(x) = \frac{1}{\lambda_+^2}\Big(\Big(\frac{\lambda_+(x)}{\lambda_+}\Big)^{l-1} < w_+|\sigma_{0x}|w_+(x) >^2 + \Big(\frac{\lambda_-(x)}{\lambda_+}\Big)^{l-1} < w_+|\sigma_{0x}|w_-(x) >^2\Big) \,, \tag{4.11}$$

where $\lambda_+ = \lambda_+(0)$ and $|w_+ >= |w_+(0) >$ .

The generating functional $\bar{G}_l(x)$ for the factorial moments of the number of links in a given interval can be defined in a similar way. A link is defined as a pair of neighbouring particles, *i.e.* $Y_i = Y_{i+1} = 1$. Using the transfer matrix method, the generating functional for links can be written as :

$$\bar{G}_l(x) = Tr\ \sigma_0^{N-l} \bar{\sigma}(x)^l \ / Tr\ \sigma_0^N \,, \tag{4.12}$$

with

$$\bar{\sigma}(x) = \begin{pmatrix} (1+x)\, e^{E-M} & e^{-M/2} \\ e^{-M/2} & 1 \end{pmatrix} . \tag{4.13}$$

In the thermodynamic limit the functional $\bar{G}$ can be expressed by the eigenvalues and the eigenvectors of the transfer matrices :

$$\bar{G}_l(x) = \Big(\frac{\bar{\lambda}_+(x)}{\lambda_+}\Big)^l < w_+|\bar{w}_+(x)>^2 + \Big(\frac{\bar{\lambda}_-(x)}{\lambda_+}\Big)^l < w_+|\bar{w}_-(x)>^2 \ . \tag{4.14}$$

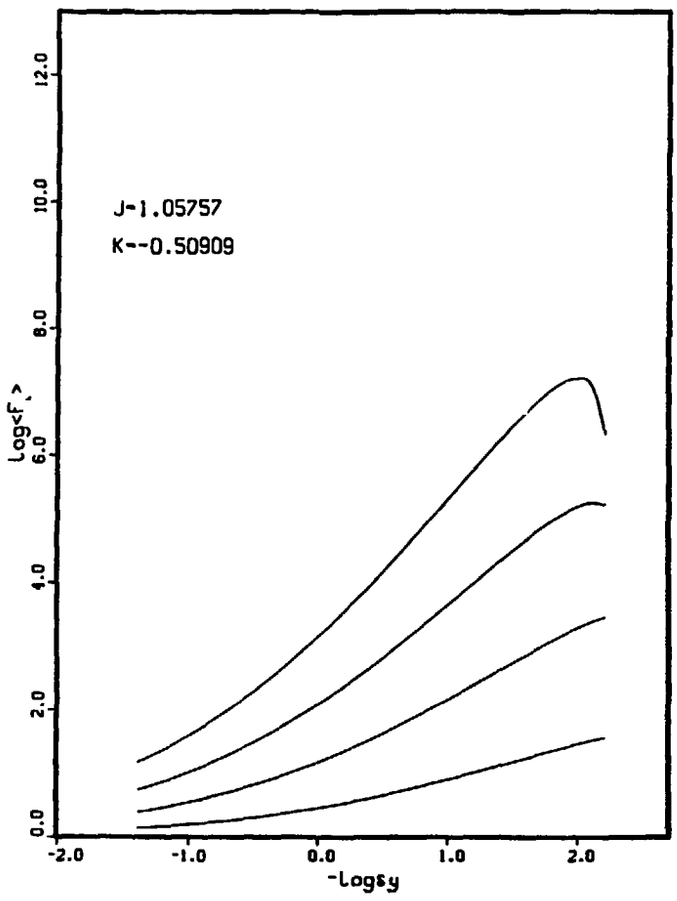


Figure 4.9: Dependence of the SFMs of the number of particles on the rapidity interval. Here the rapidity interval $\delta y = 4.0$ corresponds to the cell size $l = 561$ .

The mapping between the 1D Ising model and the 1D lattice gas model, allows us to reproduce the results of the ref. [110] in the thermodynamic limit. Using the notation of Dias de Deus and Seixas [110] the mapping between the two sets of parameters takes the form : $E = 4J$ and $M = 4J - 2K$ . Thus the parameters $J = 1.05757$ and $K = -0.50909$ correspond to $E = 4.23028$ and $M = 5.24846$ in our notation.

The mean value of the occupation number $< Y_i >= 0.0124$ should be compared to the values 0.01322, 0.01274 and 0.0126 obtained in ref. [110] for a lattice size of 256, 512 and 1024 respectively. The difference can be attributed to the finite size effect and consistently decreases with increasing lattice size.

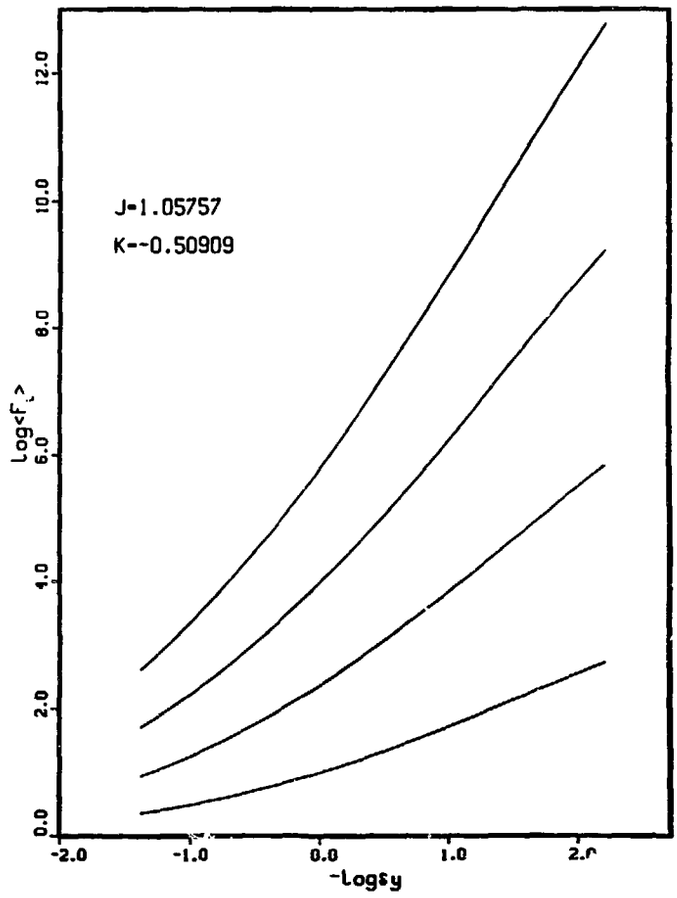


Figure 4.10: The same as in Fig. 4.9 but for SFMs of the number of links.

The dependence of the SFMs $F_i$ for $i = 2, 3, 4, 5$ on the cell size is shown in Fig. 4.9 . In order to reproduce the experimentally observed mean multiplicity $\sim$ 6.96 in the central rapidity interval [21], we have adjusted the scale of the rapidity and the scale of the length on the lattice. As a consequence of the rescaling relation $< n > = l < Y_i > \simeq 6.96$, the full rapidity interval $\Delta Y = 4$ corresponds to the length of the cell $l = 561$. The model shows intermittent-like behaviour in the whole experimentally studied range of scales. The SFMs of the number of links with the same set of parameters and for the same cell sizes are shown in Fig. 4.10 . One can see that the corresponding intermittency slopes are significantly larger than for the particle number fluctuations. The above observation demonstrate the effect of the clustering on the strength of the fluctuations. The SFMs of the clustered variables show stronger intermittency signal. This motivates the following change of the interpretation

of the model: the particles in the lattice gas correspond now to partons and the links (nearest neighbour interactions) to the observed mesons. This interpretation is only very schematic, because many partons are not linked and other are shared by two links, however it gives some insight into the mechanism of the hadron formation. Thus the intermittency signal observed in the distribution of hadrons would correspond to fluctuations in the number of produced links. These fluctuations come in some part from the clustering of partons into pairs. The interpretation of the clustering as the hadronization, leads to the conclusion that the transition from partons to hadrons enlarge the inhomogeneities which are present in the parton distribution.

The clustering of the gas of particles into links could be a simple model of the cold hadronization proposed by Van Hove [113]. This mechanism was given as a possible explanation of the intermittent behaviour. If, as proposed in ref. [113], this transition takes place as collective phenomenon involving many partons in the creation of a single hadron, then the relative increase of the fluctuations during the hadronization should be even stronger. The 1D model shows systematically stronger intermittency in all the regions of parameters where the SFMs increase. It is, however, only a very schematic and simple model of the transition from the partonic to the hadronic phase and, therefore, the quantitative conclusions would require the investigation of more realistic 3D models based on a correct gauge group structure and with the inclusion of finite mass of the quarks. The structure of the group (SU(2) or SU(3)) and the presence of quarks are known to be crucial in this issue [86]. Also an unambiguous identification of the clusters with the final hadrons is required. Finally, we would like to notice that, if this mechanism of the enhancement of the fluctuations is important, then baryons which have a more complicated structure would show stronger intermittency than mesons. The formation of baryons as topological defects in the disordered Higgs field by the Kibble's mechanism [114] could also lead to similar increase of the fluctuations in comparison to the disordered (weakly fluctuating) Higgs field.

## 4.3 The dimensional projection and the finite-size effect in critical systems

The role of dimensionality in the intermittency analysis of the high energy processes was discussed in the chapter 2. The same is true for statistical systems exhibiting intermittent behaviour. Wosiek has discussed the role of the dimensionality on the intermittency signal in critical systems [115]. He has made the comparison between the intermittency patterns on elongated cells in the 1D analysis and on square cells in the 2D analysis. To calculate the second central moment, Wosiek has used the following form of the correlation function in the vicinity of the critical point :

$$C_2(r) = e^{-r/\xi}(r/\xi)^{-2x} , \qquad (4.15)$$

where $2x$ is the critical exponent and $\xi$ is the correlation range which tends to infinity as the temperature approaches the critical value $T_c$ . He has shown that the size of the transverse dimension in the critical system [115] is important for the reduction of the intermittency signal. Moreover, in the case of the critical systems, the magnitude of this reduction increases with the elongation of the cell [115] or, for nuclear collisions,

with the transverse size of the interaction region on which we average the fluctuations [52]. In phenomenological models of the nuclear collisions, this effect may be crucial for explaining the observed dependence of the intermittency parameters on the projectile and on the impact parameter.

In chapter 3 a phenomenological model was proposed which involves a phase transition with the correlation range given only by the causality constraints [52, 64], *i.e.* the correlation range in this model is of the order of the size of the interacting system. The interpretation of the size of the transversal averaging as a new scale which is introduced in the system by the geometrical constraints on the collision, as given in that work [52, 64], goes in fact beyond some convention on the method of measurement of the intermittency patterns. The cutoff in the transverse momentum discussed in chapter 2, which is a conventional scale, has not the meaning of a physical parameter. The transverse size of the system is a physical scale built in the system, which can determine the correlations present in the system. One may therefore ask how the presence of such a finite transverse dimension influences the 1D and/or 2D intermittency analysis. It is the aim of this section to answer this question [116].

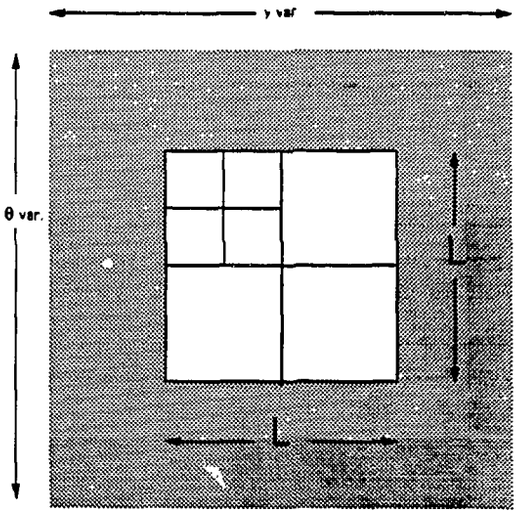


Figure 4.11: The subdivisions of the square cell in an infinite system in the 2D analysis.

To study this effect we analyze two exemplaric systems. The first one is a square cell of size L embedded in an infinite system (Fig. 4.11) and the second one is a square cell of size L embedded in an infinite strip of transverse dimension L (Fig. 4.15). The second system simulates the presence of a finite size in the critical system.

The infinite system at the critical point has an infinite correlation range and the correlation function is scale-invariant :

$$C_2(r) \sim \frac{1}{r^{2x}} \,. \tag{4.16}$$

The exponent $2x$ equals $1/4$ for the 2D Ising system [117, 103] . Assuming the appli-

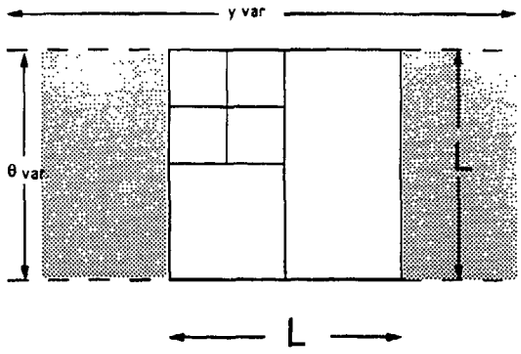


Figure 4.12: The subdivisions of the square cell in the strip geometry in the 2D analysis.

cability of the conformal invariance at the critical point, one can relate the correlation function in the z-plane :

$$C_2(z_1, z_2) = \mid w'(z_1) \mid^x \mid w'(z_2) \mid^x C_2(w(z_1), w(z_2)) \tag{4.17}$$

to the correlations in the conformally transformed geometry [118]. Using the conformal transformation:

$$w = \frac{L}{2\pi} \ln\ z \ , \tag{4.18}$$

the whole plane changes in the strip $\mid Im\ w \mid \leq L$ and the two-point correlation function becomes [118] :

$$C_2(y_1, \theta_1; y_2, \theta_2) \sim \exp -x \ln(\exp \frac{2\pi(y_1 - y_2)}{L} + \exp \frac{2\pi(y_2 - y_1)}{L} - 2\cos \frac{2\pi(\theta_1 - \theta_2)}{L}) \ . \tag{4.19}$$

For $\mid y_1 - y_2 \mid \rightarrow \infty$ this correlation attains an effective correlation range $\xi = \frac{xL}{2\pi}$ . From the correlation function one can calculate the second central moment [115] :

$$F_2^{(c)} = \frac{1}{(\Delta y)^2(\Delta\theta)^2} \int_{-\Delta y}^{\Delta y} dy_1 dy_2 \int_{-\Delta\theta}^{\Delta\theta} d\theta_1 d\theta_2 \ C_2(y_1, \theta_1; y_2, \theta_2) \ . \tag{4.20}$$

In the 2D analysis we calculate $F_2^{(c)}$ as a function of $M^2$ for $\Delta y = L/2M$ and $\Delta\theta = L/2M$ (Figs. 4.11 and 4.12). In the 1D analysis, the moment $F_2^{(2)}$ is plotted as a function of M for either $\Delta y = L/2M$ and $\Delta\theta = L/2$ (the cell is elongated transversally to the strip) or $\Delta y = L/2$ and $\Delta\theta = L/2M$ (the cell is elongated along the strip).

The dependence of the moment $F_2^{(c)}$ on the number of subdivisions of the cell is plotted in Fig. 4.13 . We find that the intermittency signal in the 1D analysis using the strip geometry differs from the signal obtained in the infinite plane. The moment calculated on cells elongated along the strip (subdivisions in the $\theta$ variable) grows slowlier than for the system of infinite size in the two directions. The reverse relation is observed when the moment is calculated on cells which are elongated transversally to the strip (subdivisions in the $y$ variable). The moment calculated in the $y$ variable and averaged over $\theta$ $(L/2 \leq \theta \leq L/2)$, grows initially even faster than in the 2D analysis.

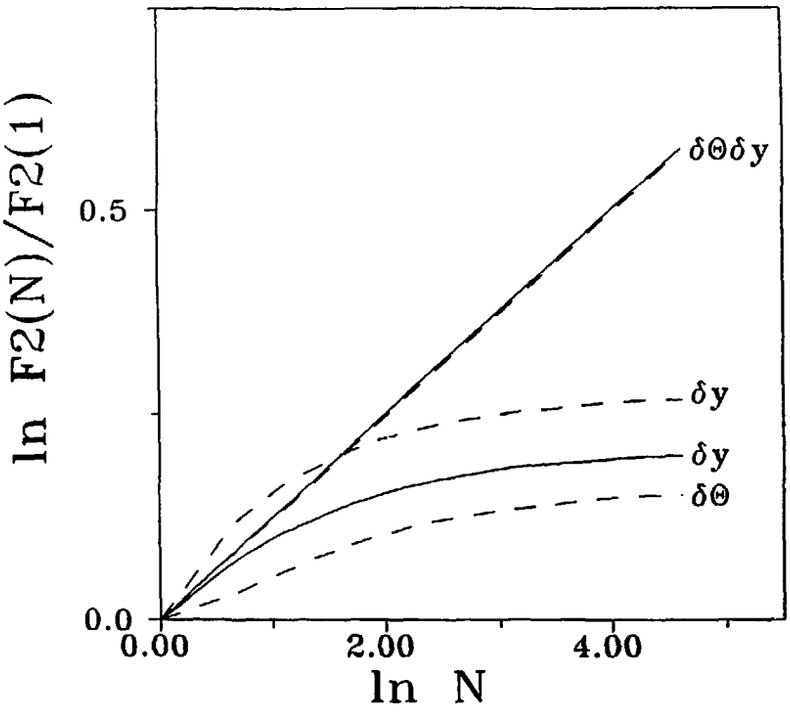


Figure 4.13: Dependence of the second SFM $F_2^{(c)}$ on the number of subdivisions of the $L \times L$ cell in the infinite strip geometry (the dashed lines) and in the infinite plane geometry (the solid lines). Moments are calculated using eq. (4.20) with $N = M^i$ where $i$ is the dimension of the intermittency analysis. All moments are normalized for the first binning.

This effect reflects the fact that the correlations in $y$ have an effective finite correlation range [118] (in our case $\xi \sim L/25$) and thus shows a faster growth in this range of M than the intermittent relation $F_2^{(c)} \sim M^x$ [115]. On the other hand, for cells smaller than the correlation range, the dependencies are asymptotically the same in all cases as one could expect when the effect of boundary conditions is negligible for small $\mid y_1 - y_2 \mid$ and $\mid \theta_1 - \theta_2 \mid$ . In this limit the correlations given by eq. (4.16) and by eq. (4.19) show the same kind of singularity. For the strip geometry the effect is the strongest one for large divisions of the cell, *i.e.* when the effective correlation range dominates the functional dependence of the moments (eq. 4.19). This feature can be clearly observed in Fig. 4.14 . Here the curves correspond to different 1D and 2D subdivisions of a cell of length $4L$ in the strip direction and $L$ in the transverse direction. So now in eq. (4.20) we have $\Delta y = 2L/M$ and $\Delta\theta = L/2M$ for the 2D analysis (Figs. 4.15 and 4.16) and $\Delta y = 2L/M$ and $\Delta\theta = L/2$ or $\Delta y = 2L$ and $\Delta\theta = L/2M$ for the 1D analysis. For the strip geometry, the initial growth of the moment, analyzed either in 2D or in 1D along the strip, is much more pronounced than seen in the analysis on square cells (Fig. 4.13). Similarly, the moment analyzed transversally to the strip grows much slowlier for the cell $L \times 4L$ than for the cell $L \times L$ . Fig. 4.14 shows the dependence of the moment $F_2^{(c)}$ in the region where the finite correlation range behaviour is dominant and hence, where the discrepancies between the two geometries

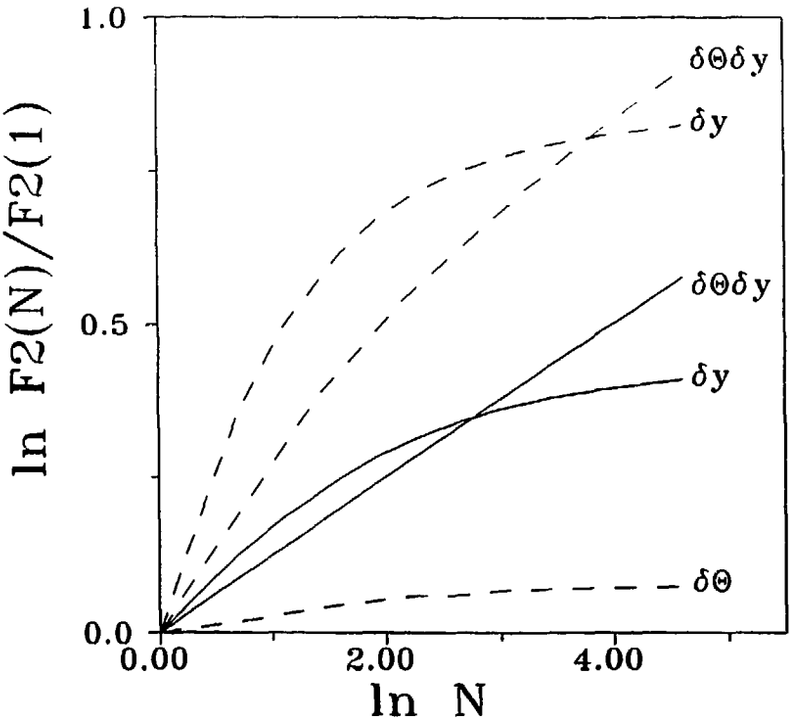


Figure 4.14: The same as in Fig. 4.13 but for a $4L \times L$ cell in the two systems.

are more pronounced. Of course, to treat the case of the $4L \times L$ cell in the strip as a quasi-one-dimensional system, its extension along the strip should be much bigger than 4L. It is obvious that these conditions are stronger and, hence, rarelier satisfied in real processes or systems than for the $L \times L$ cell. Therefore, one should be careful when applying here described intermittency analysis in square and elongated cells to realistic systems with a quasi-one-dimensional geometry. However, whenever the assumption of the infinite strip geometry is well satisfied, the simultaneous analysis on a square and on an elongated cell would be useful providing a more direct signal of finite-size effects.

As we have noticed above, the effect of an infinite strip geometry, i.e. a quasi-one-dimensionality of the system, induces some deviations from the critical scaling behaviour. These deviations are superimposed on the effect of the dimensional projection [51, 48, 52]. The projected 1D moments show different dependence on the $y$ and $\theta$ variables. The moment analyzed in the $y$ variable grows faster than the one analyzed in the $\theta$ variable. Also the moment analyzed along the strip is much more influenced by the effective finite correlation range than the projected moment in the infinite plane geometry. This effect can influence dramatically the reduction of the intermittency signal through the dimensional projection, showing a different effective correlation range than in the infinite system and a strong asymmetry in both y and $\theta$ variables. Hence, if those finite-size effects would be present in scale-invariant multiparticle production then the quantitative analysis of the dimensional projection should consider also the above observations when extracting the dimensionality and the parameters of the intermittent correlations [51, 48, 52, 49] .

We have discussed a system with finite transverse size and periodic boundary conditions. In the case of fermions, one should use antiperiodic boundary conditions. Of

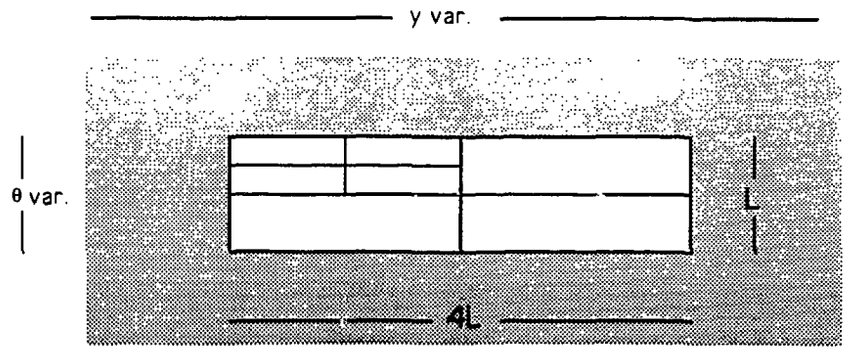


Figure 4.15: The subdivisions of the elongated cell in the infinite geometry in the 2D analysis.

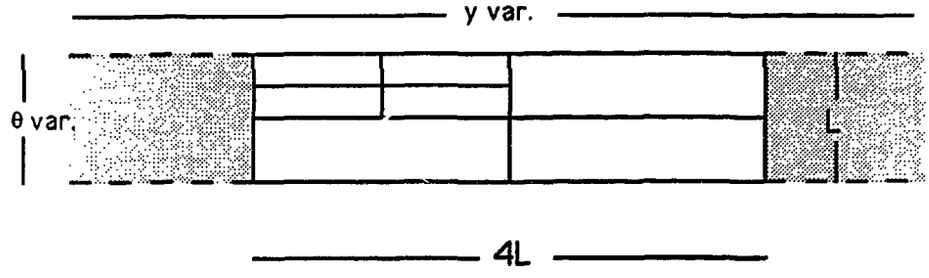


Figure 4.16: The subdivisions of the elongated cell in the 2D analysis using the strip geometry.

course, the use of antiperiodic boundary conditions changes the finite-size behaviour. For antiperiodic boundary conditions one obtains smaller effective correlation length for the same transverse size [119]. For example, in the case of the Ising system one obtains three times smaller effective correlation length [119]. This means that for the same geometry the finite-size effect should be more pronounced for fermions than for bosons.

## 4.4 Statistical systems and high energy phenomena

In section 4.2 we have analyzed the SFMs of the number of particles in a 1D lattice gas model. We have found a strong increase of the SFMs with increasing resolution. This behaviour is not related to the critical properties of the system. In fact the

two-particle correlation function is :

$$< Y_i Y_j > - < Y_i >< Y_j > = \frac{e^{-M}}{e^{-M} + (\lambda_+ - 1)^2} \left(\frac{\lambda_-}{\lambda_+}\right)^{|i-j|}$$
$$\sim \exp(-|i-j|/\xi) \,, \qquad (4.21)$$

where $\xi = 1/\ln(\lambda_+/\lambda_-)$ is the correlation length in units of the lattice size. For the parameters for which the SFMs are shown in Fig. 4.9, the correlation length is about 1.5 . The strong dependence of the SFMs on the resolution is due to the short range correlations which are integrated over a much broader range of scales. Note that this increase of the SFMs appears in a different range of rapidity separations than for the parametrization of refs. [6, 7], where the correlation range was of the order of one unit in the rapidity. Consequently, the slopes are much more important in the range of separations discussed here than in the experimental results in high energy collisions and in the fits of refs. [6, 7]. Moreover, unlike in the high energy intermittency analysis, the slopes of the higher moments are linear in the rank of the moment. This, however, does not exclude the possibility that such short range correlations are but one component of the whole $n$-particle distribution function and that the mixing of two components would give approximately the experimental slopes [120], *i.e.* smaller but faster than linear rise of the intermittency slopes with the rank of the moment.

Another feature of the critical systems is that the scaling properties are often not present in the two-field average $< \sigma(\mathbf{r})\sigma(\mathbf{r}') >$ but rather in the two-field cumulant $< \sigma(\mathbf{r})\sigma(\mathbf{r}') > - < \sigma(\mathbf{r}) >< \sigma(\mathbf{r}') > \sim |\mathbf{r} - \mathbf{r}'|^{-\nu}$. An exemple of such an observable is the number of spins up in the Ising system, for which the resulting relation of the SFMs to the scaling properties of the critical Ising system are given in ref. [105]. Different definitions of the moments give very different results in finite systems. The CA models studied in sect. 4.1 and the percolation models exhibit scaling in the SFMs. This means that the scaling in these models occurs in the two-point occupation probability or in the two-point connectivity on the percolating cluster. The problem of the correct observable to measure the scaling properties in small discrete systems has not a general solution and in each case separately one should carefully look for the correct scaling observable.

The long distance limit in which one studies scaling in statistical systems gives, by convexity, different conditions on the scaling indices :

$$\nu_i/i \leq \nu_j/j \qquad \text{for} \qquad i \geq j \qquad (4.22)$$

than in the multiparticle phenomenology [121]. The equality sign in (4.22) is true for ordered systems, like the Ising model, whereas the inequality is true for disordered systems having an infinite hierarchy of exponents like e.g. the random Ising system. The detailed structure of the correlation functions in finite and anisotropic systems was discussed in the model of a finite conformal critical system. The resulting conclusions are too schematic to be directly applied to the high energy phenomenology. This could be however an approach in studies of the detailed structure of the three momentum distribution functions. In particular such issues as the role of the $p_T$, $y$ variables and the $p_T$-dependence could be studied in such examples. Another example which could give insight into this problem is the relation of the directed vs undirected percolation model [109].

# 5. Closing discussion

The SFM analysis allows to study the multiparticle densities on small scales in the momentum space. This method of studying the high energy collisions can learn us about the mechanisms of the multiparticle production and hadronization. Several experimental groups analyzed the fluctuations in the particle distributions on small distances in the rapidity or, more generally, in the phase-space. The experimental results of the 2D and 3D analysis show a growth of the fluctuations with the resolution. This kind of behaviour is similar to the one observed in the classical turbulence and in the chaotic attractors. This observation motivates the very attractive hypothesis that similar multifractal structures may be present in the multiparticle dynamics. The presence of such fractal multiparticle distributions should be manifested by a power-law increase of the SFMs with the resolution for small phase-space cells. This concept was at the origin of a big activity in this field resulting in a good phenomenological understanding of the features of such self-similar structures. The results presented in this work were a part of these studies. On the other hand, the understanding from the "first principle" of the origin of the self-similar structures in multiparticle densities and in particular, the relation of this phenomenon to the fundamental properties of the theory of strong interactions is still missing.

In the approach proposed by Białas and Peschanski, the particle production is viewed as a multiplicative random cascade. The mechanism of the self-similar cascade could reproduce the basic features of the multiparticle final state [2, 3]. The most important prediction of the cascade model (the $\alpha$-model) is the scaling of the SFM with the resolution. This simple cascading mechanism explains how the multiparticle distributions of a very special, self-similar type are build up.

The recent SFM data in 3D momentum space for the $\mu$-$p$, $\pi^+/K^+$-$p$ and nuclear collisions seem to indicate that the scaling correlations are only a part of the whole multiparticle distribution [37]. This would be difficult to understand in the language of $\alpha$-model, and it would mean that the cascade correlates only some of the produced particles. At the origin of stronger than power-law fluctuations for small bins, could be the fluctuations in the hadronization, similar to the fluctuations in the links distribution discussed in sect. 4.2. One should subtract these hadronization fluctuations in order to find the unperturbed intermittent behaviour in high energy collisions. Note, however, that the FSS analysis indicates that the system of produced particles has a scaling multiparticle distribution in some higher dimensional space for hadron-hadron collisions. This issue still needs more experimental statistics and a better resolution in the rapidity.

As we already mentioned, the analysis performed in this work which was motivated by the analogy with classical multifractals, was based mainly on the assumption of the existence of the scale-invariant multiparticle distribution. Obviously, the assumption of the scale-invariance of the multiparticle distributions implies intermittency in the SFMs similarly as in the $\alpha$-model. In fact, the scale-invariant parametrization of the multiparticle distributions is equivalent to the $\alpha$-model prediction in many features (sects. 2.2 and 2.3). One of these features is the behaviour in the dimensional projec-

tion. The dimensional projection removes the singularities from the full-dimensional multiparticle distribution leading to the experimentally observed flattening of the dependence of the SFMs on the bin width in rapidity. The most obvious way around this problem is to perform the analysis in the 3D momentum space. Another possibility is given by the FSS analysis of the 1D SFM data (sect. 2.2). The FSS, which is the remnant of the underlying scaling-law, allows to extract the intermittency parameters of the full-dimensional scaling multiparticle distributions. Another of the common predicitions of the $\alpha$-model and of the scaling multiparticle distributions is the bin width independence of the SFCs and the scaling in the bin to bin distance. These predictions are similar also for the SFCs of the dimensionally projected denstities and are consistent with the experimental data.

The analysis of the structure of the higher order correlations in the $e^+e^-$ annihilation data of DELPHI Collaboration teaches us that the approach aiming at a simple parametrization of the $n$-particle cumulants is unsatisfactory (sect. 2.4). The multiplicity distributions in rapidity intervals were studied in the NB scheme, similar to the linked-pair-approximation and in the log-normal scheme of the multiparticle correlations. None of these schemes reproduce the DELPHI $e^+e^-$ data on SFMs in rapidity. On the other hand, as discussed in sect. 2.4, the $\alpha$-model can reproduce the shape of the multiplicity distribution both at large and small rapidity intervals. Thus, due to the correspondence between the $\alpha$-model and the scale-invariant distributions, this indicates that the self-similar parameterization of the multiparticle densities should be used instead of the correlation schemes used in sect. 2.4. However, unlike in the $\alpha$-model, there is no way in this description of relating the intermittency indices of different orders. Thus, the problem of finding a simple scheme of higher order multiparticle distribution has not a consistent solution.

For the hadron-hadron collisions the structure of the multiparticle distributions is not resolved and, formally, this structure can be changed by the independent superposition of intermittent sources [8], making the search for a simple parametrization more difficult. Moreover, one can imagine different mechanisms of fluctuations for the soft and hard production. This makes the assumption of the self-similar cascade models more doubtful for the hadron-hadron collisions. In this context, the FSS which was found in the NA22 data for $K^+/\pi^+$-$p$ collisions is very intriguing (sect. 2.2). The results of the FSS analysis for the NA22 data mean that the underlying multiparticle productions could have a simple structure in a higher dimensional space, of which the remnant is seen in the FSS of the SFMs in rapidity. The observation of the FSS provides an argument in favour of the hypothesis that the critical behaviour of the Reggeon field theory in rapidity-impact parameter space could by at the origin of the intermittency phenomena in hadron-hadron collisions. Moreover, the FSS analysis allows to test such hypothesis for which the relevant variables are not accessible experimentally.

The study of fluctuations in nuclear collisions indicates perhaps some nonlinear effect, such as a phase-transition or some regime of strongly interacting fragmenting strings. Such a nonlinear effect is needed in order to reproduce the dependence of the strength of the fluctuations on the mass of the target and projectile nuclei. We have reproduced qualitatively this dependence in a model of the spatiotemporal intermittency. The simple structure of the singular two-particle distribution was used as input for the space-time density in the interaction region of the nuclear reaction (chapter 3). This

kind of multiparticle distributions is expected to be present at the critical point of a statistical system. The observable fluctuations in rapidity distributions resulting from such singular space-time correlations were also discussed. The results allow to check qualitatively the dependence of the intermittency signal on the size of the target and projectile nuclei. This approach reproduces approximately the observed dependence, which is different than the up to now discussed $\frac{1}{dN/dy}$ scaling. The analysis of the fluctuations shows that a realistic model of ultrarelativistic collisions cannot be based on independent nucleon-nucleon collisions. The interaction between the fragmenting objects is crucial to reproduce the projectile and target dependence of the intermittency signal. In the model of sect. 3.2 this feature is due to the large correlation range of the order of the size of the interaction region. However, there is up to now no evidence that such long range correlations should be scale-invariant. The relatively strong intermittency signal observed in nuclear collisions limits the applicability of the ideal relativistic hydrodynamics in the description of the collision dynamics.

The study of SFMs in statistical systems is less interesting because, unlike in the intermittency studies in high energy collisions, one is interested in the scaling in the long distance limit. Thus, the method of SFM is not crucial in removing the statistical noise. The analysis of such systems can learn us, however, about the features of the SFM method. To illustrate the SFM analysis in the statistical systems we studied two simple CA models. For these models, we found scaling in the SFM analysis separately in the time and space directions and also in the 2D space-time analysis. We have calculated the SFMs for a noncritical 1D lattice gas model. The SFMs show an intermittent-like behaviour caused by correlations present at very small scales. This shows that the SFMs are sensitive to such non-scaling correlations and that it is better to use the SFCs which are not contaminated by the small scale correlations. We found in this model that the SFMs were larger for the links than for the particles. This can be an indication of the mechanism by which the fluctuations can build up in the scenario of the cold hadronization. The study of the conformally invariant critical systems can also be an indication of the behaviour of the SFMs in the finite system. The existence of such a finite scale changes the correlation function in 2D and in the projected distributions. This introduces an asymmetry in the projected distributions if the system has asymmetric boundary conditions. This is only one of such features, which one can also expect in the high energy phenomenology if the strong interactions possess conformal invariance in position space at small scales [122].

The study of structures in the multiparticle production at small momentum scale is very interesting, and using the method of the SFMs or SFCs this study is now possible. However, these structures should be analyzed with much care because of many difficulties, of which some have been discussed in this work. The SFM or SFC method is a powerful method of analyzing the multiparticle correlations at small scales. Using the SFM method it was demonstrated for the first time that interesting phenomena occur at small distances in the momentum. The study of those small distance correlations could give insight into the hadronization mechanism. Another objective is the demonstration of some scale-invariant structure in the multiparticle production. This issue is still not clear experimentally and its study is more difficult. In this work we analyzed the features that should possess such a scale-invariant distribution in multiparticle production both in elementary particle and in nuclear collisions. Most of the predictions

of the scale-invariant multiparticle distributions are qualitatively confirmed by the experiment. The detailed quantitative analysis still needs to be done. It requires from the experiment an unambiguous extraction of the parameters of intermittency and from the theory we need a calculation of the scaling indices.

# List of Figures

# List of Tables

# Bibliography


[1] B. Mandelbrot, J. Fluid. Mech. **62** (1974) 719;
U. Frish, P. Sulem and M. Nelkin, J. Fluid. Mech. **87** (1978) 719.

[2] A.Białas and R.Peschanski, Nucl. Phys. **B273** (1986) 703.

[3] A.Białas and R.Peschanski, Nucl. Phys. **B308** (1988) 857.

[4] D. Schertzer and S. Lovejoy, Selected papers from 4-$^{th}$ International Symposium on Turbulent Shear Flows, Karlsruhe University (1983), Eds. L.J.S. Bradbury et al., Springer, 1984.

[5] A.H.Mueller, Phys. Rev. **D4** (1971) 150.

[6] P.Carruthers and I.Sarcevic, Phys. Rev. Lett. **63** (1989) 1562

[7] A. Capella, K. Fiałkowski and A. Krzywicki, Phys. Lett. **B230** (1989) 149;
A. Capella, K. Fiałkowski and A. Krzywicki, in Festschrift L. Van Hove, eds. A. Giovannini and W. Kittel, World Scientific, Singapore, 1990.

[8] H.C. Eggers, PhD Dissertation, University of Arizona (1991).

[9] P. Carruthers, H.C. Eggers and I. Sarcevic,Phys. Rev. **C44** (1991) 1629.

[10] R. Peschanski, Nucl. Phys. **B327** (1989) 144;
A. Białas and K. Zalewski, Phys. Lett. **B238** (1990) 413;
Ph. Brax and R. Peschanski, Nucl. Phys. **B346** (1990) 65;
*ibid.* **B353** (1991) 165.

[11] A.Białas and R.C.Hwa, Phys. Lett. **B253** (1991) 436.

[12] J.Wosiek, Acta Phys. Pol. **B19** (1988) 863.

[13] B. Bambach, J. Fingberg and H. Satz, Nucl. Phys. **B332** (1990) 629;
S. Gupta, P Lacock and H. Satz, Nucl. Phys. **B362** (1991) 583.

[14] (TASSO Collab.), W.Braunschweig et al., Phys. Lett. **B231** (1989) 548.

[15] (DELPHI Collab.), P. Abreu et al., Phys. lett. **B247** (1990) 137.

[16] (ALEPH Collab.), D. Abbaneo et al. , CERN preprint (1991) CERN-PPE/91-121.

[17] (OPAL Collab.) M.Z. Akrawy et al., Phys. Lett. **B262** (1991) 351.

[18] (CELLO Collab.), H.-J. Behrend et al. , Phys. Lett. **B256** (1991) 97.

[19] I.Derado, G. Jancso, N. Schmitz and P. Stopa, Z. Phys. **C47** (1990) 23.

[20] L. Verluyten et al., Phys. Lett. **B260** (1991) 456.

[21] (NA22 Collab.), I.V.Ajinenko et al., Phys. Lett. **B222** (1990) 306;
*ibid.* **B235** (1990) 373.

[22] (NA22 Collab.), N.M. Agababyan et al., Phys. Lett. **B261** (1991) 165.

[23] (NA22 Collab.), V.V. Aivazyan et al., Phys. Lett. **B258** (1991) 487.

[24] (UA1 Collab.), C.Albajar et al., Nucl. Phys. **B345** (1990) 1.

[25] J.B. Singh and J.M. Kohli, Phys. Lett. **B261** (1991) 160.

[26] (NA22 Collab.), F. Botterweck et al., Z. Phys. **C51** (1991) 37.

[27] (KLM Collab.), R. Hołyński et al., Phys. Rev. Lett. **62** (1989) 733.

[28] (KLM Collab.), R.Hołyński et al., Phys. Rev. **C40** (1989) 2449.

[29] (EMU01 Collab.) M.I. Adamovich et al. , Phys. Rev. Lett. **65** (1990) 412.

[30] (EMU01 Collab.), M.I. Adamovich et al. , Z. Phys. **C49** (1991) 395.

[31] I. Derrado (NA35 Collab.), Proc. Ringberg Workshop on "Multiparticle production, fluctuations and fractal structure", Ringberg, FRG, June 1991, eds. R. Hwa, W. Ochs and N. Schmitz, World Scientific, Singapore, to be published.

[32] P.L. Jain and G. Singh, Phys. Rev. **C44** (1991) 854.

[33] E. Gładysz-Dziaduś, Mod. Phys. Lett. **A4** (1989) 2553.

[34] A. De Angelis and N. Demaria (DELPHI Collab.), Proc. Ringberg Workshop on "Multiparticle production, fluctuations and fractal structure", Ringberg, FRG, June 1991, eds. R. Hwa, W. Ochs and N. Schmitz (World Scientific, Singapore), to be published.

[35] I. Derrado et al., MPI preprint MPI-PhE/91-08.

[36] W. Kittel (NA22 Collab.), Proc. Ringberg Workshop on "Multiparticle production, fluctuations and fractal structure", Ringberg, FRG, June 1991, eds. R. Hwa, W. Ochs and N. Schmitz, World Scientific, Singapore, to be published.

[37] K. Fiałkowski, Phys. Lett. **B272** (1991) 139.

[38] P. Carruthers and Shih, Int. J. Mod. Phys., **A2** (1987) 1447.

[39] T. Takagi, Phys. Rev. Lett. **53** (1984) 427.

[40] K.Fiałkowski, B.Wosiek and J.Wosiek, Acta Phys. Pol. **B20** (1989) 639.

[41] A. Białas and M. Gazdzicki, Phys. Lett. **B252** (1990) 483;
W. Ochs, Z. Phys. **C50** (1991) 379.

[42] R. Peschanski, Proc. Santa Fe Workshop on "Intermittency in High Energy Collisions", Eds. F. Cooper, R.C. Hwa and I. Sarcevic, World Scientific, Singapore, 1991.

[43] A. Białas and K. Zalewski, Phys. Lett. **B228** (1989) 155.

[44] P. Bożek and M. Płoszajczak, Phys. Lett. **B271** (1991) 243.

[45] D. Seibert and S. Voloshin, Phys. Rev. **D43** (1991) 119.

[46] K. Haglin and D. Seibert, Phys. Lett. **B 273** (1991) 211.

[47] R. Peschanski and J. Seixas, CERN Preprint CERN-TH-5903/90.

[48] A. Białas and J. Seixas, Phys. Lett. **B250** (1990) 161.

[49] P. Bożek and M.Płoszajczak, Phys. Lett. **B254** (1991) 502.

[50] W.Ochs and J.Wosiek, Phys. Lett. **B214** (1988) 617.

[51] W. Ochs, Phys. Lett. **B247** (1990) 101.

[52] P. Bożek and M. Płoszajczak, Phys. Lett. **B251** (1990) 623.

[53] P. Bożek and M. Płoszajczak, GANIL Preprint, GANIL P-91-23.

[54] (UA5 Collab.), R.E. Ansorge et al., Z. Phys. **C 37** (1988) 191;
(UA5 Collab. ), G.J. Alner et al., Z. Phys. **C 33** (1986) 33;
Phys. Rep. **154** (1987) 251.

[55] L.M.Barbier et al., Phys. Rev. **D37** (1988) 1113.

[56] Ph. Brax and R. Peschanski, Saclay preprint SPhT/91-008.

[57] (NA22 Collab.), M. Adamus et al., Phys. Lett. **B185** (1987) 200.

[58] M.E. Fisher, Proc. Int. School of Physics "Enrico Fermi", Varenna, Italy, 1970, edited by M.S. Green ,Academic , New York, 1971.

[59] A. Białas, in Festschrift L. Van Hove, eds. A. Giovannini and W. Kittel, World Scientific, Singapore, 1990.

[60] P. Lipa and B. Buschbeck, Phys. Lett. **B223** (1989) 465.

[61] D. Seibert, Phys. Lett. **B240** (1990) 215.

[62] R. Peschanski, Joint Int. Lepton-Photon Symposium, Europhysics Conference on "High Energy Physics", Geneva, Switzerland, August 1991, Saclay Preprint SPhT/91-175.

[63] H.C. Eggers, P. Carruthers, P. Lipa and I. Sarcevic, Phys. Rev. **D44** (1991) 1975.

[64] P. Bożek and M. Płoszajczak, Phys. Rev. **C44** (1991) 1620.

[65] A. Białas and R. Peschanski, Phys. Lett. **B207** (1988) 59.

[66] N.Schmitz, in Festschrift L. Van Hove, eds. A. Giovannini, W. Kittel, World Scientific, Singapore, 1990.

[67] B. Buschbeck, P. Lipa and R. Peschanski, Phys. Lett. **B222** (1988) 788.

[68] E.A. De Wolf, Acta Phys. Pol. **B21** (1990) 611.

[69] L.Van Hove, Phys. Lett. **B242** (1990) 485.

[70] L. Van Hove, Physica **147A** (1987) 19.

[71] R. Szwed and G. Wrochna, Z. Phys. **C 47** (1990) 449.

[72] Ya.B. Zel'dovich, S.A. Molchanov, A.A. Ruzmaikin and D.D. Sokolov, Zh. Eksp. Teor. Fiz. **89** (1985) 2061.

[73] J.M. Alberty and A. Białas, Zeit. Phys. **C50** (1991) 315.

[74] P. Brax and R. Peschanski, Phys. Lett. **B253** (1991) 225.

[75] A. Białas, B. Błeszyński and W. Czyż, Nucl. Phys. **B111** (1976) 461.

[76] A. Białas, W. Czyż and L. Leśniak, Phys. Rev. **D25** (1982) 2328.

[77] Y.P. Chan, D. Kiang, T. Ochiai and K. Young, Can. J. Phys. **68** (1990) 145.

[78] C. Wei-qin and L. Bo, Z. Phys. **C42** (1989) 337.

[79] H. Heiselberg, G. Baym, B. Blättel, L. Frankfurt and M. Strikman, Phys. Rev. Lett. **67** (1991) 2946.

[80] J. Ftacnik, K. Kajantie, N. Pisutova and J. Pisut, Phys. Lett. **B188** (1987) 279.

[81] T. Ochiai, Phys. Lett. **B206** (1988) 535.

[82] A. Capella, J. Kwieciński and J. Tran Thanh Van, Phys. Lett. **B108** (1982) 347;
A. Capella, C. Pajares and A.V. Ramallo, Nucl. Phys. **B241** (1984) 75.

[83] B. Nilsson-Almqvist and E. Stenlund, Comp. Phys. Comm. **43** (1987) 387.

[84] L. Van Hove, Nucl. Phys. **A518** (1990) 389.

[85] B. Andersson and P. Henning, Nucl. Phys. **B355** (1991) 82.

[86] A. Patel, Phys. Lett. **B139** (1984) 394;
L. Van Hove, Z. Phys. **C27** (1985) 135.

[87] S.S. Padula and M. Gyulassy, Nucl. Phys. **B339** (1990) 378.

[88] M. Lahanas, PhD Dissertation, Frankfurt University (1991), GSI-Report GSI-91-05.

[89] J. Bartke and M. Kowalski, Phys. Rev. **C** (1984) 1341.

[90] W.A. Zajc, Nucl. Phys. **A525** (1991) 315c.

[91] A. Białas, Nucl. Phys. **A525** (1991) 345c.

[92] R. Hanbury-Brown and R.Q. Twiss, Nature **177** (1957) 27.

[93] G.I. Kopylov and M.I. Podgoretsky, Sov. J. Nucl. Phys. **15** (1972) 219;
G.I. Kopylov and M.I. Podgoretsky, Sov. J. Nucl. Phys. **19** (1974) 215;
G.I. Kopylov, Phys. Lett. **B50** (1974) 572.

[94] H. von Gersdorff, M. Kataja, L. McLerran and P.V. Ruuskanen, Phys. Rev. **D34** (1986) 794.

[95] K. Kajantie, R. Raitio and P.V. Ruuskanen, Nucl. Phys. **B222** (1983) 152.

[96] C. Meneveau and K.R. Srennivasan, Phys. Rev. Lett. **59** (1987) 1424.

[97] G. Baym, B.L. Friman, J.-P. Blaizot, M. Soyeur and W. Czyż, Nucl. Phys. **A407** (1983) 541.

[98] H. Kouno, M. Marauyama, K. Saito and F. Takagi, Phys. Rev. **D41** (1990) 2903.

[99] A. Hosoya and K. Kajantie, Nucl. Phys. **B250** (1985) 666.

[100] G. Baym H. Monien, C.J. Pethick and D.G. Ravenhall, Phys. Rev. Lett. **64** (1990) 1867.

[101] P.J.E. Peebles, "The Large Scale Structure of the Universe", Princeton University Press, Princeton (New Jersey), 1980.

[102] C.Pajares, Phys. Lett. **B258** (1991) 461.

[103] H. Satz, Nucl. Phys. **B326** (1989) 613.

[104] I. Novak, Bratislava Preprint B-3837 (1989).

[105] Z. Burda, J. Wosiek and K. Zalewski, Phys. Lett. **B266** (1991) 439.

[106] R. Bidaux, N. Boccara and H. Chate, Phys. Rev. **A39** (1989) 3094.

[107] I. Jensen, Phys. Rev. **A43** (1991) 3187.

[108] W. Kinzel, Annals of Israel Physical Society **5** (1983) 425.

[109] W. Klein and W. Kinzel, J. Phys. **A14** (1981) L405.

[110] J.Dias de Deus and J.C.Seixas, Phys. Lett.**B246** (1990) 506.

[111] P. Bożek, Z. Burda , J. Jurkiewicz and M. Płoszajczak, Phys. Lett **B265** (1991) 133.

[112] J. Seixas, Int. Jour. Mod. Phys. **A6** 1237.

[113] L.Van Hove, Annals Phys. **192** (1989) 66.

[114] J.Ellis and H.Kowalski, Phys. Lett. **B214** (1988) 161.

[115] J. Wosiek, Proc. Santa Fe Workshop on "Intermittency in High Energy Collisions", Eds. F. Cooper, R.C. Hwa and I. Sarcevic, World Scientific, Singapore 1991.

[116] P. Bożek and M. Płoszajczak, Phys. Lett. **B264** (1991) 204.

[117] B. Svetitsky and L. Yaffe, Nucl. Phys. **B210** (1982) 423.

[118] J.L.Cardy, J. Phys. **A17** (1984) L385.

[119] J.L.Cardy, J. Phys. **A17** (1984) L961.

[120] N.G. Antoniou, E.N. Argyres, C.G. Papadopoulos and S.D.P. Vlassopulos, Phys. Lett. **B260** (1991) 199.

[121] A. Ludwig, Nucl. Phys. **B330** (1990) 639.

[122] K.G. Wilson, Phys. Rev. **179** (1969) 1499.